12-21-2021

DESIGN AND ANALYSIS OF FLEXIBLE INSULATED PAVEMENT FOR COLD REGION APPLICATIONS

Zhuang Zhuo
Rowan University

DESIGN AND ANALYSIS OF FLEXIBLE INSULATED PAVEMENT FOR COLD REGION APPLICATIONS

by
Zhuang Zhuo

A Dissertation

Submitted to the
Department of Civil and Environmental Engineering
College of Engineering
In partial fulfillment of the requirement
For the degree of
Doctor of Philosophy
at
Rowan University
November 24, 2021

Dissertation Chair: Cheng Zhu, Ph.D., PE

Committee Members:
Yusuf Mehta, Ph.D., PE
William T. Riddell, Ph.D.
Gilson R. Lomboy, Ph.D., PE
Hamed Hosseinzadeh, Ph.D.

Dedication

To my grandmother, Ms. Rong-Shi Li.

Acknowledgments

I hereby acknowledge my appreciation to my advisors, Dr. Cheng Zhu, Dr. Yusuf Mehta, Dr. Gilson Lomboy, Dr. William Riddell, and Dr. Hamed Seyyedhosseinzadeh for their valuable time spent serving on my dissertation committee.

I deeply appreciate the invaluable support from my research collaborators at the Center for Research and Education in Advanced Transportation Engineering Systems (CREATEs): Dr. Daniel Offenbacker, Dr. Andrae Francois, Mr. George Shackil, Mr. Dorin Papuc, Mr. Ahmed Saidi, Mr. Ahmad Alfalah, Ms. Rahaf Hassan, Mr. Ian Sennstrom, Ms. Caitlin Purdy, and Mr. Kommini Chandu; and my collaborators from the Geomechanics Laboratory for Underground Exploration and Storge (GLUES): Mr. Rui Liu, Mr. Chenchen Huang, Ms. Kaniz Roksana, and Dr. Shaini Aluthgun Hewage.

This study was conducted as part of a Department of Defense (DoD) Research Project entitled "Development of Innovative Materials and Methods to Solve United States Department of Defense (DoD) Horizontal Infrastructure Challenges in Cold Regions." I would like to thank the DoD and the United States Army Corps of Engineers (USACE) for their support in funding this research study.

I also would like to thank my grandparents, Ying-Wei Zhuo and Rong-Shi Li, my parents, Zheng-Yu Zhuo and Xiu-Ying Lv, my sister Ling Zhuo, my brother Hao Zhuo, and all other family members.

Abstract

Zhuang Zhuo
DESIGN AND ANALYSIS OF FLEXIBLE INSULATED PAVEMENT FOR COLD REGION APPLICATIONS
2021-2022
Cheng Zhu, Ph.D., PE
Doctor of Philosophy

Pavements in cold regions suffer from additional deterioration due to the influences of extreme climate on frost-susceptible subgrade layers. To address this problem, one efficient strategy is to add a thermal insulating layer above the frost-susceptible layer. This study aims to evaluate the insulating effects of four materials: XPS boards, tire chips, foamed glass aggregates, and foamed concrete. Large-scale insulated pavement boxes (1.2m×1.2m×0.8m) were constructed to compare the thermal performance of different materials. The thermal performance of each box was evaluated and graded based on indicators related to the short-term temperature decrease and long-term temperature variation. Experimental results show that with the same insulation layer thickness, XPS boards have the best overall performance (65.8/100), followed by foamed glass aggregates (60.1/100), foamed concrete (52.7/100), tire chips (48.8/100), and the control box (38.8/100). Furthermore, finite element method (FEM) models were developed and calibrated to predict the thermo-mechanical coupled performance of insulated pavement structures. Parametric analyses using FEM enable the formulation of a thermally-mechanically balanced insulation pavement design procedure, which can be used to predict the maximum allowable load repetitions under specific local climate conditions. The cost analysis indicates that using an insulation layer could save approximately $1M/mile in construction costs.

Table of Contents

Table of Contents (Continued)

Table of Contents (Continued)

Table of Contents (Continued)

Table of Contents (Continued)

Table of Contents (Continued)

List of Figures

Figure Page

List of Figures (Continued)

Figure Page

List of Figures (Continued)

Figure Page

List of Tables

Table Page

Chapter 1

Introduction

The performance of flexible pavements is highly dependent on several factors such as traffic and environmental conditions. Flexible pavements experience deterioration, during their service life, due to damage accumulation from traffic loading and variations in environmental conditions (e.g., freeze-thaw cycles, temperature fluctuations, moisture content changes, etc.). One of the major distresses flexible pavements experiences is cracking (fatigue and thermal related); which is also the predominant pavement distress in cold regions. This is the case because of uneven frost heave, excessive settlements due to spring thaw, and the recurring freeze-thaw cycling in cold regions; making pavements more prone to cracking. Consequently, a long-lasting pavement structure should be able to withstand these excessive deformations and freeze-thaw cycling in cold regions.

The typical strategies for designing pavements in cold regions involve selecting proper asphalt binders (proper Performance Grade (PG)), replacing frost-susceptible natural (subgrade) soils, and providing proper drainage. While these strategies are beneficial, the ability of a pavement structure to resist environmental impacts is not always guaranteed because of the unavoidable natural variation in materials and inherent variability in design and construction processes. A non-traditional solution to mitigate environmental impacts on pavements, which has gained increased attention in recent years, is insulating pavements (or insulated pavements) to reduce temperature variation in unbound, frost-susceptible layers.

Insulated pavements are those that include a layer of thermal insulation material; typically placed between subgrade and base layers. The insulation layer is placed to impede heat transfer from top layers to frost-susceptible layers; thus, reducing heat loss from the pavement structure when its surface is exposed to cold air. Research indicates that the use of insulation layers in flexible pavements might be a viable option for mitigating the impacts of cold environments on pavement performance and durability. Several pavement insulation materials were evaluated, and their thermal conductivities were investigated. Polystyrene (extruded or foamed) is reported to be the best material at insulating pavements. Other materials, such as saw wood; tire chips; plastic crumbs; and bottom ash, may also be beneficial in reducing the impacts of freeze-thaw cycles and insulate pavements. Additional research to evaluate the effectiveness of alternative materials for pavement insulation is still needed.

1.1 Research Hypothesis

The three research hypotheses are:

1) Except for the traditional insulating material, extruded polystyrene (XPS) boards, there are other alternative materials that fit the requirements when used as the insulation layer.
2) The thermal and mechanical performance of the insulated pavement system could be simulated by a finite element model.
3) The design procedure of insulated pavements is different from the design of conventional pavement systems due to the need of balancing the thermal and mechanical performance.

1.2 Study Objectives

The main goal of this dissertation is to investigate the application of insulated pavement in the aspects of materials, modeling, design, and cost-effectiveness. The objectives to achieve this goal are summarized as follows:

1) Identify and evaluate cost-effective, lightweight, readily available, and easily installable/constructible material for insulating pavements.
2) Propose a finite element method (FEM) model with the consideration of moisture phase change in the base and subgrade layer to quantify the performance of different material.
3) Develop an insulated pavement design methodology based on the concept of balancing the thermal and mechanical benefits of the developed insulation materials.
4) Estimate and compare the cost-effectiveness of the materials used in this dissertation.

1.3 Dissertation Outline

This dissertation is divided into eight chapters. The first chapter provides a brief introduction and goals of the study. Chapter two presents a summary of current literature pertaining to materials for insulating materials, heat transfer in pavement structures, and more. In Chapter three an experimental test used to compare the performance of different insulating is provided. Chapter four includes the details of the finite element model used in this study. Chapter five presents a discussion of a procedure developed for a thermal-mechanical balance design for insulated pavement. Chapter six details the exploration of

using foamed concrete as an insulation layer in pavements in cold regions. Chapter seven presents a cost comparison of different insulated pavement structures, highlighting the relative cost-effectiveness of each material. Finally, chapter eight presents a summary of findings and conclusion for this study.

Chapter 2

Literature Review

2.1 Pavement in Cold Regions

Pavements in cold regions are subject to differential frost heave in winter months and thaw settlement and weakening during spring months. This in turn, coupled with the formation and melting of ice lenses, the properties of unbound pavement layers (e.g., porosity, density, and resilient modulus) experience seasonal changes. A description of differential frost heave, spring thaw, and the impacts of freeze-thaw cycling on pavement structures is presented in the following subsections.

2.1.1 Differential Frost Heave

Frost heave is described as an upward swelling of soil under cryogenic conditions in cold regions. It is caused by the accumulation of moisture inside the soil and the formation of ice lenses [1]. Differential frost heave causes pavement structure to deform differently in certain locations than in others; thus, causing pavement cracking.

According to Peterson and Krantz (1998), four major factors that cause differential frost heave in pavement structures. These are: 1) instability of one-dimensional freezing process, 2) variability in frost susceptibility of subgrade soils, 3) variability of the thermal regime (air temperature), and 4) inherent material heterogeneity. Peterson and Krantz (1998) also reported that one-dimensional frost heave tends to evolve into multidimensional differential frost heave as a function of soil properties and environmental conditions.

2.1.2 Thaw Weakening

Thaw weakening is a phenomenon that occurs in early spring due to a rise in temperatures and the melting of snow. When a frozen pavement structure starts to thaw, especially unbound layers, water gets entrapped within the unbound pavement layers. When saturated, these unbound layers become significantly weaker; thus, any applied heavy loads end up damaging the pavement. This is mainly due to the weaker bearing capacity of saturated unbound layers, especially the subgrade soil layer.

From a technical standpoint, spring thaw increases the pore water pressure within unbound pavement layers which in turn reduces the effective stresses within the soils' skeleton. Based on the falling weight deflectometer (FWD) test conducted by Salour [2], an increase in moisture content in unbound layers largely decreases the stiffness of these layers.

2.1.3 Impacts of Freeze-Thaw Cycling

In addition to differential frost heave and thaw weakening, another factor that may affect the performance of pavements in cold regions is freeze-thaw cycling. Various studies showed that freeze-thaw cycling may change the mechanical properties of granular base and subgrade soil layer in the pavement structure, thus reducing the bearing capacity of the pavement structure. For instance, Viklander [3] pointed out that the density of soil subjected to several freeze-thaw cycling increased for an initially loose soil and decreased for an initially dense soil based on laboratory tests. The influence of freeze-thaw cycling on the mechanical properties causes the resilient modulus of soil to decrease by 25% to 60% [4]. The weakening of the resilient modulus of the subgrade

layer induces more rutting depth and decreases the load-bearing capacity. Hydraulic permeability of subgrade soils also increases by one to two orders of magnitude after freeze-thaw, according to the research of Chamberlain [5], Zimmie [6] and Viklander [3]. The increases of subgrade permeability in return accelerate the moisture movement and strength degradation. Therefore, freeze-thaw cycling creates weaker unbound pavement layers with heavy loads easily damaging these pavements.

2.2 Strategies to Protect Cold Regions' Pavements Against Freeze-Thaw Cycling

Several strategies (or design considerations) can be employed for protecting pavement structures from the detrimental impacts of freeze-thaw cycling. These include improving subgrade soils (or replacing frost-susceptible soils) [7, 8], improving drainage conditions [9], and the use of insulation materials to insulate the subgrade layer [10, 11]. A brief description of each of these techniques is presented in the following subsections.

2.2.1 Improving Subgrade Soils

This strategy revolves around the concept of ensuring uniform subgrade soils for pavements constructed in cold regions and also the removal/replacement of frost-susceptible natural subgrade soils. The use of non-frost-susceptible subbase layers is one additional way of protecting the subgrade from freeze-thaw cycling impacts. Such a subbase layer helps: 1) resist frost penetration, 2) reduce differential movements; and 3) help in load distribution and drainage of water.

2.2.2 Improving Pavement Drainage

The detrimental impacts of freeze-thaw cycling on pavements can be minimized by improving their ability to drain water away from subgrade layers. Such a drainage

improvement can be achieved by installing deep drains or capillary barriers to maintain the water table a depth below the unbound pavement layers. If it is not possible to maintain a deep-water table level, the pavement structure can be protected by removing all frost-susceptible soils to a sufficient depth below frost penetration.

2.2.3 Insulation of Subgrade Layers

Insulation of subgrade layers is another approach for protecting pavement structures against the negative impacts of freeze-thaw cycling. In this approach, an "insulating" pavement layer is placed on top of the subgrade to resist frost penetration. A discussion of the typical materials used for insulating pavement structures is provided in Section. 2.3 of this report.

2.3 Typical Insulated Materials Used in Pavement

Several materials were identified from the literature as insulators of flexible pavement structures. These include extruded polystyrene (XPS) boards, expanded polystyrene (EPS), tire chips, bottom ash, wood residues, foamed concrete, foamed glass aggregates, among other materials. A description of each of these materials is provided in the following subsections.

2.3.1 Polystyrene Foam Boards

Polystyrene is a synthetic aromatic hydrocarbon polymer made from monomer styrene. Foamed polystyrene is a super-lightweight material, approximately 1% the weight of soil. Generally, two types of foamed polystyrene, expanded polystyrene (EPS) and extruded polystyrene (XPS) are used for insulating pavements. EPS has interconnected voids between the beads that can provide pathways for water to penetrate

the insulation. XPS, on the other hand, is a uniform closed-cell rigid foam insulation board with no voids or pathways for moisture to enter. XPS has higher strength and lower water absorption than EPS, making it more desirable by designers. Physical properties required when using these materials as pavement insulators are provided in ASTM C578–18 specifications Table 1 presents examples of physical properties for XPS as specified in ASTM C578-18.

Table 1

Example Physical XPS Boards Properties for Thermal Insulation Applications (ASTM C578)

Classification	Type XI	Type I	Type VIII	Type II	Type IX	Type X/V	Type XV	Type XII
Compressive resistance (psi)	5	10	13	15	25	40	60	15
Thermal resistance ($F \cdot ft^2 \cdot h/Btu$)	3.1	3.6	3.8	4	4.2	4.2	4.3	4.6
Flexural strength (psi)	10	25	30	35	50	60	75	40
Water absorption (perm)	4	4	3	3	2	2	2	0.3

2.3.2 Tire Chips

Tire chips (or shredded tires) are recycled materials made by shredding scrap tires. Generally, tire chips are smaller than 2-in. (Humphrey et al. 1993). It is estimated that 1-2 billion waste tires were disposed of in the United States [12]. Tire chips are not only an effective pavement insulation material they also have high permeability; allowing them to drain excess water from a pavement's substructure (Humphrey et al. 1993, 1995). Tire chips have a thermal conductivity ranging between and 0.071 to 0.10 BTU/(h·ft·°F).

2.3.3 Bottom Ash

Bottom ash is a byproduct of coal combustion when burned in the furnace of electric power plants. The size of bottom ash is smaller than 0.5 mm, and it is composed of silica, alumina, and iron [13]. A carefully compacted ash is not susceptible to frost because of its low permeability and hardening. The thermal conductivity of bottom ash ranges between 0.17 and 0.52 BTU/(h·ft·°F) [14].

2.3.4 Foamed Concrete

Foamed concrete is a mixture of cement, water, and foam. Typically, foamed concrete contains 20% or more entrapped foam within its structure. This material contains no coarse aggregates. Foamed concrete is produced at densities ranging from 43.7 lb/ft^3 to 87.4 lb/ft^3 [15]. Foamed concrete has excellent thermal insulating properties due to its cellular microstructure, which is about one-sixth that of typical cement–sand mortar [16]. The thermal conductivity of foamed concrete ranges between 0.14 to 0.43 BTU/(h·ft·°F) [15].

2.3.5 Foam Glass Aggregates

Foamed glass aggregate is lightweight fill material made from 100-percent-recycled container glass. It is 85-90% lighter than quarried aggregates, has a high friction angle, and is a good insulator due to its closed-cell structure [17]. The initial use of this material was to prevent frost heave in frost susceptible soils throughout Scandinavia. It is also used as building roof insulation and lightweight fill over compressible soils and/or utilities [18]. The thermal conductivity of foamed aggregates ranges between 0.03 to 0.12 BTU/(h·ft·°F) [19].

2.4 Performance of Insulated Pavement Structures

Most studies on evaluating the performance of insulated pavement structures focused on using polystyrene boards as the insulation layer. Research on other pavement insulation materials has been conducted. However, these efforts were not as extensive as those conducted on polystyrene materials. The following subsections present a summary of the studies focusing on polystyrene and other pavement insulation materials.

2.4.1 Performance of Polystyrene Foam Boards as Pavement Insulators

Several studies were conducted to evaluate the performance of polystyrene boards as pavement insulation layers. For instance, Penner [20] insulated a field pavement section (100 ft. long with have being insulated) using polystyrene boards and monitored for 3 years. Penner monitored the temperature distribution and moisture change within the control (uninsulated) and insulated portions of the section. Based upon these measurements, inward frost penetration from the edge of an insulated area is about the same as the downward penetration on the control segment. Penner (1976) also reported

that the time for cooling the insulated pavement structure surface is faster than that in the control segment. This might lead to surface icing on insulated pavements.

In 1982, Gandahl [11] investigated the frost resistance capacity, frost heaving, surface icing, and road repair cost of polystyrene foam insulated pavements. Gandhal reported that the frost resistance capacity of a polystyrene foam insulated base layer is dependent on: properties and thickness of the polystyrene foam and water content in layers beneath the foam. The researcher also concluded that the surface temperature of the polystyrene insulated section is -3.6 °F lower than the non-insulated sections.

Esch [21] reported the observations of a series of field test results from four insulated pavement sections (i.e., foamed-in-place polystyrene, molded polystyrene, extruded-expanded polyurethane, and a control) constructed from 1967 to 1994 in Alaska. After 25 years of monitoring the sections, Esch reported that extruded polystyrene foam had better performance than polyurethane due to is lower moisture absorption. The extruded-expanded polystyrene foam showed excellent resistance to moisture absorption.

Kestler and Berg [22] evaluated four polystyrene insulated pavement sections in Maine. Frost penetration, insulation discontinuities, frost heave, cracks, and surface icing from each section were collected. Kestler and Berg reported that the insulated pavement did not exhibit strength loss and the subgrade layer of the insulated section didn't experience a frost-thaw weakening process. Cote and Konrad [23] reported that the use of insulation layers create the potential of differential icing for surface layers. According to Cote and Konard, a pavement insulation layer may reduce the upward heat flow, resulting in a

sharp increase in the rate of cooling of the pavement surface when exposed to cold air temperatures.

2.4.2 Other Pavement Insulation Materials (Tire Chips, Bottom Ash, Foamed Concrete, and Foamed Glass Aggregates)

In 1995, Dore et al. [24] constructed 12 fields insulated sections to investigate the performance of two alternative insulating materials: sawdust and tire chips. The thermal and mechanical behavior (e.g., penetration depth and maximum heaving deformation) of the insulated sections with different insulating materials and thicknesses were compared. A combined performance evaluation equation, which considers both the thermal performance and the mechanical performance of insulated pavement, was proposed to find the optimum design. The experimental results indicated that the mechanical performance (deflection and vertical strain) of sawdust is similar to the reference (uninsulated) section, while the deflection and strain in the tire chips insulated section is much larger than that in the reference section. As for the thermal performance such as frost penetration depth and heaving displacement, the test results showed that the two insulated sections had less frost penetration depth and heave displacement compared with the reference section. The thermal performance of sawdust and tire chips was similar.

Research on bottom ash includeded that by Haghi, Nassiri et al. [13]. In this study, the researchers constructed three field-sections of insulated pavements; one control with no insulating layer and the other two were insulated sections (one insulated with 1000 mm thick bottom ash layer and 100 mm thick polystyrene boards). Comparing temperature distributions in base and subgrade layers and frost depth for each of the sections suggests

that the base layer in the polystyrene section experienced higher temperatures in summer and lower temperatures in winter compared with the other two sections. The polystyrene-insulated section also had the lowest temperature variation in the subgrade layer. Nassiri et al. [13] concluded that the polystyrene insulating layer decreased the frost depth by 40%, while the bottom ash insulating layer decreased the frost depth by 28%. Field et al. [25] reported that polystyrene and bottom ash insulating layers could effectively prevent the freezing of subgrade soils and subsequent heave, while the polystyrene insulating layer might generate transverse cracking of the pavement due to the abrupt temperature gradient.

In the case of foamed concrete and foamed glass aggregates, it is noted that no studies were found in literature where these materials are evaluated as pavement insulation layers.

2.5 Heat Transfer in Pavement Structures

2.5.1 Importance and Formulation of Heat Transfer Constitutive Equations

Pavements in cold regions are more prone to distresses due to severe swings in temperature and moisture levels. Mallick (2007) reports three cold regions factors that impact pavement performance: 1) temperature, 2) moisture, and 3) the effect of temperature on moisture. The third factor (effect of temperature on moisture) is controlled by the degree of heat transferred within the layers of a pavement structure and the amount of moisture present in these layers.

In any medium, there are three fundamental modes of heat transfer: 1) conduction (direct contact heat transfer), 2) convection (heat transfer by fluid mass motion), and 3)

electromagnetic radiation (e.g., U.V. lights from the sun). In most situations, convection and radiation are negligible when studying heat transfer through mediums; in comparison to conduction heat transfer.

For isotropic homogeneous materials, Joseph Fourier (1768-1830) postulated that heat flow rate is proportional to the temperature gradient. The proportionality factor that defines this relationship is thermal conductivity (Equation 1).

$$q = k\nabla T = k\frac{dT}{dx} \tag{1}$$

where k is thermal conductivity, represents the rate at which heat energy flows across a unit area of a material due to a unit temperature gradient, q is the heat flux per unit area (W/m^2), and ∇T is temperature gradient (K/m).

By substituting Equation 1 into the balance equation (Equation 2):

$$\frac{dq}{dx} = \rho c\frac{\partial T}{\partial t} \tag{2}$$

the conduction heat transfer constitutive equation is derived as:

$$k\frac{\partial^2 T}{\partial x^2} = \rho c\frac{\partial T}{\partial t} \tag{3}$$

where ρ is density (kg/m^3), c is heat capacity (J/K), and t is time (s).

Based on Equation 3, it can be seen that an understanding of heat transfer in pavement applications is possible through defining changes of thermal conductivity (k) and heat capacity (c). Note that most paving materials (e.g., granular base aggregates and subgrade soils) are not homogeneous. In these materials, thermal conductivity is temperature-dependent. This is the case due to the dependence of the different phases of these materials (e.g., solid particles, air, vapor, ice particles when frozen) on temperature.

The following subsection presents models in literature defining the thermal conductivity of unbound paving materials.

2.5.2 Thermal Conductivity of Soils and Aggregates

The main factors affecting the thermal conductivity of soils and aggregates include: grain distribution, connectivity of the porous network, a volumetric fraction of each component, and properties of these components[26]. To capture the relation between the thermal conductivity and each of these factors, several semi-theoretical and empirical models were developed. These models allow for estimating the thermal conductivity of soils and aggregates in both frozen and unfrozen states. These models are summarized in Table 2.

From Table 2, it can be observed that thermal conductivity is related to porosity, degree of saturation, and soil type. For a specific kind of soil, the thermal conductivity estimated by the formulas in Table 2 will remain constant under different temperatures. Therefore, these formulas (Table 2) are not suitable for characterizing the thermal conduction process for pavements in cold regions.

In addition to the empirical and semi-theoretical models, several other theoretical models were also derived (Table 2). These theoretical models take into consideration the effects of ice content, mineral content, and vapor pressure. Therefore, they are more suitable for estimating the thermal conductivity of soils and aggregates while also accounting for the temperature dependency of thermal conductivity in these materials.

Table 2

Semi-Theoretical and Empirical Models for Estimating Thermal Conductivity of Soils and Aggregates

Author (reference)	Thermal conductivity formula (k)
Kersten [27]	For silty and clayey soils, Unfrozen: $k = [0.9\log w - 0.2]10^{0.01\gamma_d}$ Frozen: $k = 0.01(10)^{0.022\gamma_d} + 0.085(10)^{0.008\gamma_d} w$ ($w \geq 7\%$) For sandy soils, Unfrozen: $k = [0.7\log w + 0.4]10^{0.01\gamma_d}$ Frozen: $k = 0.076(10)^{0.013\gamma_d} + 0.032(10)^{0.0146\gamma_d} w$ ($w \geq 1\%$) w = water content; γ_d = dry density
	The proposed correlations are found to be suitable only for frozen soils. Limited saturation level ≤ 90%
Van Rooyen and Winterkorn [28]	$\frac{1}{k} = A \cdot 10^{-BS} + G$ S = degree of saturation A, B, G = functions of dry density, mineral type, and granulometry respectively
	Limited to unfrozen sands and gravels; Limited to saturation level 1.5% ~ 10%

Author (reference)	Thermal conductivity formula (k)
Johansen [29]	$k = (k_{sat} - k_{dry})k_e + k_{dry}$ k_{sat} = Soil thermal conductivity in the saturated state $k_{dry}\left(\frac{W}{mK}\right) = \frac{0.135\rho_{dry}+64.7}{\rho_{solid}-0.947\cdot\rho_{dry}} \pm 20\%$ (ρ in kgm^{-3}) for dry natural soils $k_{dry}\left(\frac{W}{mK}\right) = 0.039n^{-2.2} \pm 25\%$ for crushed rock materials k_e = Kersten number, a dimensionless function of soil saturation n = porosity
	Suitable for both coarse and fined grained soils in the frozen and unfrozen states. Limited to saturation level > 20%
Gavriliev [30]	$k_{dry} = 0.025 + 0.238\rho_{dry} - 0.193\rho_{dry}^2 + 0.114\rho_{dry}^3$ ρ_{dry} = dry density ($\leq 2\ gcm^{-3}$)
	Applicable for mineral and organic soil (air-dry soils)

Author (reference)	Thermal conductivity formula (k)
Becker, Misra [31]	Correlation with saturation $S = \lambda_1[\sinh(\lambda_2 k + \lambda_3) - \sinh(\lambda_4)]$ S = degree of saturation k = thermal conductivity [unit: Btu in. / (ft^2 hr ^oF)] $\lambda_1 \sim \lambda_4$ = coefficients that depend on the soil type
	This correlation is developed for 5 soil types in both the frozen and unfrozen states: gravel, sand, silt, clay, and peat.

Table 3

Theoretical Models for Estimating the Thermal Conductivity of Soils and Aggregates

Author (reference)	Model	Effective thermal conductivity ($\boldsymbol{\phi}$ = porosity, $\mathbf{k_a}$ = thermal conductivity of air, $\mathbf{k_m}$ = thermal conductivity of mineral particle)
De Vries [32]	Two/three-phase material model	$k = \frac{x_f k_f + F x_s k_s}{x_f + F k_s}$ x_f and x_s = fluid and solid volume fraction x_f and x_s = fluid and solid thermal conductivity $F = \frac{1}{3}\sum_i \left[1 + (\frac{k_s}{k_f} - 1)g_i\right]^{-1}$ (I = a, b, c.) g = shape factor
		Applicable for unfrozen coarse soils Limited saturation level 10% ~ 20%

Author (reference)	Model	Effective thermal conductivity ($\boldsymbol{\phi}$ = porosity, $\mathbf{k_a}$ = thermal conductivity of air, $\mathbf{k_m}$ = thermal conductivity of mineral particle)
Gemant [33]	Geometrical model of soil particles with point contacts	$\frac{1}{k} = \frac{[\frac{1-a}{a}]^{4/3}\arctan[\frac{k_s-k_w}{k_w}]^{1/2}}{(\frac{h}{2})^{1/3}[k_w(k_s-k_w)]^{1/2}} + \frac{(1-z)}{k_s a} f(\frac{b^2}{a})$ $a = 0.078\rho_{dry}{}^{1/2}$ $h = 0.16 * 10^{-3}\rho_{dry} w - h_0$ $z = (\frac{1-a}{a})^{2/3}(\frac{h}{2})^{1/3}$ $b^2 = (\frac{a}{1-a})^{2/3}(\frac{h}{2})^{2/3}$ ρ_{dry} = soil dry density w = water content h = apex water (water collected around the soil particle contact points) h_0 = water absorbed as a film around the soil particles k_s, k_w = thermal conductivity of the soil solid and water

Author (reference)	Model	Effective thermal conductivity ($\boldsymbol{\phi}=$ porosity, $\mathbf{k_a}=$ thermal conductivity of air, $\mathbf{k_m}=$ thermal conductivity of mineral particle)
summarized in DeVera and Strieder [34]	Series (2 phases)	$\frac{1}{k_{eff}}=\frac{\phi}{k_a}+\frac{1-\phi}{k_m}$
	Parallel (2 phases)	$k_{eff}=\phi\cdot k_a+(1-\phi)\cdot k_m$
Maxwell and Thompson [35]	Randomly distributed and non-interacting homogeneous spheres (2 phases)	$k_{eff}=k_m[\frac{k_f+2k_m-2\phi(k_f-k_m)}{k_f+2k_m-\phi(k_f-k_m)}]$ for dry soil, fluid is taken as air $k_f=k_a$
summarized in Kumlutas, Tavman [36]	Geometric mean (2 phases)	$k_{eff}=k_a^{\phi}\cdot k_m^{1-\phi}$
	Two phase system with particle shape and the orientation/type of packing considered (2 phases)	$k_{eff}=k_m\frac{1+a\cdot B\cdot\phi}{1-\psi\cdot B\cdot\phi}$ $B=\frac{\frac{k_a}{k_m}-1}{\frac{k_a}{k_m}+a}$, $\psi=1+(\frac{1-\phi_m}{\phi_m^2})\cdot\phi$ αand ϕ_m are particle shape and packing parameters

Author (reference)	Model	Effective thermal conductivity ($\boldsymbol{\phi}$ = porosity, $\mathbf{k_a}$ = thermal conductivity of air, $\mathbf{k_m}$ = thermal conductivity of mineral particle)
Hashin and Shtrikman [37]	Hashin and Shtrikman boundaries (2 phases)	$k_{eff} = k_m + \frac{\phi}{\frac{1}{k_a - k_m} + \frac{1-\phi}{3k_m}}$ upper boundary $k_{eff} = k_a + \frac{1-\phi}{\frac{1}{k_m - k_a} + \frac{1-\phi}{3k_a}}$ lower boundary
Nimick and Leith [38]	solid-continuous material and regions of fluid-continuous material.	$k_{eff} = k_{sc}\left[1 - \frac{3 \cdot \phi(1-A)}{2 + A + \phi(1-A)}\right], A = \frac{k_{fc}}{k_{sc}}$ $k_{sc}\ and\ k_{fc}$ = Hashin and Shtrikman's upper and lower bound.
Tarnawski, Leong [39]	Self-consistent method (3 phases)	$k_{eff} = \frac{1}{3}[\sum_{i=1}^{3} \frac{\phi_i}{2k_{eff} + k_i}]^{-1}$
Gori and Corasaniti [40]	Cubic cell model (2 phases)	$\frac{1}{k_{eff}} = \frac{\beta-1}{k_a \cdot \beta} + \frac{\beta}{k_a \cdot (\beta^2 - 1) + k_m}$, $\beta = [\frac{1}{1-\phi}]^{1/3}$ for dry soil

As illustrated in Table 2, the theoretical models utilize mineral content and ice content for the estimation of thermal conductivity. There are two advantages of this: 1) when using ice content as one of the variables, temperature drops cause an increase in ice content, and thus the estimated thermal conductivity might reflect phase changes; and 2) considering mineral content makes these theoretical models applicable for estimating the thermal conductivity of different soil and aggregate types. However, even though the thermal conductivity could be estimated by the mineral content and ice content (or unfrozen water content), it is still necessary to understand the icing mechanism of soils and aggregates when determining their ice content. Additional details are provided in Section 2.5.3.

2.5.3 Estimation of Temperature Distribution in Pavement Structures

To comprehensively understand the deterioration process under environmental loadings and evaluate the efficiency of different insulation materials, an accurate heat transfer model of the pavement system is required. The performance of flexible pavement in cold regions involves multiphysics behavior: the frost penetration is related to the thermal field, the frost heaving cracking is the coupling behavior of the thermal, hydraulic, and mechanical field. A few heat transfers models have been proposed to characterize the temperature distribution inside the pavement structures.

In 1970, Ho et al. [41] proposed a finite difference numerical model to predict the temperature distribution of insulated pavement. In this model, the moisture migration, thermal expansion, and properties change of the soil body were neglected. Besides, the heat transfer process of this model is only by conduction and phase change. The heat

transfer process in this model used the Fourier's thermal conduction equation (Equation 4), and the heat transfer caused by phase change was expressed by:

$$Q_{pc} = -L\gamma_d w \Delta g(\Delta x \Delta y \Delta z) \quad (4)$$

where L is the latent heat, γ_d and w are the dry unit weight and water content of the soil, Δg is the fraction of total moisture content that changes in phase during the interval.

The thermal conductivity, moisture content, and percent of water frozen were all set as constant due to the limitation of the computation method. The comparison of predicted temperature and measured temperature shown in Figure 1 indicated that this method is efficient in estimating the long-term heat transfer process for insulated pavement.

Figure 1

Comparison of Predicted Temperature and Measured Temperature from Ho's Study [41]

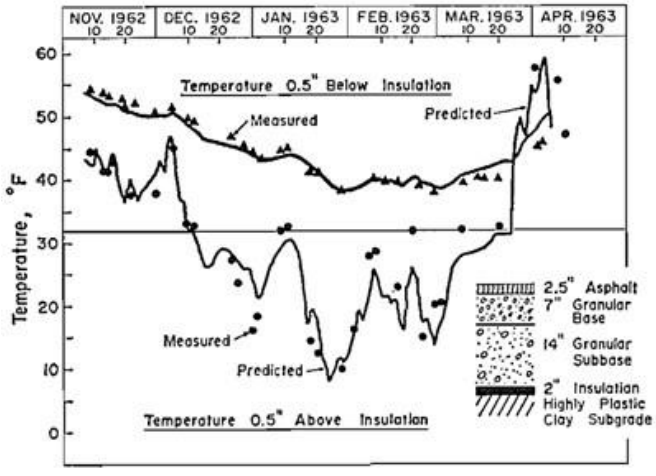

Frivik et al. (1977) [42] developed a finite element model to solve the nonlinear heat transfer problem in soils. In this model, heat conduction, heat convection, and radiation were all considered into account in the heat transfer process, the techniques of evaluating the thermal properties and boundary conditions were improved. This model could predict both the long-term and short-term temperature variations. Fourier heat conduction (Equation 1) was used in this model to calculate the heat transfer from conduction. The calculation of heat convection and radiation used a semi-empirical method:

$$Q_{cv} = \alpha(T - T_a) \tag{5}$$

$$\alpha = \begin{cases} 3W/m^2 \cdot k, & T < T_a \\ 4W/m^2 \cdot k, & T > T_a \end{cases} \tag{6}$$

$$Q_r = e\sigma(T^4 - T_r^4) \tag{7}$$

where Q_{cv} is the heat transfer from convection, α is the convection coefficient, T is the temperature, T_a is the air temperature, k is the thermal conductivity, Q_r is the heat transfer from radiation, e is the emissivity of the boundary surface, σ is the Stefan-Boltzmann constant ($1.714\times10{-}9$ BTU/(h·ft^2·°R^4)), T_r is the sky-radiation temperature.

The thermal conductivity used in this study is modeled by the semi-empirical equation derived by Johansen (listed in Table 2). The temperature prediction result was acceptable as shown in Figure 2.

Figure 2

Comparison of Predicted Temperature and Measured Temperature from Frivik's Study [42]

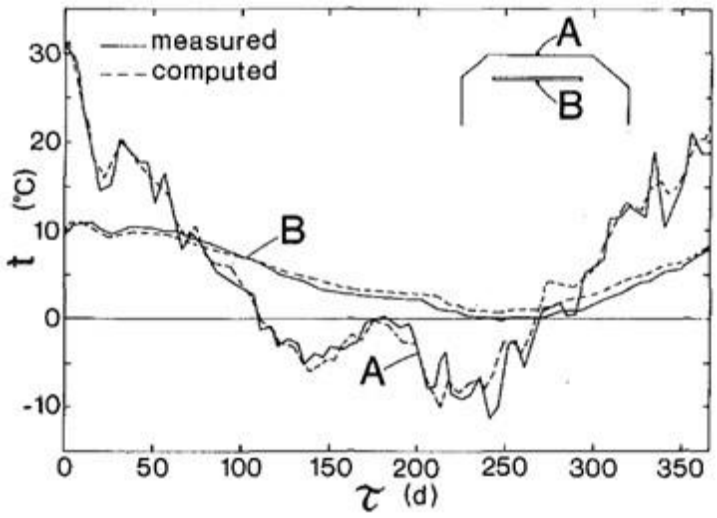

Dempsey and Thompson [43] proposed a heat-transfer model for evaluating frost action and temperature-related effects for a multilayered pavement system. This model is based on the one-dimensional finite difference method, and the climatic data were the major input information in this model. The heat transfer from conduction, convection, short-wave radiation, and long-wave radiation were all taken into account. The heat conduction was expressed with the Fourier equation (Equation 1), the heat convection and heat radiation were expressed with Equations 5 and 7. The model accuracy is acceptable as shown in Figure 3.

Figure 3

Comparison of Predicted Temperature and Measured Temperature from Dempsey's Study [43]

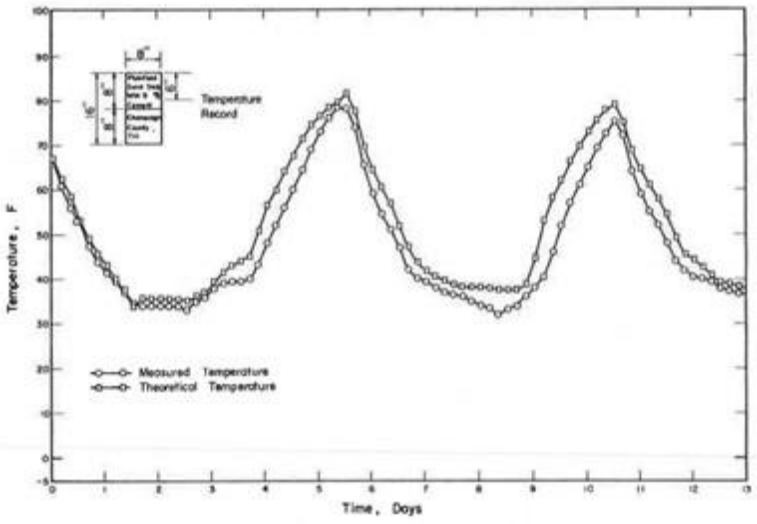

Berg et al. (1980) proposed a mathematical model of coupled heat and moisture flow in soil with consideration of phase change of soil moisture. However, this method is not fully coupled based on the method and computation technique at that time. The heat and moisture fluxes were essentially decoupled to facilitate the evaluation of the model. For the heat transfer process, conduction (Equation 1) and latent heat generation were taken into account. The moisture transportation was expressed by Darcy's law, and the heat convection was expressed by:

$$Q_{cv} = \frac{\partial}{\partial x}(C_w v T) \tag{8}$$

where C_w is the heat capacity of water, v is the velocity flux.

The thermal conductivity in this model was estimated by the theoretical model developed by DeVries (Table 3). The results predicted from this were similar to the lab test results.

Padilla and Villeneuve (1992) used the finite element method to solve the water flow, heat and solute transport of the frost-susceptible soil. They selected hydraulic head, soil temperature and solute concentration as the degrees of freedom in this problem. This method considered the presence and formation of ice lenses in saturated, partially saturated, colloidal and noncolloidal soils based on Miller's theory. Besides, the dispersion, convection, solute redistribution, and overburden were also considered in this simulation. The heat transfer process was expressed by:

$$c(H)\frac{\partial T}{\partial t} = \frac{\partial}{\partial z}\left\{k(H)\frac{\partial T}{\partial z}\right\} - \rho_w c_w v\frac{\partial T}{\partial z} + \left((c_w - c_i)T + L_f\right)i \qquad (9)$$

where c is the thermal capacity by unit volume of the porous medium, c_w, c_i are the specific heat of water and ice, v is the Darcy velocity, L_f is the latent heat.

The developed model established a reasonable degree of confidence to simulate soil freezing conditions related to saturated, unsaturated soils. However, this coupling method was not involved the mechanical field and the objective of this problem is only soil without the multilayer pavement structure.

Luo et al. (2018) proposed a thermos-hydro-mechanical model to investigate the stress changes in pavement subjected to freeze-thaw. Heat conduction, heat convection, and latent heat were calculated by Equation 9. In this model the elastic modulus of materials is specified as a temperature-dependent value and changes before and after the

freeze-thaw process. However, this model could not give the stress changes after multiple freeze-thaw cycling.

2.6 Design Methods of the Insulated Pavement in Cold Regions

2.6.1 Design Methods of Pavements in Cold Regions

Due to the limited understanding of the mechanism behind the frost heave and thaw weakening, most of the primary pavement design methods do not explicitly account for the frost effects [44].

The United State Army Corps of Engineers (USACE) provided two methods on the design of pavement in cold regions: limited subgrade frost penetration method and reduced subgrade strength method [45].

The limited subgrade frost penetration method requires a sufficient thickness of the layers above the frost-susceptible subgrade to ensure the penetration of the frost into the subgrade layer within an acceptable amount. The first step is to estimate the average moisture content in the base course and subgrade layer, and estimate the dry unit weight of the base. The second step of this method is to estimate the frost penetration depth based on the design curve (Figure):

Figure 4

Design Curve of Estimating Frost Penetration Beneath Pavements [45]

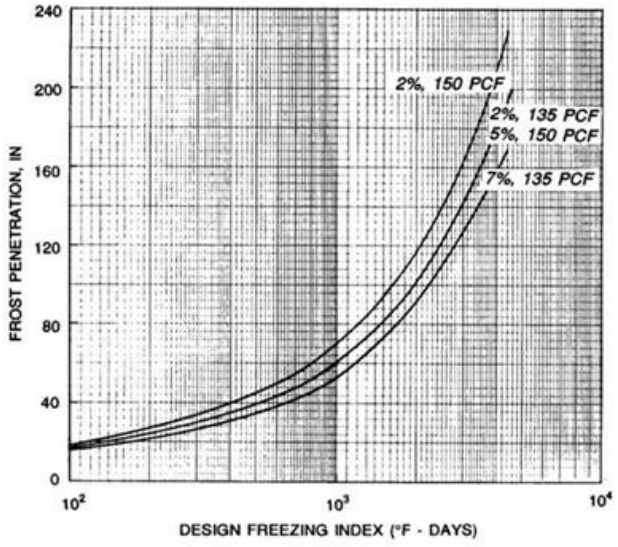

The thickness above the frost-susceptible layer can be determined based on the frost penetration depth. However, using this method to protect the subgrade layer is usually uneconomical and unnecessary.

The reduced subgrade strength method does not require the limitation of the frost penetration depth. This method seeks to build the surface layer, base layer, and subbase layer strong enough to adequately carry the traffic loads when the subgrade experienced thaw weakening. A series of design curves were provided by this method, the thickness of each layer can be determined by the CBR value.

The AASHTO flexible pavement design method (or MEPDG method) [46] considered the seasonal variation in the strength of the subgrade layer, but did not

account for the strength variation of the base and subbase layer. The detail of using this method to design the pavement structure was presented in Chapter 5.

In addition to these two design methods provided above, other methods also provide the design process account for the influence of temperature. The Asphalt Institute (AI) method only accounts for the influence of the maximum temperature on the pavement performance, but fail to consider the influence of seasonal frost heave and thaw weakening [47]. The National Stone Association (NSA) method provided the flexible pavement design method that provides the procedure for minimizing the frost damage, but it is not widely used [44].

2.6.2 Design Method of Insulated Pavements

USACE also provided the design procedure of insulated pavements [45]. According to the design procedure given by the USACE, the first step of designing the insulated pavement is to determine the thickness of the layers above the insulation layer to ensure the vertical stress on the insulation layer does not exceed one-third of the compressive strength. After the thickness of the overlying layer is determined, the thickness of the insulation layer can be determined based on the climate by design curves shown in Figure 5. However, this method is only applicable to the insulation layers made by extruded polystyrene boards (XPS). Besides, the design procedure only considers the thermally protection of the subgrade layer, while the mechanical performance of the designed structure is not included.

Figure 5

Example Design Curve of Determining Insulation Thickness

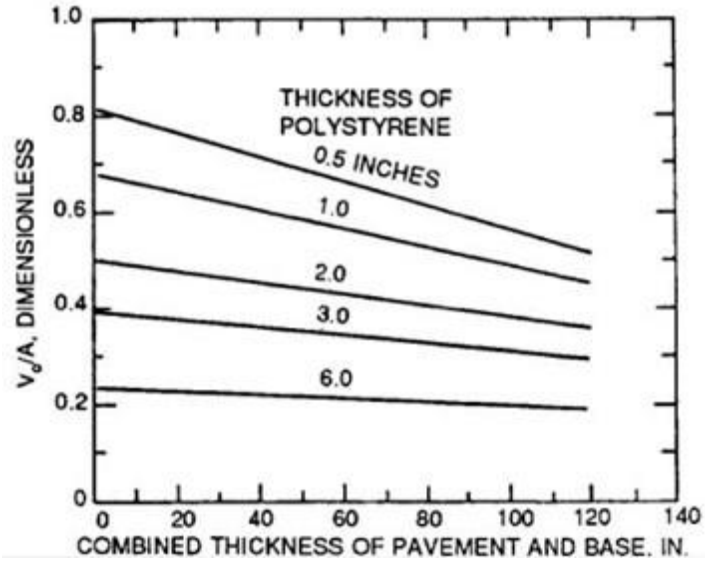

In addition to the design procedure from USACE, Côté and Konrad [48] explored the design of granular thickness in the insulated pavement to mitigate the potential of differential icing effect for near-surface. Design curves of determining the granular protection thickness were provided based on this research:

Figure 6

Design Charts for the Minimum Value of Granular Protection Thickness in the Province of Quebec [48]

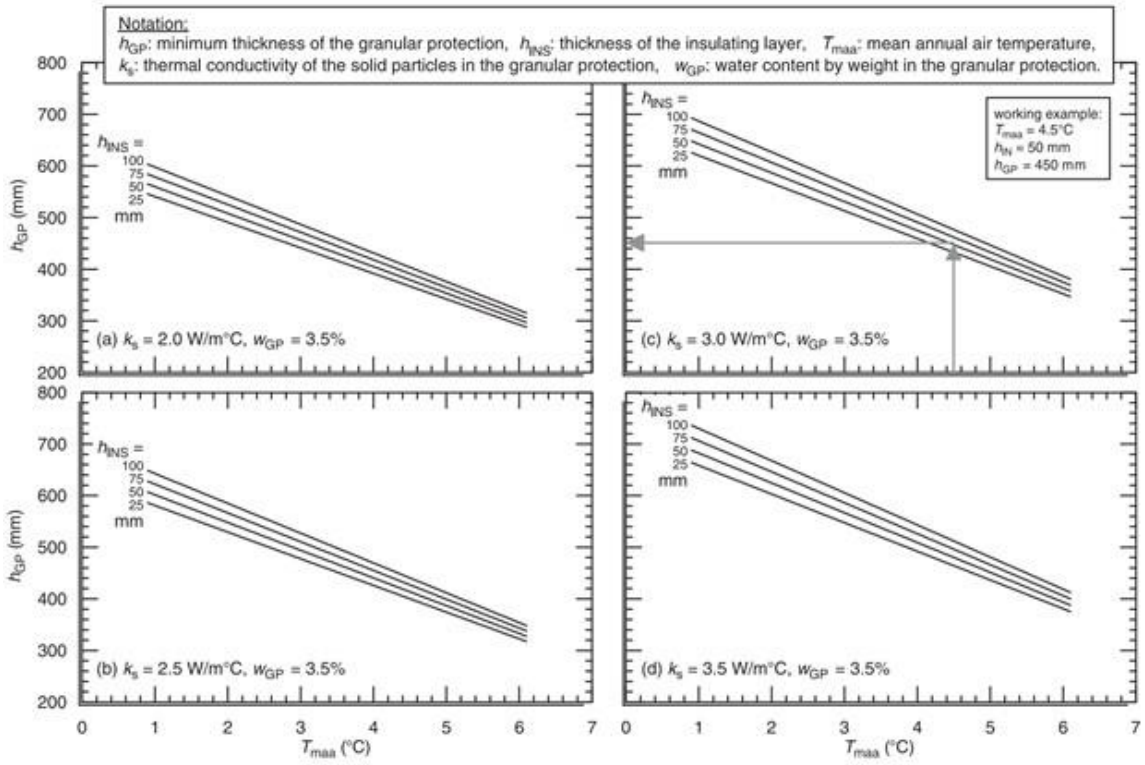

2.7 Literature Review Summary

Field tests indicated that adding an insulation layer above the frost-susceptible subgrade can efficiently mitigate the damage process caused by frost penetration such as uneven frost heave, thaw weakening, and the strength degradation caused by frost-heave cycles. Compare with the other strategies to protect the pavement in cold regions (i.e. improving subgrade soils and improving pavement drainage), insulating the subgrade

layer is more cost-effective. Based on the information provided in the literature review, the following points can be drawn:

Substantial research has been conducted to explore the potential of using alternative insulating materials other than extruded polystyrene (XPS) boards such as tire chip and bottom ash. The mechanical and thermal performance of these materials were compared with the XPS insulated section and control (uninsulated section), but most of the research failed to conduct the quantification analysis.

In addition to the traditional insulating materials, some new types of insulating materials such as foamed concrete and foam glass aggregates exhibited good mechanical and insulating properties, while the potential of using these materials as an insulation layer in pavements was not investigated yet.

The temperature prediction within the pavement structure is the basis of the quantification analysis of insulated pavement. The heat transfer process was investigated by substantial research, and the heat transfer equations that account for heat conduction, convection, radiation, and phase change were well developed.

Limited primary pavement design methods considered the influence of frost penetration for pavements in cold regions. The current design approach related to the insulated pavement [45] has a limitation on the insulating material type, and the design process was not well established.

In summary, there is a need to explore the use of alternative insulating materials. The thermal and mechanical performance of different insulation materials needs to be

quantified in the application. The current design method on insulated pavement needs to be updated and improved by building a heat transfer model of insulated pavements.

Chapter 3

Comparative Study of Different Materials for Insulated Pavement in Cold Regions

3.1 Abstract

Pavements in cold regions suffer from additional deterioration due to the influence of extreme climate on frost-susceptible subgrade layers. To mitigate this effect, one efficient strategy is to add a thermal insulation layer above the frost-susceptible layer (or subgrade) in a pavement structure. This paper was initiated to adopt both the experimental and numerical methods to evaluate the performance of different types of insulating materials. In this study, five large-scale insulated pavement boxes were built, one without an insulation layer, and the other four were insulated with different materials: XPS boards, tire chips, foamed glass aggregates (FGA), and foamed concrete. The five pavement boxes were tested under two different conditions, constant freezing and outdoor environment, and the temperature distributions were collected to compare the insulation performance. Based on the large-scale pavement tests, a finite element model was developed with the consideration of moisture phase change in the unbound granular layers. The numerical simulation was used to extrapolate the temperature distribution of pavement structures different from the structures in the large-scale boxes. The results indicated that the XPS and FGA have the best overall insulation performance, followed by foamed concrete and tire chips. This study provides new insights into the evaluation of insulating materials for pavement in cold regions.

3.2 Introduction

Pavements in cold regions are prone to more severe deterioration than those under temperate climates [49]. Due to the formation and melting of ice lenses, these pavements undergo differential frost heave in winter months and thaw weakening during spring months [50-54]. This causes considerable degradation of the engineering properties (e.g., porosity, density, and resilient modulus) of unbound pavement layers [5, 55-57]. Differential frost heave causes pavement structures to deform differently at varying locations, resulting in pavement cracking [58-60]. On the other hand, thaw weakening occurs in early spring due to a rise in temperature and the melting of ice, leading to significant reductions in the shear strength and stiffness of the unbound pavement layers. Under this weakening effect, heavy loads applied on the pavement could easily damage the pavement [61, 62]. Such degradations accumulate and become worse under repeated freeze-thaw cycles. Various experimental studies have shown that the freeze-thaw cycle significantly lowers the mechanical integrity of the granular base and subgrade soil layers in a pavement structure [3, 63].

To mitigate such potential hazards associated with extreme climates, one efficient strategy is to add a thermal insulation layer above the frost-susceptible layer [49]. The studies related to the insulated pavement were initiated in the 1960s [64]. Since then, a large number of field tests showed that the insulation layer decreased the frost depth and mitigated frost heave. For example, in 1976, Penner [20] investigated the frost penetration depth in two field pavement sections (one with and one without insulated strips). His research showed that the insulation layer kept the temperature of the subgrade

layer relatively constant and reduced the frost depth. Esch [21] evaluated the long-term performance of insulated pavements for over 30 years, focusing on the frost heave deformation, permafrost thickness, and thaw depth. His results indicated that the use of an insulation layer reduced settlements to half of those of adjacent uninsulated road segments. Haghi [65] investigated the thermal and mechanical performance of three full-scale test roads, including one control section and two insulated sections. The field test results showed that the insulation layer decreased the frost depth by 0.5 m in comparison to the control section.

However, despite the apparent benefits of insulated pavements, research revealed that the insulation layer increased the temperature variation of the layers above the insulation layer [11, 20, 22]. In a freezing environment, the presence of the insulation layer accelerates the temperature decreasing in the layers above the insulation layer and causes surface icing. In a hot environment, the insulation layer increases the temperature of the surface layer and negatively influences the performance of the asphalt concrete. This is because the heat transfer process mainly occurs within the layers above the insulation layer. To mitigate these thermal effect, one efficient way is to increase the thickness of the base layers above the insulation layer [21, 49]. In 2006, to minimize the differential icing effect caused by the insulation layer, Côté and Konrad [48] tested the effectiveness of adding a granular protection layer and developed a design procedure. In summary, the negative influence on the surface layer temperature is one of the primary drawbacks of the insulation layer technique.

In recent years, there has been an increasing number of kinds of literature exploring the appropriate materials for the insulation layer. The most commonly used material for the insulation layer is the extruded polystyrene (XPS) board due to its excellent insulating effect and mechanical strength. XPS board is also currently the only material accepted by the U.S. Department of Defense for insulated pavement construction [66]. The efficiency of using XPS boards as an insulation layer was proved by a large number of field tests [10, 11, 20-22, 64]. Despite its satisfactory field performance, the XPS board suffers from several major drawbacks: (1) the XPS board is more expensive than the traditional construction materials; (2) the installation of the XPS board is labor-intensive; and (3) the insulating effect degrades due to the long-term moisture accumulation [67]. Therefore, researchers have started to explore alternative materials for constructing insulation layers. For example, Lee [12] and Kardos [68] used tire chips as the backfill materials in pavement construction. Their results proved the efficiency in utilizing shredded tires, particularly mixed with sand or cement, as reinforced soil structures. Shao [69] and Dore [24] investigated the potential of using the tire chips as the insulation layer in pavements and found that tire chips have relatively good insulating effect (with thermal conductivity ranging from 0.1 to 0.17 W/(m·K)) and mechanical strength (with resilient moduli ranging from 648 to 1482 kPa). Bottom ash is another material tested for insulated pavement construction and has shown satisfactory insulating performance in field experiments [13, 25, 65, 70-72]. More recently, lightweight foam-based materials, such as foamed glass aggregates (FGA) and foamed concrete, draw substantial attention in the construction industry due to their unique lightweight and

insulating features [17, 18, 73-77]. Typical applications include ground engineering, retaining wall, back filling [78], trench reinforcement [16], and pavement insulation [79, 80].

As summarized above, previous research efforts mainly focused on the positive insulating effect of the materials on the subgrade layer, whereas the negative influence of insulation materials on the overlying layers requires further analyses. Moreover, to the best of the authors' knowledge, the potential of using foamed glass aggregates (FGA) and foamed concrete as a possible insulation layer, has not been investigated. These facts highlight the necessity to compare the insulating effect of different materials and quantify their engineering performance under a similar test or simulation condition.

3.3 Study Goal and Objectives

The primary aim of this study is to evaluate and quantify the insulating performance of four materials (XPS boards, tire chips, FGA, and foamed concrete) as the insulation layer. Experiments compared the influence of different types of insulation layers on the pavement structure. A numerical model was developed for further quantitative analysis of the four materials. To achieve this goal, the following specific objectives were completed:

(1) Construct five large-scale pavement samples, one uninsulated sample as the control sample and four insulated samples with the four selected materials, to compare the influence of the insulation layer on the pavement under a similar condition.

(2) Establish a grading baseline with the consideration of different indicators under two environmental conditions.

(3) Develop a finite element method (FEM) model with the consideration of moisture phase change in the base and subgrade layer to quantify the performance of different materials.

3.4 Materials and Methodology

3.4.1 Description of the Large-Scale Boxes

To directly compare the efficiency of different insulating materials, five large-scale pavement boxes, including one uninsulated pavement box as the control sample and four insulated pavement boxes, were built. Figure 7 shows the schematic view of the pavement structure of the control box and insulated boxes. The width and length of all boxes are 122 cm, and the height of the control box is 74 cm, the height of the insulated boxes is 79 cm. Each pavement box contained an HMA layer as the surface layer, a recycled concrete aggregates layer as the base layer, and a clayey sand layer as the subgrade layer. The four insulated pavement boxes contained an additional insulation layer embedded between the base and subgrade layer. The four insulated boxes were insulated by the extruded polystyrene (XPS) boards, tire chips, foamed glass aggregates (FGA), and foamed concrete, respectively. To monitor the temperature distribution, all pavement boxes were instrumented with thermocouples along with the depth as shown in Figure 7. Besides, the sides and bottom of the pavement boxes were thermally insulated with XPS boards to ensure the vertical heat transfer process. These pavement boxes first experienced constant freezing for 200 hours and then moved outdoors for long-term

testing under the outdoor environment. To create a constant freezing environment, a frosted panel made by pipes and chillers was placed on the top of pavement boxes for over 200 hours. After the constant freezing, these pavement boxes were kept indoors for a month to restore the internal temperature to room temperature and then moved outdoors and tested for 280 days (Jan 16, 2020 ~ Oct 22, 2020). The pictures of the test setup under two test conditions were presented in Figure 8.

Figure 7

Schematic View of the Experimental Pavement Boxes: (a) Control Box; (b) Insulated Box

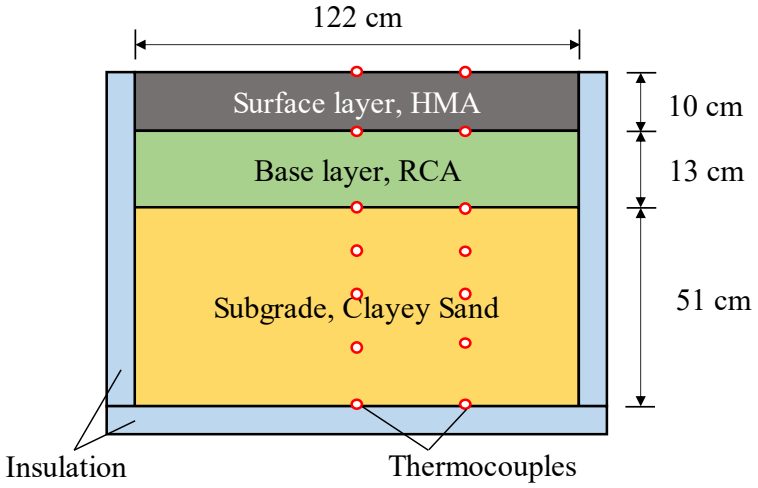

(a)

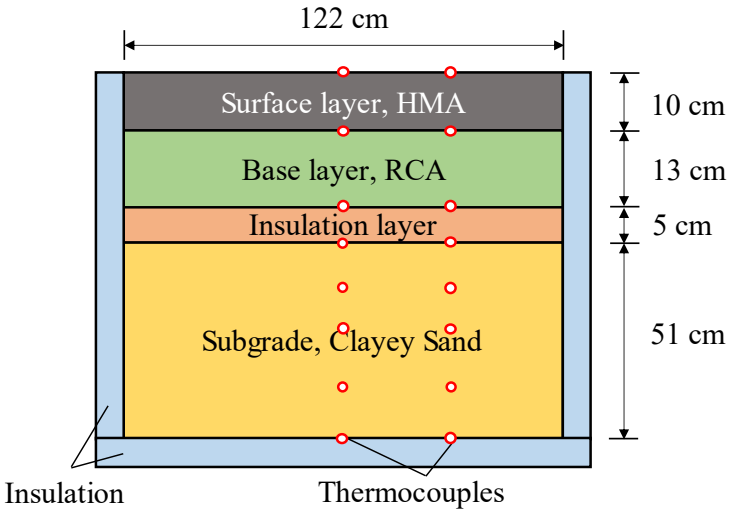

(b)

Figure 8

Test Setup of Pavement Sample under Two Conditions: (a) Constant Freezing; (b) Outdoor Environment (Datalogger Covered Under the Waterproof Wrap)

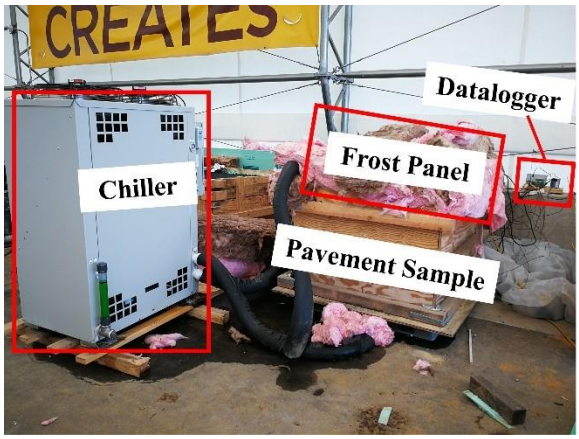

(a)

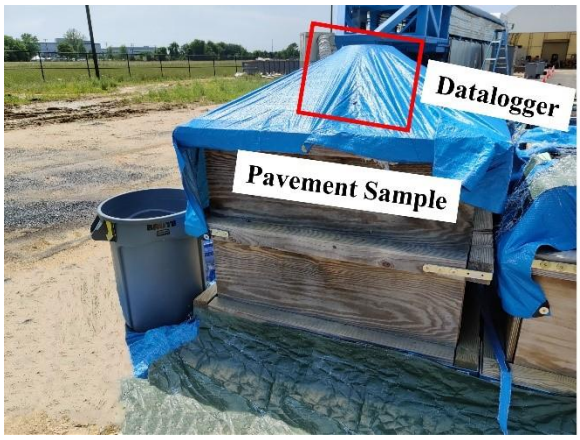

(b)

3.4.2 Materials

3.4.2.1 Hot Mix Asphalt (Surface Layer). The HMA mix used in this study was a dense-graded mixture with a nominal sieve size of 9.5 mm, obtained from a local plant in New Jersey. This mix met all New Jersey Department of Transportation (NJDOT) specifications for HMA. The mix was prepared at an optimum binder content of 5.8% (by total weight of mix) using the binder PG64-22. A hand tamper and an electrical vibratory compactor were used to control the thickness, compaction degree, and density of the HMA layer. The measured densities of the surface layer in all boxes are presented in Table 4.

3.4.2.2 Recycled Concrete Aggregates (Base Layer). Recycled concrete aggregates (RCA) are materials obtained by crushing old Portland cement concrete into aggregates of the desired size range. In New Jersey, this material is densely graded and frequently used in the base layers of flexible pavements. The RCA used in this study contains 56% gravel (size larger than 4.76 mm), 35% sand (size between 4.76 mm to

0.074 mm), and 9% fines (particle size smaller than 0.074 mm). The optimum moisture content of RCA was determined as 12.4% using the modified Proctor test (AASHTO T180). Similar to the HMA layer, the thickness, density, compaction degree, and moisture content of the base layers in all boxes were strictly controlled in a similar range. The measured densities and moisture contents of the base layer in all boxes were presented in Table 4.

3.4.2.3 Clayey Sand (Subgrade Layer). Frost-susceptible clayey sand from a local plant in New Jersey was used as the subgrade layer for the pavement boxes. This clayey sand contains 35.2% (by weight) fine materials (particle size smaller than 0.074 mm). The optimum moisture content of clayey sand was determined as 12.1%. The subgrade layer was constructed by four 12 cm thick sublayers to ensure the uniformity of the properties. The thickness, density, compaction degree, and moisture content of the subgrade layer in all boxes are similar. The measured densities and moisture content of the subgrade layer in all boxes were presented in Table 4.

Table 4

Measured Density and Moisture Content of Layers in The Pavement Boxes

Pavement Layer		Control	XPS	Tire Chips	FGA	Foamed Concrete
Surface (HMA)	Density(kg/m^3)	1885	1909	1900	1898	1905
	Water Content (%)	--	--	--	--	--

Pavement Layer		Control	XPS	Tire Chips	FGA	Foamed Concrete
Base (RCA)	Density(kg/m^3)	1927	2163	2187	2097	2007
	Water Content (%)	13.0	13.7	12.3	13.0	12.3
Subgrade (Clayey sand)	Density(kg/m^3)	1932	1967	1977	1957	1948
	Water Content (%)	11.0	10.2	11.5	11.0	10.5

3.4.2.4 Extruded Polystyrene (XPS) Boards (Insulation Layer). XPS boards have been extensively used as the thermal insulation layer in the insulated pavement. The density of the selected XPS boards is 50 kg/m^3, and their thermal conductivity is approximately 0.02-0.04 W/(m·K) [67].

3.4.2.5 Tire Chips (Insulation Layer). Tire chips are recycled materials that are widely used for tire-derived fuel, tire retreading applications, highway crash barriers, breakwaters, reefs, and crumb rubber asphalt pavement [12]. Its thermal conductivity has been determined to be approximately 0.25-0.6 W/(m·K) [24].

3.4.2.6 Foamed Glass Aggregates (FGA) (Insulation Layer). Foam glass aggregates are recycled lightweight fill materials, increasingly used in civil engineering and infrastructure applications. Due to high porosity, FGA is an ideal material for thermal insulation. The thermal conductivity of FGA is approximately 0.15- 0.25 W/(m·K) [80].

3.4.2.7 Foamed Concrete (Insulation Layer). Foamed concrete is manufactured by mixing a relatively large volume of air with cement paste through the use of a chemical foaming agent [73]. Due to the presence of air cellular, foamed concrete has

very good thermal insulating properties. The thermal and mechanical properties of foamed concrete are dominated by density. With a higher density, the mechanical strength of the foamed concrete is higher, but the thermal conductivity is lower [15]. In this study, the density of foamed concrete is 880 kg/m^3. The thermal conductivity of foamed concrete is approximately 0.1-0.66 W/(m·K) [16].

3.5 Description of the FEM Model

Although each layer's thickness and physical properties in all five boxes were strictly controlled in a similar range, the test condition of each box has an unavoidable difference due to the large size of the pavement sample. For example, the five pavement samples were cooled down one by one when testing under the constant freezing condition for 200 hours. This results in a different initial temperature distribution because the samples were not tested in the same season. Furthermore, the influence of the depth and thickness of the insulation layer was not investigated in the laboratory tests because all these insulated pavement boxes have the same layered structure. To bridge this gap, a 2D heat transfer finite element method (FEM) model with the consideration of the phase change process of the unbound layers (i.e., the base and subgrade layers) was developed.

3.5.1 Model Configuration

In this study, we developed a symmetric finite element model of asphalt pavement using the commercial finite element software COMSOL Multiphysics to predict the temperature responses of pavement structures. The developed FEM model was first set as the same structure as the large-scale pavement boxes; then, the FEM model was calibrated by adjusting the thermal properties (i.e., thermal conductivity and heat

capacity) until the predicted temperature distribution match the measured temperature distribution. After that, the calibrated model was used for parametric study by changing the thickness and depth of the insulation layer. With the parametric study, the equivalent thickness of different insulating materials that have similar insulating effects was calculated. The equivalent thickness was then used for a cost-effectiveness evaluation.

The symmetric 2D FE model was meshed by triangular elements, as shown in Figure 9. No heat exchange was allowed on the model's sides and bottom surface to ensure the developed model has the same test condition as the large-scale pavement box test.

Figure 9

Mesh And Boundary Conditions of the Developed FE Model

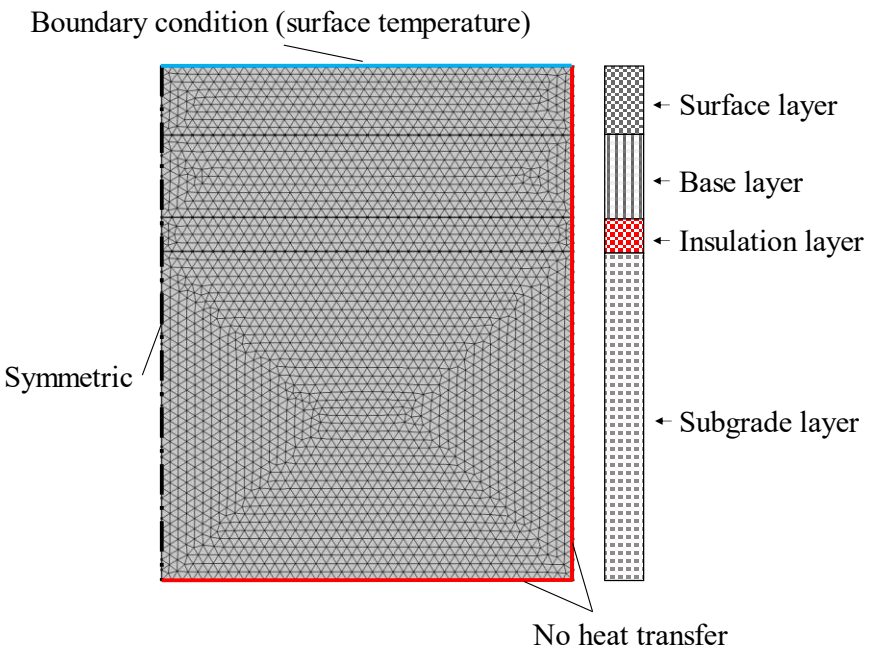

3.5.2 Governing Equations

For pavements in cold regions, the thermal field is usually the main cause of multi-physical processes. The phase change of the moisture plays a critical role in the heat transfer process when the temperature reaches the freezing point of water [81]. Phase change influences the heat transfer process in two ways: one is the different thermal properties between the unfrozen water and ice; the other is the latent heat generated when unfrozen water turns into ice. For instance, when unfrozen water freezes into ice, the thermal conductivity increases from 0.56 W/(m·K) to 2.18 W/(m·K). To precisely formulate energy transport in the pavement layers, a multi-layer finite element model was built based on the following assumptions:

(1) Phase change only happens in the base and subgrade layers. For the surface and insulation layer, the moisture content is close to zero.

(2) Moisture movement and associated heat convection are not considered in this model.

(3) The effects of the surface's albedo, the incoming solar radiation, the wind speed, and the air phase on temperature distribution are neglected.

A modified Fourier's equation with the conduction terms was adopted as shown in Equation (10):

$$(\rho C)_{eq}\frac{\partial T}{\partial t} + \nabla \cdot \left(-k_{eq}\nabla T\right) = Q \tag{10}$$

where $(\rho C)_{eq}$ is the equivalent product of the density (ρ) and heat capacity (C), T is the temperature, t is time, k_{eq} is the equivalent thermal conductivity, Q is the heat source.

Because the phase change and air phase in the surface and insulation layer are neglected, the equivalent terms in Equation (10) equals the properties of the solid mass as shown in Equation (11) and (12).

For the base and subgrade layer, the equivalent term is calculated by the volumetric content of solid mass (v_s) and water (v_w).

$$(\rho C)_{eq} = \begin{cases} \rho_s C_s & \text{Surface and insulation layers} \\ \rho_s C_s v_s + \rho_w C_w v_w & \text{Base and subgrade layers} \end{cases} \quad (11)$$

$$k_{eq} = \begin{cases} k_s & \text{Surface and insulation layers} \\ k_s v_s + k_w v_w & \text{Base and subgrade layers} \end{cases} \quad (12)$$

The density (ρ_w), heat capacity (C_w), and thermal conductivity (k_w) of water are calculated by Eq. (13) – (17):

$$\rho_w = \theta_i \rho_i + \theta_{uw} \rho_{uw} \quad (13)$$

$$C_w = \frac{1}{\rho_w}(\theta_i \rho_i C_i + \theta_{uw} \rho_{uw} C_{uw}) + L \frac{\partial \alpha_m}{\partial t} \quad (14)$$

$$\alpha_m = \frac{1}{2} \frac{\theta_{uw} \rho_{uw} - \theta_i \rho_i}{\theta_i \rho_i + \theta_{uw} \rho_{uw}} \quad (15)$$

$$k_w = \theta_i k_i + \theta_{uw} k_{uw} \quad (16)$$

$$\theta_i + \theta_{uw} = 1 \quad (17)$$

where the subscript *i* and *uw* denote ice and unfrozen water, respectively (e.g., θ_i = ice content and ρ_{uw} = the density of unfrozen water). L is the latent heat of water (334 kJ/kg), and α_m characterizes the phase transition between the ice and water.

3.5.3 Back-Calculated In-Situ Thermal Properties in the FEM Model

The developed FEM model was first calibrated by adjusting each layer's thermal properties until the predicted temperature distribution matches the measured temperature distribution. The FEM model was calibrated based on the measured temperature results under the constant freezing environment. An optimization algorithm was applied to ensure the back-calculated thermal properties were comparable with values obtained from related literature [82]. The back-calculated thermal properties (i.e., the thermal conductivity (k) and heat capacity (C)) of each box are shown in Table 5. The thermal conductivity values of the base and subgrade layer refer to the soil solids. For the surface, base, and subgrade layer, the different values were caused by the inherent inhomogeneity of the material and the inevitable construction difference. The comparison of the measured and predicted temperature is presented in Figure 10. The calibrated model is capable of predicting the temperature distribution accurately.

Table 5

Back-Calculated Thermal Properties in Each Layer

Thermal Properties	Control	XPS	Tire Chips	FGA	Foamed Concrete
$k_{surface}$ (W/m·K)	1.07	2.21	2.25	2.32	1.00
$C_{surface}$ (J/kg·K)	3736	2497	3578	3402	3963
k_{base} (W/m·K)	2.14	2.79	2.85	2.78	2.20
C_{base} (J/kg·K)	1065	1973	1213	1817	1838
$k_{Insulation}$ (W/m·K)	--	0.04	0.42	0.31	0.61
Typical range (W/m·K)	--	0.02-0.04 [67]	0.25-0.6 [24]	0.15-0.25 [80]	0.1-0.66 [16]
Thermal Properties	Control	XPS	Tire Chips	FGA	Foamed Concrete
$C_{Insulation}$ (J/kg·K)	--	1478	738	1254	1711
$k_{Subgrade}$ (W/m·K)	2.71	2.49	2.21	2.08	2.81
$C_{Subgrade}$ (J/kg·K)	2162	1520	2924	2710	2941

Figure 10

Comparison of the Measured and Predicted Temperature with the Calibrated Model

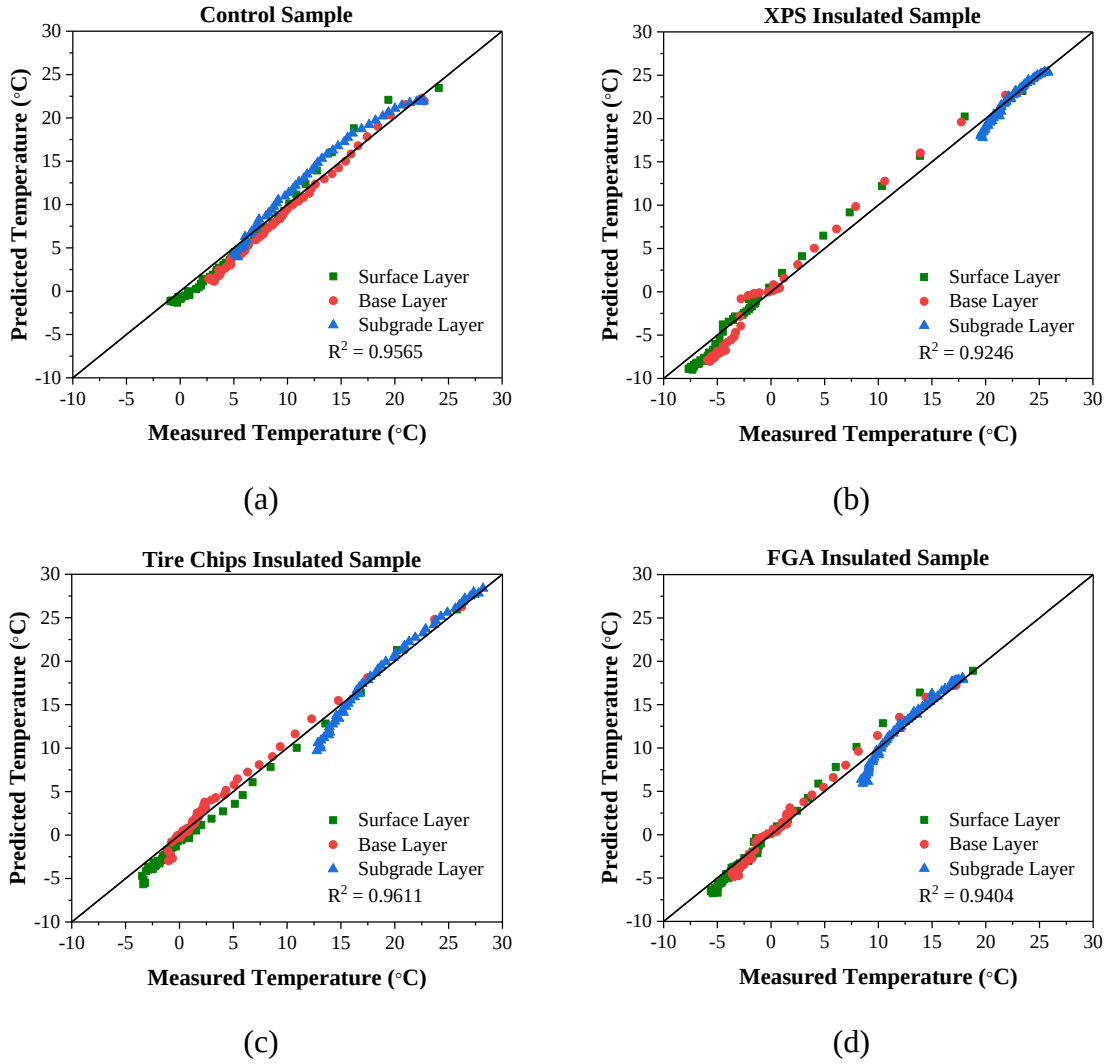

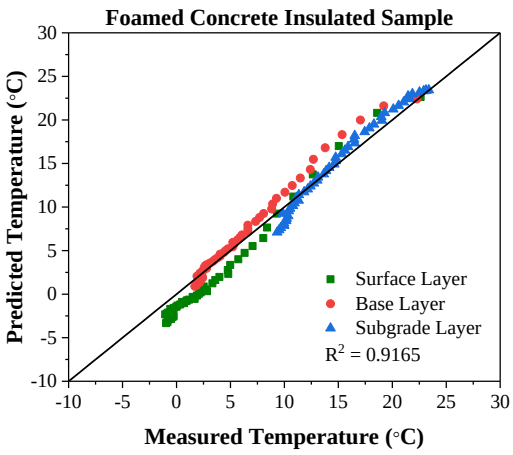

(e)

Figure 11 shows an example of the phase of water (left column) and temperature distribution changes (right column) with time-based on the FEM simulation results. The phase of water in the surface and insulation layer is empty because the moisture phase change in these layers is neglected. According to the temperature distribution changes, it can be seen that due to the presence of the insulation layer, the frost front was kept above the subgrade layer. At t = 50 h and t = 100 h, the phase of water in the base layer turned from unfrozen water to ice (grey color) when the temperature is lower than the freezing point of water (0 ℃).

Figure 11

An Example of the Phase of Water and Temperature Distribution Change with Time in the FEM Model

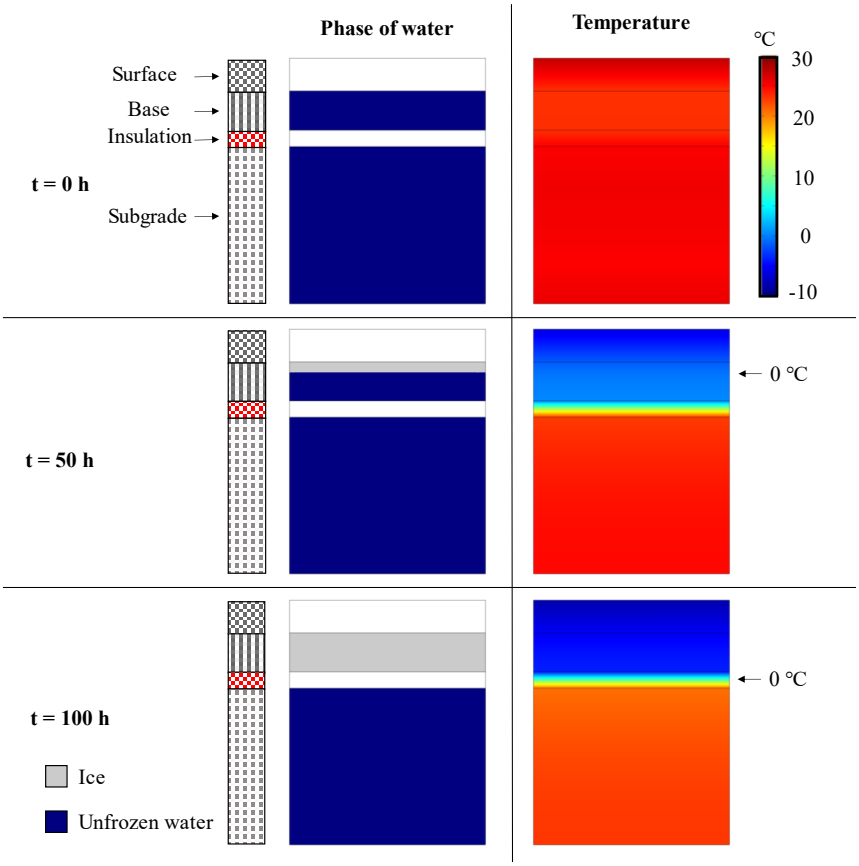

3.6 Results and Discussion

3.6.1 Temperature Distribution of the Pavement Boxes Under the Constant Freezing Environment

The temperature distributions under a constantly freezing environment of each box are shown in Figure 12. The bottom of the surface layer, the bottom of the base layer/top of the insulation layer, and the middle of the subgrade layer were selected as the

representative locations of the surface, base, and subgrade layer, respectively. The "Top of the surface layer" shown in Figure 12 indicates the temperature on the top surface of the pavement box (or input temperature). The temperature profiles were different over time for the five boxes. For the FGA and foamed concrete samples, the surface temperature reached the lowest near-constant temperature within a small period (around 50 hours), whereas it took around 100 hours for other samples. One possible reason is that these pavement boxes were tested during different seasons. The other reason is that the insulation layer accelerated the temperature decreasing process of the surface layer. According to the measurement, the presence of the insulation layer mitigated the temperature variation of the subgrade layer but accelerated the temperature decrease of the layers above the insulation layer. This result matches the findings from related studies [20]. During the 200-hour cooling period, the subgrade temperature of the control sample decreased the most (16.9 ℃), followed by the tire chips insulated sample (15.4 ℃), the foamed concrete insulated sample (13.8℃), the FGA insulated sample (9.3 ℃), and XPS insulated sample (5.8 ℃). In contrast, the surface temperature of the XPS sample decreased the most (30.8 ℃), followed by the tire chips insulated sample (29.1 ℃), the foamed concrete insulated sample (23.6 ℃), the control sample (24.4 ℃), and the FGA insulated sample (24.2 ℃). The temperature decrease was influenced by three factors, including the effect of the insulation layer, the boundary temperature input (temperature on top of the surface layer), and the initial temperature of the pavement boxes. Based on Figure 12, the temperature dropping rate decreased when the temperature is lower than 0 ℃. For this reason, the pavement box with a lower initial temperature, such as the FGA

insulated sample (starting at 18 ℃), had a lower temperature decrease in the surface layer compared with other samples (initial temperature: control 24 ℃, XPS 25 ℃, tire chips 28 ℃, and foamed concrete 23 ℃).

The "bottom of the surface layer" shown in Figure 12 is at the interface between the surface layer and the base layer. When the frost front reached the base layer (i.e., the "surface layer" curve shown in the figure reached 0 ℃), the moisture in the base layer started to freeze, resulting in a transition point as shown in Figure 12.

Figure 12

Temperature Changes of the Surface Layer, Base Layer, and Subgrade Layer in the Five Pavement Boxes Under the Constantly Freezing Environment

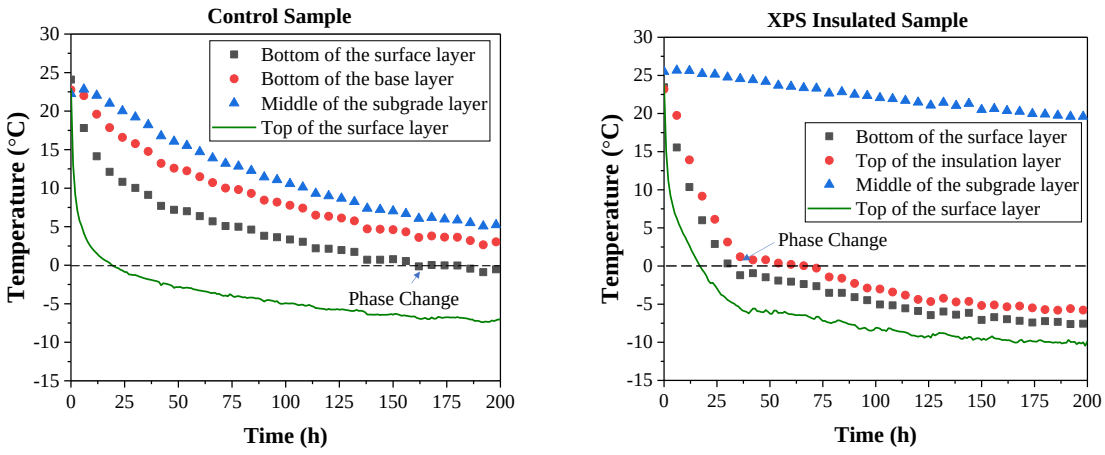

(a) (b)

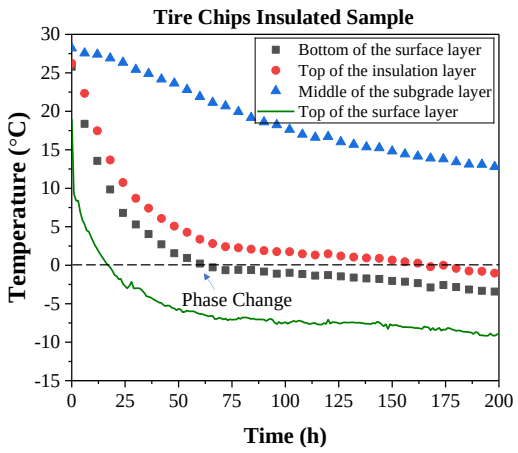

(c)

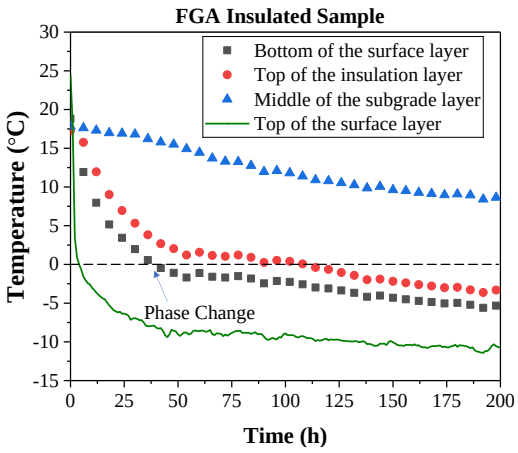

(d)

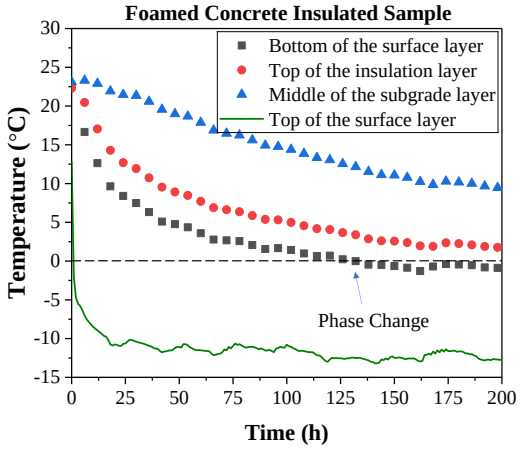

(e)

To compare the insulating effect of different materials, the temperature difference between the subgrade and surface layers was calculated and presented in Figure 13. As discussed in the previous section, the temperature difference between the surface and subgrade layers is influenced by both the insulating effects and the initial temperature distribution. For this reason, a higher temperature difference does not necessarily lead to a better insulating effect. This study shows that the temperature difference increased in

the first 35 hours and then became stable. The XPS insulated sample has the largest temperature difference at t = 200 h (27 ℃), followed by the tire chips sample (16 ℃), FGA sample (14 ℃), foamed concrete sample (10 ℃), and the control sample (6 ℃). The temperature difference was taken as one indicator for the insulating effect and will be further discussed in the next section.

Figure 13

The Temperature Difference Between the Subgrade Layer and Surface Layer in All Pavement Boxes Under a Constant Freezing Condition

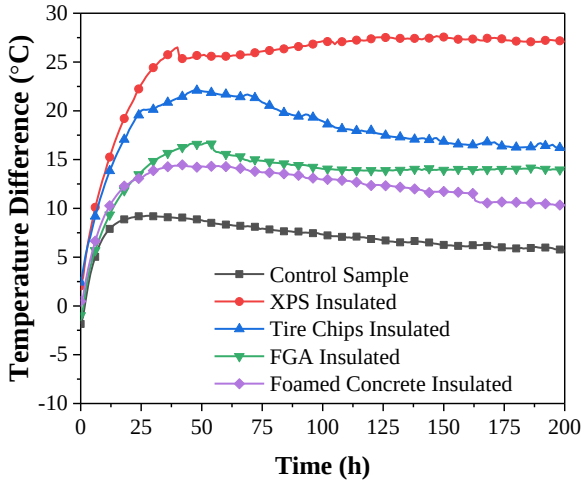

3.6.2 Temperature Distribution of the Pavement Boxes Under the Outdoor Environment

After the constant freezing test, these pavement boxes were kept indoor for a month to restore to ambient temperature and then moved outdoors. The five boxes were covered with waterproof cloth to avoid direct sunlight and rain. Figure 14 provided the

temperature distribution of the five pavement boxes under a 280-day outdoor thaw environment (from Jan 16, 2020, to Oct 22, 2020). As in the previous section, the temperatures of three locations (the bottom of the surface layer, the bottom of the base layer, and the middle of the subgrade layer) were selected as the representative locations of the surface, base, and subgrade layers. The air temperature during the test period is shown in Figure 14 (a). The discontinuity in the data from July 17, 2020, to July 22, 2020 was caused by an unexpected power shortage. To quantify the temperature variation during the test period, the standard deviation (shown as "σ" in Figure 14) of each curve was calculated. A higher temperature standard deviation means more variability during the test period. The temperatures of the surface, base, and subgrade layers in the conventional pavement (control sample) are similar. In contrast, in the insulated samples, the surface and base layer temperature significantly differ from the subgrade. We also calculated the maximum temperature difference between the surface layer and the subgrade layer of each sample as shown in Figure 15. The results show that the XPS insulated sample has the largest maximum temperature difference (9.19 ℃), followed by the FGA insulated sample (6.81 ℃), the tire chips insulated sample (5.77 ℃), the foamed concrete insulated sample (5.60 ℃), and the control sample (2.75 ℃). As discussed previously, a higher temperature difference does not necessarily mean a better insulating effect because the insulation layer has a positive effect on the subgrade layer and a negative effect on the surface and base layers. Compared with the temperature difference, the standard deviation of the subgrade layer is a more representative indicator of the insulating effect. According to the results, the XPS insulated sample has the lowest

temperature standard deviation (8.56 ℃) in the subgrade layer, followed by the FGA insulated sample (8.59 ℃), the foamed concrete sample (8.60 ℃), the tire chips insulated sample (8.63 ℃), and the control sample (8.97 ℃). As for the temperature variation in the surface layer, the XPS insulated sample has the largest standard deviation (9.82 ℃), followed by the tire chips insulated sample (9.36 ℃), the FGA insulated sample (9.35 ℃), the foamed concrete insulated sample (9.21 ℃), and the control sample (9.18 ℃).

Figure 14

Temperature Changes of the Surface Layer, Base Layer, and Subgrade Layer in the Five Pavement Boxes Under the Outdoor Environment Measured in 2020

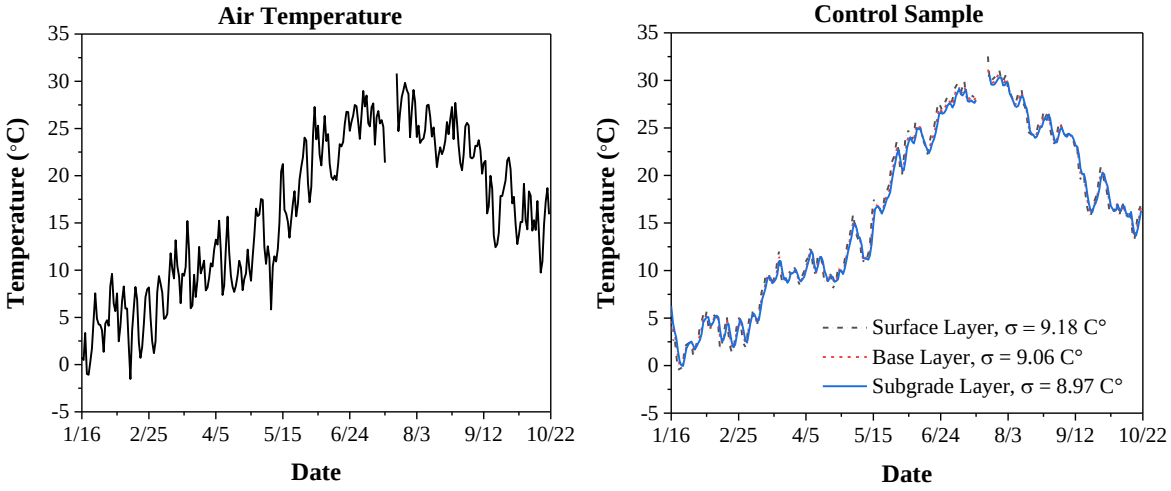

(a) (b)

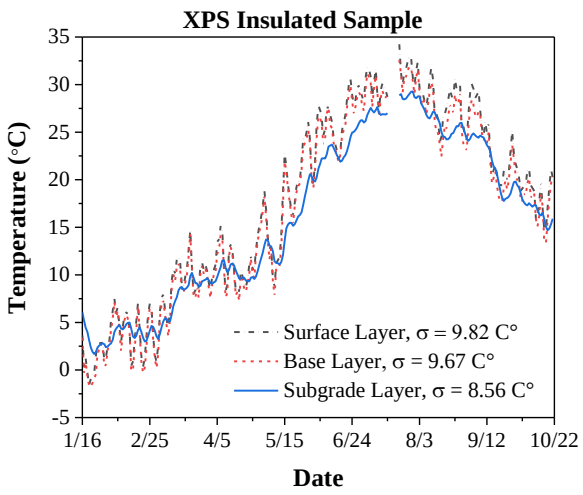
XPS Insulated Sample
Temperature (°C)
Date
Surface Layer, σ = 9.82 C°
Base Layer, σ = 9.67 C°
Subgrade Layer, σ = 8.56 C°
1/16
2/25
4/5
5/15
6/24
8/3
9/12
10/22

(c)

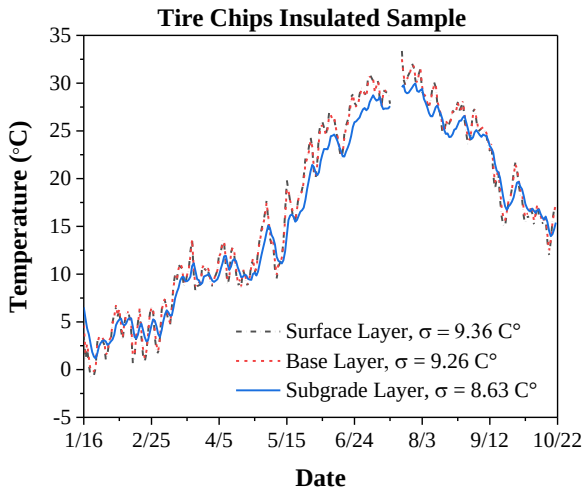
Tire Chips Insulated Sample
Temperature (°C)
Date
Surface Layer, σ = 9.36 C°
Base Layer, σ = 9.26 C°
Subgrade Layer, σ = 8.63 C°
1/16
2/25
4/5
5/15
6/24
8/3
9/12
10/22

(d)

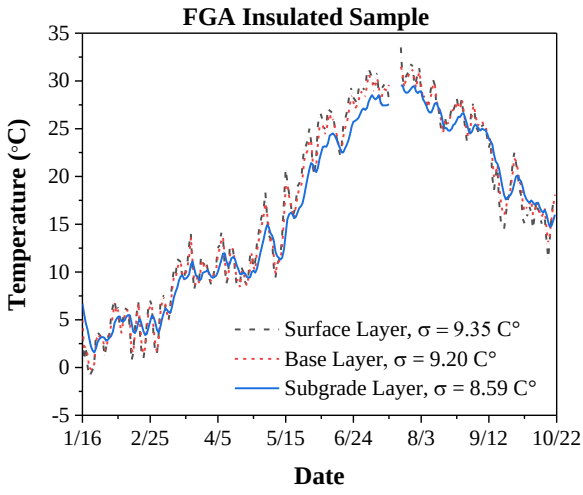
FGA Insulated Sample
Temperature (°C)
Date
Surface Layer, σ = 9.35 C°
Base Layer, σ = 9.20 C°
Subgrade Layer, σ = 8.59 C°
1/16
2/25
4/5
5/15
6/24
8/3
9/12
10/22

(e)

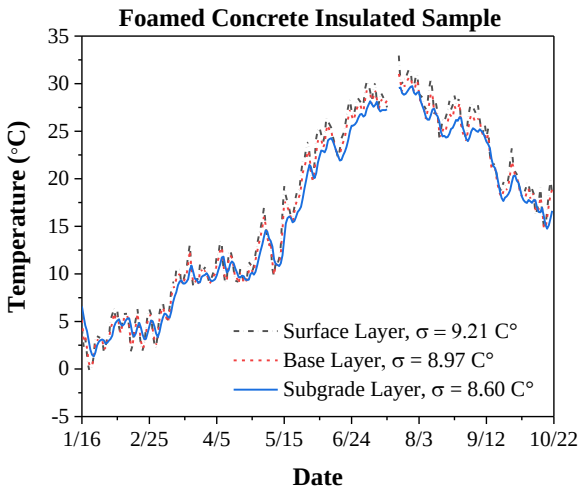
Foamed Concrete Insulated Sample
Temperature (°C)
Date
Surface Layer, σ = 9.21 C°
Base Layer, σ = 8.97 C°
Subgrade Layer, σ = 8.60 C°
1/16
2/25
4/5
5/15
6/24
8/3
9/12
10/22

(f)

Figure 15

The Temperature Difference Between the Subgrade Layer and Surface Layer in All Pavement Boxes Under an Outdoor Environment

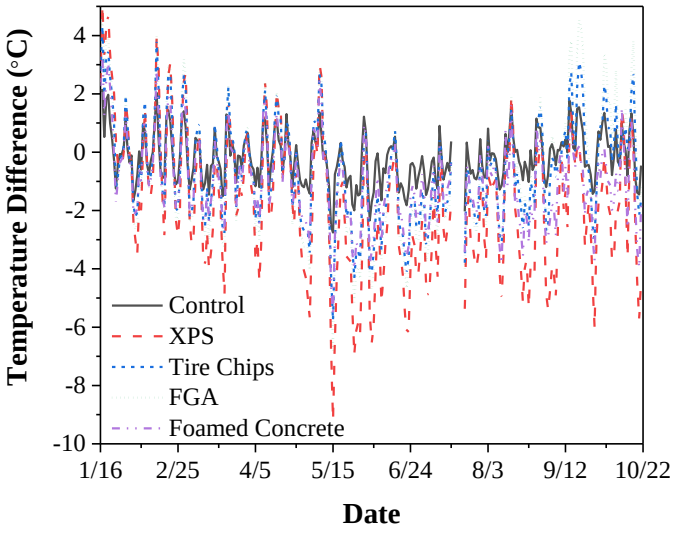

To quantify the performance of each pavement box, we summarized and graded each material based on the six evaluation indicators discussed above. The grading standards was listed in Table 6a, with a higher grade representing better performance (i.e., a lower temperature variation in the surface and subgrade layer). For example, the XPS insulated sample has a 5.8 ºC temperature decrease in the subgrade layer, so the grade is 20-5.8=14.2; whereas the XPS insulated sample has a 30.8 ºC temperature decrease in the surface layer, so the grade is 30-30.8=-0.8. The grades under the six indicators were shown in Table 6b. According to the grades, the XPS boards had the best insulating effect in the subgrade layer but also caused the most significant variation in the overlying surface layer. FGA has the second-best insulating effects in the subgrade layer. The XPS boards have the best overall performance, followed by FGA, foamed concrete,

and tire chips. The overall performance of all these insulated pavement boxes is better than the control box.

Table 6a

Grading Standard of Each Indicator

Environment	Indicators	Grading Standard			
		Value	Grade	Value	Grade
Constant freezing	Subgrade temperature decrease (20)	0 ºC	20	20 ºC	0
	Surface temperature decrease (10)	20 ºC	10	30 ºC	0
	Temperature difference (20)	0 ºC	20	30 ºC	0
Outdoor environment	Maximum temperature difference (20)	8 ºC	20	10 ºC	0
	Subgrade temperature variation (20)	9 ºC	10	10 ºC	0
	Surface temperature variation (10)	10 ºC	20	0 ºC	0

Table 6b

Grades of Each Material Under Different Indicators

Environment	Indicators	Control	XPS	Tire Chips	FGA	Foamed Concrete
Constant freezing	Subgrade temperature decrease (20)	4.7	14.2	5.6	10.5	6.2
	Surface temperature decrease (10)	5.6	-0.8	0.9	5.7	6.4
	Temperature difference (20)	4.9	18	10.7	9.3	6.9

Environment	Indicators	Control	XPS	Tire Chips	FGA	Foamed Concrete
Outdoor environment	Maximum temperature difference (20)	5.6	18.4	11.6	13.6	11.2
	Subgrade temperature variation (20)	10	14	14	14	14
	Surface temperature variation (10)	8	2	6	7	8
Summary (100)		38.8	65.8	48.8	60.1	52.7

3.7 Main Finding in This Chapter

In this study, five large-scale insulated pavement boxes were built, one without an insulation layer, and the other four insulated with different materials (XPS boards, tire chips, FGA, and foamed concrete). The temperature distributions inside the pavement boxes were collected under two different environmental conditions to compare the insulating effects. In addition, we also developed a FEM model with the consideration of moisture phase change to investigate the cost-effectiveness of different pavement types. The results obtained from this study led to the following conclusions:

(1) The presence of an insulation layer has both a positive effect on the layer underneath it and a negative effect on the layers above it. The temperature decrease of the subgrade layer in insulated boxes, depending on the materials, ranges from 5.8 ºC to 15.4 ºC, while in the control box, it is 16.9 ºC. In contrast, the temperature decrease of the surface layer in insulated boxes ranges from 24.2 ºC to 30.8 ºC, which is larger than that in the control box (24.4 ºC).

(2) Based on the measured temperature distribution, the XPS boards presented the best insulating effect on the subgrade layer (grades 14.2/20 and 14/20 in the subgrade layer), but also caused the most significant variation in the surface layer (grades -0.8/10 and 2/10). The FGA has the second-best insulating effect (10.5/20 and 14/20), and its influence on the surface layer is less than that of the XPS boards (5.7/10 and 7/10). The tire chips and foamed concrete have a similar insulating effect.

(3) Considering the positive effect on the subgrade layer and the negative effect on the surface layer, XPS boards have the best overall performance (65.8/100), followed by foamed glass aggregates (60.1/100), foamed concrete (52.7/100), tire chips (48.8/100), and the control box (38.8/100).

Chapter 4

Insulated Pavement Analysis Based on a Thermo-Hydro-Mechanical (THM) Coupled Finite Element Model

4.1 Abstract

Flexible pavements in cold regions are subjected to severe environmental conditions. Adding an insulating layer into a regular flexible pavement structure can reduce the frost penetration depth and mitigate uneven frost heave. This study used a thermo-hydro-mechanical coupled model to evaluate the pavement responses for pavements insulated with extruded polystyrene (XPS) boards. Model input parameters were calibrated with experimental and simulation data obtained from a large-scale insulated pavement box and Layered Elastic Analysis. Moreover, the potential application of the simulation results for the structure design of insulated pavement was demonstrated. Numerical simulation results validate that the presence of the insulation layer can efficiently reduce the frost penetration depth, whereas might induce loading capacity and drainage issues.

4.2 Introduction

Flexible pavements built in cold regions are more vulnerable than those in regular areas [54]. Unlike pavements in areas under temperate climates, the design and construction of pavements in cold regions must consider the effect of extreme freezing temperature on both interior moisture distribution and stress-strain relation [49]. Factors that cause damage in cold regions pavements can be categorized into 3 groups: differential pavement surface heave due to freezing effects [1], load capacity decrement caused by

spring thawing [54], and repetitive damage accumulation because of periodic freeze-thaw cycling [83]. Therefore, the study of flexible pavements in cold regions must consider the coupled effect of thermal, hydraulic, and mechanical fields.

To minimize the deterioration of flexible pavements in cold regions, adding an insulation layer inside the pavement structure has gained increased attention in recent years [48, 84]. The use of insulated pavements was investigated since the 1970s, with studies suggesting that an insulation layer has both beneficial and detrimental impacts on pavement structures. Substantial field tests were performed showing that an insulation layer could efficiently reduce the frost penetration depth and frost heave depth [22]. However, installing an insulation layer may cause two other problems. One is that, due to the mechanical weakness of insulating materials, the insulation layer could result in a weaker structure and thus experience more deflection under the same traffic load compared with regular pavement [20]. Moreover, prior studies [48] also revealed that the presence of the insulation layer could increase the cooling rate for layers above the insulation layer (i.e. differential icing effect). For these reasons, the design of insulated pavements needs to quantify both the positive and negative effects of the insulation layer on the whole pavement structure.

Several investigations have been conducted on the balanced design of the insulated pavements. To mitigate the differential icing effect caused by the insulation layer, a common strategy is to add a protection base layer with a certain thickness. Côté and Konrad [48] discussed the influence of the protection base layer thickness on the predicted frost penetration depth using a surface heat balance model. Doré and Zubeck

[49] introduced a design chart to determine the minimum thickness of the insulation layer based on the numerical model. However, the model used in these studies only considered thermal and mechanical responses, limited or no study investigated the pavement responses by a THM coupled model. To bridge this gap, this work aimed at proposing a THM coupled model to accurately quantify the pavement responses under extreme climate conditions. The calculated responses could be used to predict the mechanical performance (e.g. fatigue cracking and rutting depth) based on the experimental relation given by the Mechanical-Empirical Pavement Design Guide (MEPDG).

4.3 Numerical Modeling of Insulated Pavement

4.3.1 Model Configuration

A THM coupled numerical model was built in COMSOL Multiphysics to calculate the pavement responses such as temperature distribution, stress, and strain as well as pressure heads at critical locations. The axisymmetric model contained 13,152 four-node free tetrahedral solid elements (Figure 16a). The top surface was allowed to deform while all other boundaries were fixed. No heat transfer or moisture distribution was assigned on the four sides. 12-month of temperature and precipitation historic data was used as top boundary conditions. The temperature and precipitation for each month were set as the historical average data of Glassboro, New Jersey, acquired from the National Oceanic and Atmospheric Administration (NOAA). An 827 kPa (120 psi) tire pressure was applied on the top surface to mimic the tire load of an 18-kips single axle truck. The shape of this load is shown in Figure 16b, with the loading area calculated as [47]:

$$L = \sqrt{\frac{A}{0.5227}} \tag{18}$$

where A is the contact area, L is the length of the loading area.

Figure 16

Finite Element Model: (a) Geometry and mesh; (b) Loading Area

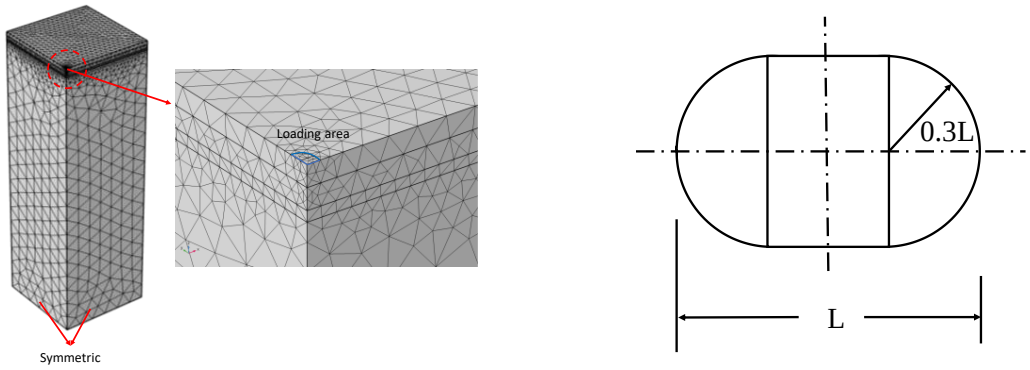

(a) (b)

4.3.2 Governing Equations

In this model, the Fourier-Biot equation was applied to account for heat transfer:

$$\rho C \frac{\partial T}{\partial t} + \nabla J_s = Q \tag{19}$$

where ρ is density, C is specific heat capacity (J/(kg·K)), T is the temperature (℃), and t is time (hours). J_s is heat flux, calculated as:

$$J_s = -\lambda \nabla T \tag{20}$$

where λ is thermal conductivity.

An unsaturated hydraulic constitutive relation was adopted in the model. The relation between the matric head and time is expressed by Richard's equation:

$$C(h)\frac{\partial h}{\partial t} - \frac{\partial}{\partial x}\left[K(h)\left(\frac{\partial h}{\partial x}\right)\right] = -\alpha_B \frac{\partial}{\partial t}\varepsilon_{vol} \tag{21}$$

where h is the matric head induced by capillary action, t is time, K is the hydraulic conductivity, $C(h)$ is a function describing the rate of change of saturation with respect to the matric head.

A viscoelastic constitutive model was used to calculate the mechanical responses of the HMA layer, and elastic models were used for the rest of the layers. Non-linear models will be considered in future studies for base and subgrade layers. The relaxation modulus of the asphalt mixtures was modeled as a generalized Maxwell solid model in terms of the Prony series:

$$E(t_r) = E_0\left(1 - \sum_{i=1}^{N} E_i\left(1 - e^{\frac{-t_r}{t_i}}\right)\right) \tag{22}$$

where E_0 is instantaneous elastic modulus, E_i and t_i are Prony series parameters, t_r is reduced time. The Prony series parameters were assigned with the values obtained from laboratory tests done by Katicha [85].

The thermal and mechanical processes were coupled through the temperature dependency of resilient modulus for the (Hot Mix Asphalt) HMA layer. The temperature dependency of asphalt concrete modulus is characterized by the time-temperature superposition principle. The relation between the time-temperature shift factor and temperature can be expressed by the Williams-Landell-Ferry (WLF) function:

$$\log a_T = -\frac{C_1(T - T_R)}{C_2 + (T - T_R)} \tag{23}$$

where T_R is reference temperature (in this study, 21.1℃), C_1 and C_2 are regression parameters. The values of C_1 and C_2 are assigned by the laboratory measured values provided in [86].

Moreover, the hydraulic field and mechanical field were also coupled to each other in the model. On one hand, the hydraulic head was influenced by the volumetric strain given by the mechanical field through equation (4). On the other hand, the mechanical field was also influenced by the hydraulic field with the equation below:

$$\begin{bmatrix}\sigma_{xx}\\ \sigma_{yy}\\ \sigma_{xy}\end{bmatrix} = \frac{E}{(1+\upsilon)(1-2\upsilon)}\begin{bmatrix}1-\upsilon & \upsilon & 0\\ \upsilon & 1-\upsilon & 0\\ 0 & 0 & 1-2\upsilon\end{bmatrix}\begin{bmatrix}\varepsilon_{xx}\\ \varepsilon_{yy}\\ \varepsilon_{xy}\end{bmatrix} - \begin{bmatrix}\alpha_B p & 0 & 0\\ 0 & \alpha_B p & 0\\ 0 & 0 & \alpha_B p\end{bmatrix} \tag{24}$$

where υ is Poisson's ratio and the term $\alpha_B p$ amounts to the fluid pressure that represents the fluid-to-structure coupling expression.

4.4 Full-Scale Experimental Test

4.4.1 Pavement Materials

4.4.1.1 Hot Mix Asphalt (HMA) Layer. The HMA mix used was a dense-graded mixture with a nominal sieve size of 9.5 mm, which satisfies the New Jersey Department of Transportation (NJDOT) specifications. The mix was prepared using an optimum binder content of 5.8% (by total weight of mix) and a binder grade of PG 64-22. The gradation curve of the aggregates is shown in Figure 17a.

4.4.1.2 Recycled Concrete Aggregates (RCA) Layer. RCA is a recycled material made through the crushing of old Portland cement concrete into the desired size range, commonly used as base layers for flexible pavements in New Jersey. The

constituents of RCA include 56% gravel materials (retained above Sieve No. 4), 35% sandy materials (passing Sieve No. 4), and 9% fines (passing sieve No. 200). The gradation curve of this material is shown in Figure 17a. The optimum moisture content to achieve maximum dry density for RCA was determined as 12.4% using the modified Proctor test (AASHTO T180) (Figure 17b).

4.4.1.3 Clayey Sand Layer. A frost susceptible clayey sand obtained from a local New Jersey contractor was used as the subgrade layer. 35.2% of this material (by weight) are fines (i.e., passing sieve No. 200, plasticity index = 8.23, medium-high frost susceptibility). The gradation curve of this material is shown in Figure 17a. As shown in Figure 17b, this subgrade material has an optimum moisture content of 12.1%.

Figure 17

(a) Gradation Curve of HMA, RCA and Subgrade Soil, and (b) Compaction Curves of RCA and Subgrade Soils Obtained from the Modified Proctor Test

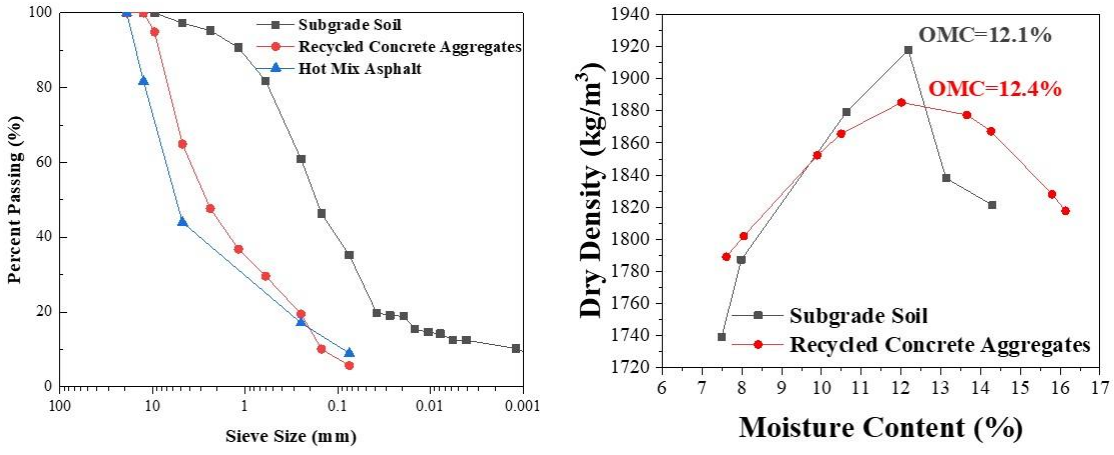

(a) (b)

4.4.1.4 Extruded Polystyrene (XPS) Board. 5.1 cm thick XPS boards were placed between the subgrade and base layers as an insulation layer. This material was selected because of its relatively good thermal insulating properties [67] and its extensive usage in practice [11, 20, 22]. However, the mechanical performance of the XPS board is weaker than regular construction materials such as RCA or clayey sand. The modulus of the XPS board used in this study is 2930 psi (20.2 MPa), while the compressive strength of the RCA ranges from 40-80 MPa.

4.4.2 Large-Scale Pavement Samples Fabrication and Freezing Plan

To compare the insulating performance of different materials under a consistent condition, two large-scale 1.21 m by 1.21m by 0.91 m deep pavement boxes shown in Figure 18 were constructed for one-dimensional heat transfer tests, one as a control sample without insulation layer and the other was insulated with extruded polystyrene (XPS) boards. The pavement boxes were thermally insulated on the sides and bottom with 2 in. XPS boards to ensure the heat exchange into and out of the pavement boxes mainly took place on the top surface. Then the pavement boxes were tested under a constantly freezing environment. The pavement boxes were placed under this constantly freezing environment for 200 hours. The control pavement box consisted of a hot mix asphalt (HMA) layer as the surface layer, a recycled concrete aggregates layer as the base layer, and a clayey sand layer as the subgrade layer. For insulated pavement boxes, an additional insulation layer was embedded between the base layer and the subgrade layer.

Figure 18

Schematic View of the Experimental Pavement Structures: (a) Control Sample (No Insulation Layer); (b) Insulated Sample

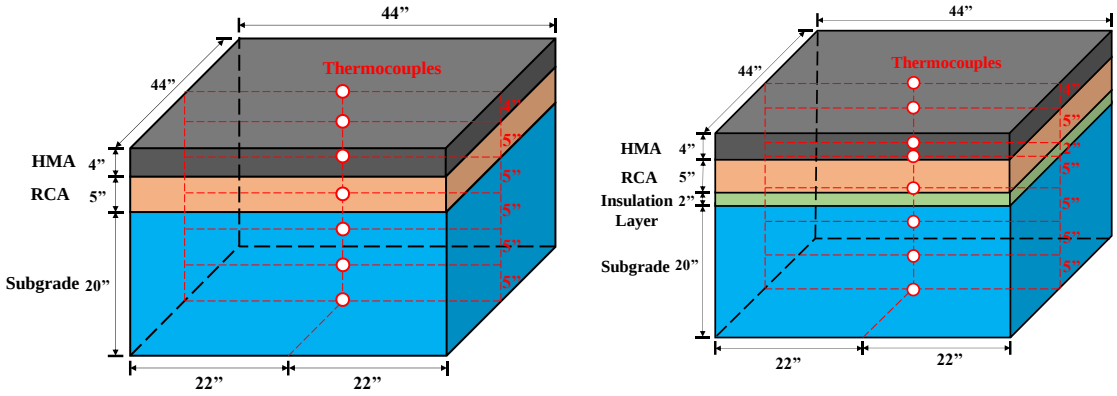

Several steps were taken when building the boxes to ensure the similarity of HMA, RCA, and subgrade material properties in two boxes. The density and moisture content of the subgrade layer and the base layer were controlled to reach the optimum compaction for both boxes. For the surface layer, the HMA mix was preheated to 175℃ to facilitate placement and compaction. Like the unbound layers, the weight of HMA materials was controlled by placing the same amount of materials to compact a 10.2 cm thick surface layer. Compaction of all layers was performed using a vibratory plate compactor. The density of all layers was determined using two non-nuclear gauges available commercially.

To apply a constant freezing condition to the sample surface, a freezing panel was utilized to cool down from the top of the HMA layer to mimic the low-temperature

environment in cold regions. The cooling system was built in-house using copper pipes and fittings and was connected to a chiller capable of lowering the temperature of the liquid inside the pipes to around -15℃. A number of thermal couples were installed to monitor the spatiotemporal distribution of temperature across the depth.

4.5 Results and Discussion

4.5.1 Model Validation

To validate the accuracy of the mechanical prediction results from the coupled model, the predicted mechanical responses were compared with analytical solutions given by the widely used layered elastic analysis software known as KENPAVE. The elastic constitutive analytical solution was compared with the numerical solution obtained from an elastic FEM (no thermal or viscoelastic behavior is modeled). In the validation model, the geometry of the first three layers (HMA, base, and insulation) are the same as the large-scale boxes. The thickness of the subgrade layer in the FEM model was assumed to be 2.54 m (100 in.) thick to mimic the simi-infinite assumption adopted in KENPAVE. After the configuration of equivalent pavement structures in the elastic FEM and KENPAVE models, the predicted vertical displacement, vertical stress, and horizontal strain were compared at the same depths. The comparison of the analytical solution and numerical solutions was presented in Figure 19. The high R-square values between the analytical solution and elastic constitutive numerical solution indicated that the proposed FE model could accurately predict the mechanical responses of pavement structures. This suggests that boundary conditions, the load applied, and the mesh generated in the FEM model are sufficient to reflect the experiments.

Figure 19

Comparison of the Numerical Results to (a-b) Experimental (Temperature) and (c) Theoretical Results (Displacement, Stress and Strain)

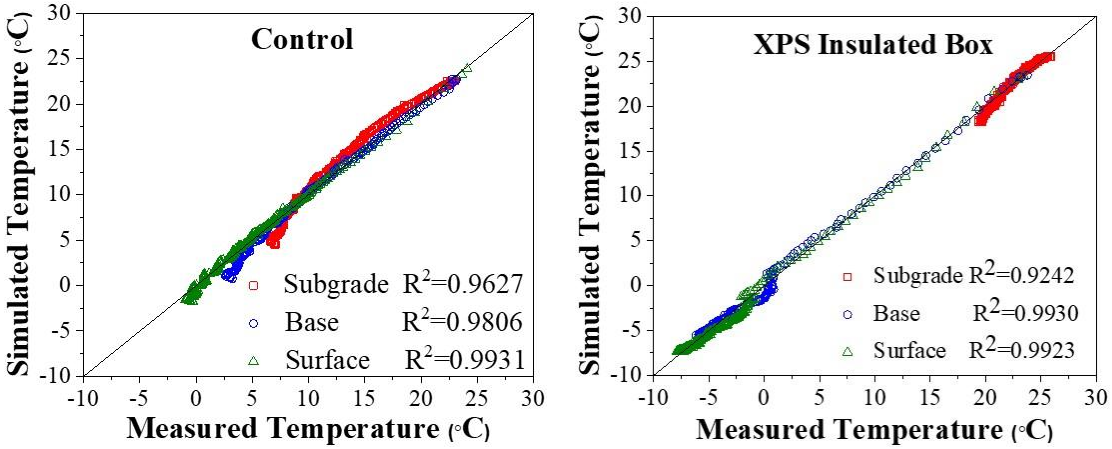

(a) (b)

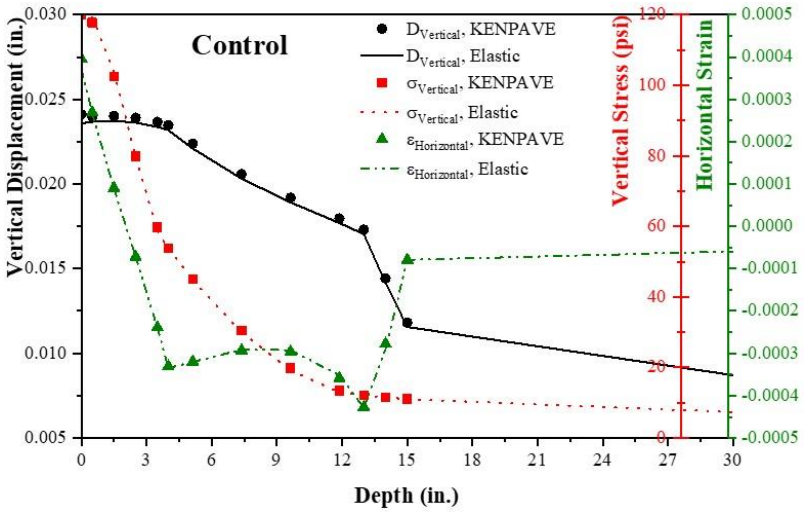

(c)

4.5.2 Finite Element Modeling Results

Figure 20 presented an example of the simulation results on the thermal (temperature), mechanical (vertical strain), and hydraulic (pressure head) fields.

Figure 20

THM Modeling Results for Regular and Insulated Pavement Structures

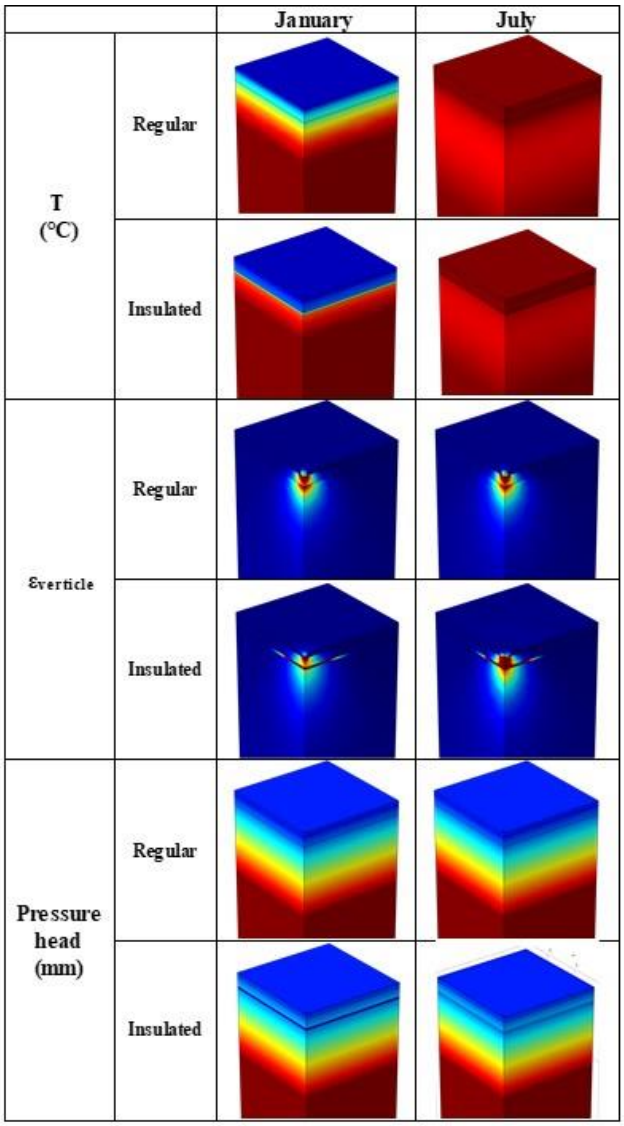

According to the comparison of the regular pavement and insulated pavement, the insulation layer can efficiently reduce the frost penetration depth. The temperatures below the insulation layer is all above 0 ℃ in January and December, while in the regular

pavement the subgrade layer (the fourth layer) has a frozen area. However, the temperature above the insulation layer for the insulated pavement is lower than that of regular pavement (i.e. differential icing), which agrees with the findings of related researches. As for the mechanical responses, the numerical model shows that for the regular pavement, the maximum vertical strain at the bottom of the base layer throughout the whole year is 1.4×10^{-4}, while for the insulated pavement, the maximum vertical strain at the same location is 4.4×10^{-4}. Besides, due to the low hydraulic conductivity of the XPS board, the insulation layer could also cause moisture accumulation. Based on the simulation results, the water pressure at the insulation layer was lower than the water pressure in the same location of regular pavement, which represents that the moisture transportation in this area was lower than in the regular case. This phenomenon might cause a drainage issue for the insulated pavement.

4.5.3 Potential Application of the Proposed THM Model in Insulated Pavement Design

The calculated thermal and mechanical responses by the proposed THM coupled model can be used in the design process of the insulated pavement. According to the MEPDG, the pavement design process includes selecting failure criteria and reliability levels, calculating the mechanical responses of the trial structure, evaluating the pavement performance based on the mechanical responses, and changing the trial structure if it does not meet the criteria. Once the failure criteria and trial structure are determined in the design process, the proposed THM coupled model in this study can calculate the mechanical and thermal responses of the trial structure. The pavement performance can

be predicted with the calculated vertical and tensile strain based on the equations given by MEPDG:

$$\Delta_{p(HMA)} = \beta_{1r} k_z \varepsilon_{r(HMA)} 10^{k_{1r}} N^{k_{2r}\beta_{2r}} T^{k_{3r}\beta_{3r}} \quad (25)$$

$$\Delta_{p(soil)} = h_{soil} \beta_{s1} k_1 \varepsilon_v \left(\frac{\varepsilon_0}{\varepsilon_r}\right) e^{-\left(\frac{\rho}{N}\right)^{\beta}} \quad (26)$$

$$N_{f-HMA} = k_{f1}(C)(C_H)\beta_{f1}(\varepsilon_t)^{k_{f2}\beta_{f2}}(E_{HMA})^{k_{f3}\beta_{f3}} \quad (27)$$

where *Δp(HMA)* is the accumulated permanent deformation in the HMA layer, *Δp(HMA)* is the accumulated permanent deformation in the unbound layer, $N_{f\text{-}HMA}$ is the allowable number of axle-load applications for a flexible pavement and HMA overlays. *N* is the load repetitions, ε_r is the resilient strain in the sublayers, *T* is the layer temperature, h is the thickness of each layer, ε_t is the tensile strain in the critical location, E_{HMA} is the modulus of the HMA layer. The rest of the parameters are experimental fitting values. In this study, these values adopted the global value recommended by MEPDG.

With the proposed numerical model, the optimal pavement structure can be calculated. For example, the trial pavement structure consists of three layers: 15 cm (6 in.) thick HMA layer, 13 cm (5 in.) thick base layer, and 10 cm (4 in.) thick of XPS insulation layer. For a local pavement in Glassboro, New Jersey, with the recommended criteria of 20% alligator cracking and 1.3 cm (0.5 in.) maximum rutting depth, the maximum load repetitions N this trial structure can withstand is 14,005,379. If the insulation thickness is reduced by 2.5 cm (1 in.), the allowable maximum load repetition increased to 16,311,448. This is because, with a thinner mechanically weak layer (insulation layer), the pavement can withstand more vehicle repetitions. Combined with

the historical and estimated traffic capacity, the optimum pavement structure can be determined based on the calculation above.

4.6 Main Findings in this Chapter

In this study, a design procedure for insulated pavements was proposed. A THM coupled finite element model was built to investigate the influence of insulation on pavement performance. Compared with the experimental test and analytical solution, the numerical model shows a relatively good agreement. Based on the numerical model and experimental test, the following conclusions were drawn:

The insulation layer can efficiently preserve the temperature of the underlayers, but it is also mechanically weak in pavement structures and might have the potential of causing the drainage problem.

The bottom of the HMA layer has the largest tensile strain, while the insulation layer has the largest vertical strain. Compare with the regular pavement structure, the insulated pavement induced 214% vertical strain at the bottom of the base layer.

The insulation layer could induce differential icing on the layers above the insulation layer. The design of insulated pavement should take this phenomenon into account.

Chapter 5

Investigation of Thermally and Mechanically Balanced Structural Design of Insulated Pavements for Cold Region Applications

5.1 Abstract

Adding an insulation layer above the frost-susceptible layer in regular pavement structures was proved to be an efficient way to mitigate the influence of climates such as frost heave and thaw weakening on pavements in cold regions. However, there is limited research in the area of insulated pavement performance evaluation and design procedures. To bridge the gap and design the structure of insulated pavements, we develop an approach that integrates the selection of the failure criteria, the generation of a trial structure, the evaluation of the thermal and mechanical responses based on a finite element (FE) model, and the prediction of the pavement rutting and cracking performance. To calibrate the heat transfer process and the thermal field of the FE model, four large-scale pavement boxes were constructed, with one as the control box (no insulation layer) and three others insulated by extruded polystyrene (XPS) boards, tire chips, and foamed concrete, respectively. The spatiotemporal variations of temperature distributions in each box using thermocouples were monitored, and the thermal properties of the insulation materials were back-calculated by a simulated annealing method. Based on the mechanical and thermal responses of various insulated pavements, we calculated the maximum axle load repetitions and developed a sample design table for insulated pavements. The design table indicates that the pavements insulated by XPS boards and foamed concrete can bear more load repetitions than uninsulated pavements, while the

tire chips insulated pavement can bear more traffic repetitions only when the overlay thickness is greater than 35 cm. The temperature of the subgrade layer in the insulated pavements is more stable than that in the uninsulated pavements, and a thicker insulation layer results in less temperature variation in the subgrade layer. This study provides new insights into the behavior of insulation layers under cold temperature conditions and helps guide the design of insulated pavements in cold regions.

5.2 Introduction

The design of pavements in cold regions is more complex than in temperate regions due to various factors that must be taken into consideration. For instance, pavements in cold regions are subjected to traditional mechanical loads (from traffic) [87, 88] and several other environmental conditions such as changes in moisture content (hydraulic effects), wide swings in temperatures (between hot and cold temperatures, thermal effects), and frost heave and spring thaw (thermal-hydraulic coupled effects) [50-52]. In addition, damage to pavements in cold regions accumulates with freeze-thaw cycles [3, 55, 89, 90]. Because of these environmental effects, compared to temperate regions, pavements in cold regions are more prone to distresses. Consequently, it is important to design a long-lasting pavement structure that is able to withstand excessive deformations and freeze-thaw cycling in cold regions by taking into consideration of mechanical and thermal effects.

To minimize the influence of frost penetration on pavements in cold regions, one of the most efficient strategies is to add a thermal insulation layer above the most frost-susceptible layer (usually the subgrade layer) [49]. Such an insulation layer is built with

materials with low thermal conductivities (ranging from 0.01 to 0.1 W/(m·K); [67]). This layer impedes frost penetration from upper pavement layers and reduces heat dissipation from the supporting layer; thus, protecting the frost-susceptible layer from wide changes in temperatures [11, 84]. The efficiency of an insulation layer is determined by its ability to minimize changes in temperatures within a frost-susceptible layer.

Extensive research on the use of insulated pavements was conducted by various researchers, dating back to the late 1970s. For instance, Penner [20] compared the temperature distribution for two test strips (one uninsulated control strip and one insulated with extruded polystyrene, XPS, boards) within a field pavement section. At the same depths (layer below insulation) within these pavement strips, Penner [20] reported that temperatures in the insulated pavement strip were 3 to 4°C higher than those in the uninsulated section. Other researchers (Gandahl [11], Esch [91], Kestler and Berg [22]) reported similar findings to those of Penner. Penner [20] also concluded that the use of insulation pavement layers could potentially reduce differential frost heave and minimize temperature variations in frost-susceptible layers.

Several investigations have been conducted on the design of insulated pavements. Côté and Konrad [48] developed design charts to determine the minimum thickness of the granular protection layer in the insulated pavement. This has been applied to control the occurrence of differential icing on the pavement surface. Doré and Zubeck [49] introduced design charts for determining the minimum thickness of the insulation layer based on simulation results. However, these design charts are only valid for pavement, including 150 mm of HMA over 450 mm of the granular base material.

Despite the apparent benefits of insulated pavements, the use of an insulation layer introduces a new set of concerns and challenges that must be addressed to ensure construction of long-lasting, well-performing pavements. One concern with the use of insulated pavement layers is the mechanical weakening of the overall pavement structure. This is originated from the use of weaker materials (insulation materials) when compared to traditional pavement materials (e.g., dense-graded base aggregates) [71]. To elaborate, consider the use of XPS boards as an example, which has a compressive modulus ranging from 6.9 to 27.6 MPa (Yoshihara et al.[92]), which is considerably softer than typical paving materials (more than 69 MPa). More recent research focused on the evaluation of alternative insulating materials such as tire chips [12, 24], bottom ash [13, 25], foamed glass aggregates [17, 18, 79, 80], and foamed concrete [73, 76]. However, these materials are still mechanically weaker than traditional paving materials and they pose similar design challenges.

Another concern with the use of insulation layers in pavement structure is the accelerated cooling of the layers (e.g., hot mix asphalt, HMA, and aggregate base) above the insulation layer, resulting in a lower temperature that is 2-5 ℃ below normal ranges [20]. Several field studies [20, 23, 48] reported that the presence of an insulation layer increases the cooling rate in the layers above the insulation layer due to the absence of latent heat release. With the same heat dissipation, energy extraction in insulated pavement structures is mostly from layers above the insulation layer. In conventional pavements, energy extraction occurs from the whole pavement system (all layers). For these reasons, it is important to balance the mechanical and thermal benefits and

challenges posed using insulating layers when designing insulated pavement structures. This in turn warrants a thorough understanding of thermal, hydraulic, and mechanical impacts on pavement structures.

To understand temperature variations within a pavement structure and consequently the thermal and hydraulic impacts on pavements, a number of heat transfer models have been developed. These models can be divided into three categories, namely, analytical, numerical, and empirical models [93]. One sample model was proposed by Lukannen et al. [94]. This regression model was developed using data from the long-term pavement performance (LTPP) database for 41 roadways in North America. However, this model is based on uninsulated pavements and may not be applicable for insulated pavement. This model is also limited to HMA layers with thicknesses ranging from 46 to 305 mm and surface temperature ranging from 0 to 40℃.

As for finite difference approximation (FDA) and finite element method (FEM) numerical models, Dempsey [43] proposed a one-dimensional, forward-FDA model to evaluate temperature-related effects in a multilayered pavement system. In 1991, Braley and Zarling [95] developed a similar FDA model using implicit finite difference techniques. Hermansson [96-98] proposed a mathematical model for the calculation of pavement temperatures, in which the temperature of pavements is influenced by radiation, convection, and heat transfer. More recently, Côté and Konrad [48] incorporated the heat conduction approach proposed by Braley and Zarling [95] into the surface heat balance model to predict temperature distributions within insulated pavement structures. Chen et al. [99] presented an analytical approach to predict temperature field in asphalt pavement

for urban heat island (UHI) effect. These models were reported as accurate at predicting the temperature distribution within a pavement structure in cold regions, validating the reliability of using such numerical models for insulated pavement design.

In summary, extensive research was conducted to quantify the benefits of insulated pavement structures and gain a better understanding of temperature distribution within these pavements. However, limited research exists on the structural design of insulated pavements, especially research that takes into consideration the challenges pavement insulation layers present. It is evident from the previously presented studies that the use of insulation layers offers several benefits and poses challenges, such as subjecting HMA and other pavement layers to faster cooling rates (or colder temperatures). Insulated pavements are also mechanically weaker than typical pavement layers. As a result, a structural design approach that optimizes and balances the thermal and mechanical performances of insulated pavements is needed. The study presented in this paper bridges this gap by introducing an approach account for both thermal and mechanical effects.

5.3 Study Goal and Objectives

The goal of this study is to present a thermally and mechanically balanced design approach to determine the adequate thickness of the pavement insulation layer. The developed approach balances the mechanical performance and thermal effects in insulated pavements. An optimal design that offers the best insulation effects without significantly compromising mechanical performance is presented. To achieve this goal, the following specific objectives were completed:

- Construct large-scale samples of insulated and uninsulated pavement structures. The aim of building these samples was to calibrate the heat transfer process and the thermal field of the FE model. These samples were used to measure the actual temperature distribution within the control (uninsulated) and insulated pavement structures. Different insulating materials were used in these sample boxes.
- Develop a finite element model (FEM), taking the temperature dependency of materials into consideration. The model will be used to estimate the temperature distribution and mechanistic responses within insulated and uninsulated pavement structures.
- Predict pavement performance using FEM estimated thermal and mechanistic responses and identify proper/design thickness of insulation layer.
- Develop design charts/tables to easily estimate the minimum adequate insulation layer thickness that balances load-carrying capacity and heat-transfer requirements.

5.4 Experimental Test Program

Four large-scale (1.2m long by 1.2m wide by 0.9m deep) pavement box samples were constructed to provide temperature data under controlled cold conditions aiming to calibrate the proposed finite element model. One of these samples was not thermally insulated (control, as shown in Figure 21(a)), and the other three were insulated with extruded polystyrene (XPS) boards, tire chips, and foamed concrete, respectively (as shown in Figure 21(b)). The control sample consisted of an HMA surface layer, a dense-graded (Recycled Concrete Aggregates, RCA) base layer, and a natural (frost-susceptible)

subgrade soil layer. The insulated sample boxes used the same materials as the control sample for surface, base, and subgrade layers. In addition, a 5 cm thick insulation layer was placed between the subgrade and base layers. The following subsections present a discussion of the materials used to construct control and insulated samples.

Figure 21

(a) Schematic View of the Control Sample (No Insulation Layer); (b) Schematic View of an Insulated Sample; (c) Experiment Setup

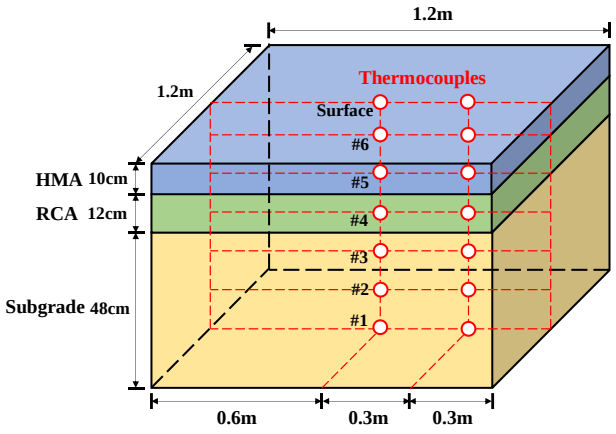

(a)

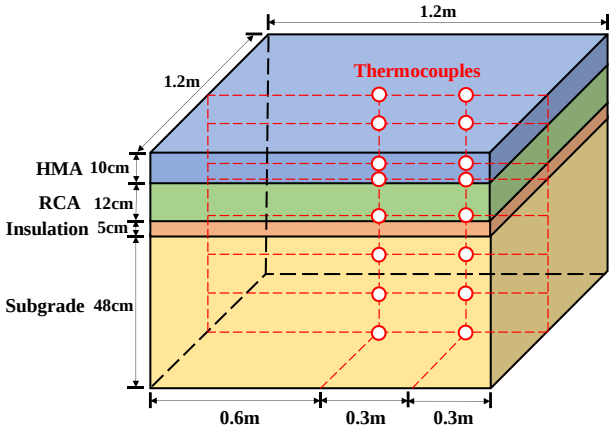

(b)

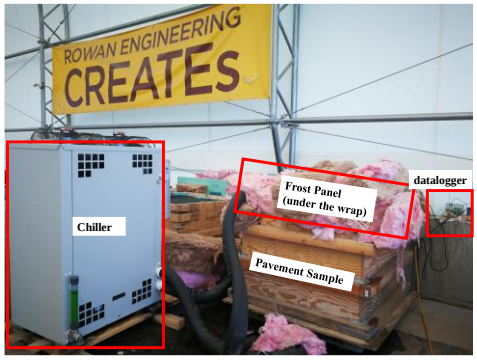

(c)

5.4.1 Description of Pavement Materials

5.4.1.1 Hot Mix Asphalt (HMA) Materials for Surface Layer. The HMA mix used in this study was a dense-graded mixture with a nominal maximum sieve size of 9.5 mm, which satisfies the New Jersey Department of Transportation (NJDOT) specifications. The mix was prepared using an optimum binder content of 5.8% (by total weight of mix) and a binder grade of PG 64-22.

5.4.1.2 Recycled Concrete Aggregates (RCA) for Base Layer. RCA is a recycled material made through the crushing of old Portland cement concrete into the desired size range. This material is commonly used as base layers for flexible pavements in New Jersey as it is typically crushed to have a well-graded, dense gradation. The constituents of RCA used in our study include 56% coarse materials (retained on Sieve No. 4), 35% sandy materials (passing Sieve No. 4), and 9% fines (passing sieve No. 200). The optimum moisture content to achieve maximum dry density for RCA was determined as 12.4% using the modified Proctor test (AASHTO T180).

5.4.1.3 Clayey Sand for Frost Susceptible Subgrade Layer. A frost susceptible clayey sand from a local New Jersey contractor was used as the subgrade layer for the pavement boxes. This material contains 35.2% (by weight) fine materials that pass sieve No. 200 (i.e., < 75μm). Similar to RCA, a modified Proctor test (AASHTO T180) was conducted to determine the clayey sand's optimum moisture content. The subgrade material (clayey sand) had a Proctor test optimum moisture content of 12.1%. According to the Unified Soil Classification System (USCS), the soil can be classified as clay of low plasticity (CL).

5.4.1.4 Extruded Polystyrene (XPS) Boards for the Insulation Layer. XPS boards (5cm thick) were placed between the subgrade and base layers as an insulation layer in one of the insulated large sample boxes. This material was selected because of its relatively good mechanical and thermal insulating properties [67] and its extensive usage in practice [11, 20, 22, 24]. The density of the selected XPS boards is 50 kg/m^3, and their thermal conductivity is approximately 0.025~0.1 W/(m·K).

5.4.1.5 Tire Chips for the Insulation Layer. Another type of insulating material used is tire chips, which were also placed as a 5cm-thick layer between the base and subgrade layers. Tire chips are recycled materials widely used for tire-derived fuel, tire retreading applications, highway crash barriers, breakwaters, reefs, and crumb rubber asphalt pavements [12]. Several prior studies were performed to investigate the potential of using tire chips as an alternative insulation layer due to their low thermal conductivity (approximately 0.1~0.6 W/(m·K)) [24, 100].

5.4.1.6 Foamed Concrete for the Insulation Layer. In addition to XPS boards and tire chips, a 5cm thick cellular material named foamed concrete was used as an insulating material. Foamed concrete is manufactured by mixing a relatively large volume of air with cement paste through the use of a chemical foaming agent [73]. Due to the presence of air cellular, foamed concrete has excellent thermal insulating properties. The thermal conductivity of foamed concrete ranges from 0.1 to 0.66 W/(m·K), influenced by the proportion of chemical foam and cement paste.

5.4.2 Procedure for Preparing Large Box Samples

To ensure consistency between the control (uninsulated) and insulated pavement boxes, several steps were taken when building these boxes. For instance, the weight and moisture content of materials placed for each of the layers were controlled to achieve the desired thickness. The pavement structures were constructed from the bottom up inside the thermally insulated (XPS boards placed on sides and bottom) wooden box. During the preparation of the subgrade and base materials, soil materials were dried then mixed with water outside the box before filling into the pavement box to ensure a similar moisture content for each lift. As a result, the construction of the pavement structure started by placing four 12cm lifts of the subgrade to achieve a total thickness of 48cm (Figure 21). The amount of water to add was calculated based on the target moisture content. Water was then mixed with the dried materials in a concrete mixer to meet the optimal moisture content. The weight of materials used for each lift was the same to ensure consistency. This process was also used to produce the RCA base layer (12cm thickness).

For the surface layer, the HMA mix was preheated to 175℃ to facilitate placement and compaction. Like the unbound layers, the weight of HMA materials was controlled by placing the same amount of materials to compact a 10cm thick surface layer. Compaction of all layers was performed using a vibratory plate compactor. The density of all layers was determined using two non-nuclear gauges available commercially. In addition, thermocouples were installed at the bottom of each lift from the bottom of the sample to the top surface. Each lift has two thermocouples, one at the midpoint and the other at the quarter-point. These thermocouples were connected to a data acquisition system for the continuous recording of temperature (rate of recording: 1 point every 5 minutes).

Table 7 presents the measured density and moisture content of each of the layers in the control and insulated pavement boxes. The density and moisture content of the unbound layers were determined by a nuclear gauge, and the density of the HMA layer was determined by an electromagnetic density indicator. Besides, the density was also determined by the quotient of the weight and filled volume for each lift. The moisture content readings from the nuclear gauge were calibrated with laboratory tests as well. As can be seen from this table, the densities are similar (i.e., within acceptable variability for such large boxes and materials), implying that pavement boxes were prepared in a consistent way. Therefore, for all practical reasons, the three boxes were considered similar, with the only difference being the placement of different insulation materials. A freezing panel was utilized to cool down the top of the HMA layer to mimic the low-temperature environment in cold regions. The cooling system was built in-house using

copper pipes and fittings and was connected to a chiller capable of lowering the temperature of the liquid inside the pipes to around -15℃. Insulation wrap was also placed on top of the freezing panel to ensure efficient pavement cooling. A number of thermal couples (14 for the control sample and 16 for the insulated samples) were installed to monitor the spatiotemporal distribution of temperature across the depth. For the control and insulated boxes, two weeks were set as the cooling period to ensure that the subgrade temperature reaches sub-freezing conditions. In this study, the chosen time period was sufficient to cool down the control box (top of subgrade) to subzero temperatures (i.e., less than 0℃).

Table 7

Measured Density and Moisture Content of Pavement Layers in Control and Insulated Pavement Large Box Samples

Pavement Layer		Control	XPS	Tire Chips	Foamed Concrete
Surface (HMA)	Density (kg/m^3)	1899	1923	1912	1918
Base (RCA)	Density (kg/m^3)	1940	2177	2201	2020
	Moisture Content (%)	12.96	13.66	12.34	12.31
Subgrade (Clayey Sand)	Density (kg/m^3)	1945	1981	1990	1961
	Moisture Content (%)	10.96	10.23	11.52	10.52

5.5 Numerical Modeling of Insulated Pavement

5.5.1 Description of the Finite Element Model

The performance of the trial pavement structure in the proposed design procedure is evaluated based on a proposed finite element model. A symmetric FE model of asphalt pavement was developed using the commercial finite element software COMSOL Multiphysics to predict the temperature and mechanical responses of pavement structures. The geometry of this model changes with different trial structures. The FE model was meshed by four-node free tetrahedral solid elements, as shown in Figure 22(a). The mechanical boundary conditions for the model included assigning its four sides to only move in the vertical direction (vertical displacement) while the bottom face was fixed with no movement allowed. Layers were fully bonded at the interface. No heat exchange was allowed on the model's sides and the bottom surface to ensure that a one-dimensional heat transfer process is simulated. An 827 kPa static load was applied on the top surface of the model to mimic the tire load of an 18-kips single axle truck. The load was applied on a designated area, including a rectangle and two semi-circles, as shown in Figure 22(b). Equation 28 was used to calculate the contact area [47, 101]:

$$L = \sqrt{\frac{A_c}{0.5227}} \tag{28}$$

where A_c is the contact area. L is the length of the loading area.

In addition, a 12-month temperature cyclic was applied on the top surface of the coupled model to simulate climate change throughout a whole year. The temperature for

each month was set as the historic average temperature of Glassboro, New Jersey acquired from the National Oceanic and Atmospheric Administration (NOAA).

Figure 22

FE Model Layout: (a) Mesh and Boundary Conditions (b) Loading Area

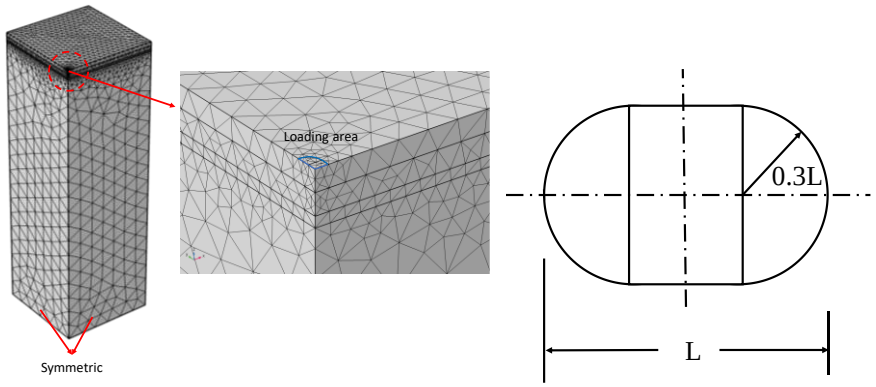

(a) (b)

5.5.1.1 Thermal Field. The thermal field is the main cause of multiphysical processes in insulated pavements. The heat transfer process could influence pavement performance by inducing thermal stress and changing the properties of the material in each layer. The Fourier-Biot equation was used in this study as the governing equation of the heat transfer process:

$$\rho C \frac{\partial T}{\partial t} + \nabla J_s = Q \tag{29}$$

where ρ is density (kg/m^3), C is specific heat capacity (J/(kg·K)), T is the temperature (°C), t is time (hours), J_s is heat flux (W/m^2), Q is heat source (J).

The heat flux can be calculated by Equation 30:

$$J_s = -\lambda \nabla T \tag{30}$$

where λ is thermal conductivity (W/(m·K)).

For insulated pavement structures, when the temperature reaches subzero, the moisture inside the subgrade soil will be frozen (phase change), and the thermal properties such as the thermal conductivity and specific heat capacity will change due to the difference of liquid water and solid water [102, 103]. To characterize the influence of the phase change process, a simplified temperature-dependent thermal conductivity was considered in the heat conduction model while other material properties were kept constant for each layer. Based on the laboratory test of the thermal conductivity changes with temperature [102-104], a temperature-dependent thermal conductivity expression was used in the heat conduction model:

$$\lambda = P_1 T^2 + P_2 T + P_3 \tag{31}$$

where T is the temperature (℃), P_1, P_2 and P_3 are fitting parameters.

5.5.1.2 Mechanical Field. A linear elastic constitutive model was adopted to simulate the mechanical behavior of the HMA layer, and elastic models were used for the rest of the layers. The mechanical properties of the base layer, insulation layer, and subgrade layer used in the FE model are listed in Table 8.

5.5.2 Determination of Thermal Properties Based on the Large-Scale Heat Transfer Tests

Before applying the proposed TM coupled model into the insulated pavements design process, the thermal properties in Equation 2-4 for each material were determined by experimental data. To determine the thermal properties of each layer, the FE model

was combined with an engineering optimization algorithm known as the simulated annealing (SA) method. Random thermal properties were generated and evaluated by the fitting effects until the preset stop criteria is satisfied. The optimized thermal properties with the best fitting effects were used as an input of the FE coupled model, and these properties were shown in Table 8. The comparison of measured and predicted temperature (Figure 23) indicated that the thermal field of the TM coupled model had an acceptable accuracy in determining the temperature distribution of pavement structures.

Table 8

Thermal and Mechanical Properties Used in This Study

Layer	Property	Control	XPS	Tire Chips	Foamed Concrete
HMA	λ [W/(m·K)]	1.23	1.77	1.58	0.93
	C [J/(kg·K)]	1750	1414	1870	2061
	E[MPa]	3447			
	ν	0.35			
Base	λ [W/(m·K)]	$0.00077T^2$-0.0187T+2.75	$0.0006T^2$-0.0593T+2.82	$0.0008T^2$-0.01178T+3.818	0.0004T2-0.0629T+3.11
	C [J/(kg·K)]	1562	1384	1076	1555
	E[MPa]	689			
	ν	0.25			

Layer	Property	Control	XPS	Tire Chips	Foamed Concrete
Insulation	λ [W/(m·K)]	--	0.11	0.38	0.26
	C [J/(kg·K)]	--	1889	1149	2887
	E[MPa]	--	6.9	1	1100
	ν	--	0.35	0.35	0.35
Subgrade	λ [W/(m·K)]	$0.00065T^2$-0.0305T+2.4	$0.00041T^2$-0.0302T+2.41	$0.000803T^2$-0.03738T+4.84	$0.0007T^2$-0.003711T+4.12
	C [J/(kg·K)]	3062	3979	3421	4289
	E[MPa]	69			
	ν	0.4			

5.5.3 Validating the Mechanical Section of the FE Model

To validate the accuracy of the mechanical prediction results from the coupled model, the predicted mechanical responses were compared with analytical solutions given by the widely used layered elastic analysis software known as KENPAVE. The elastic constitutive analytical solution was compared with the numerical solution obtained from an elastic FEM (no thermal or viscoelastic behavior is modeled). Similar pavement structures were built in the elastic FEM and KENPAVE separately, and the predicted vertical displacement, vertical stress, and horizontal strain were compared at the same depths.

Figure 23

Comparison of Simulated Temperature and Measured Temperature of: (a) Control Box, (b) XPS Insulated, (c) Tire Chips Insulated, and (d) Foamed Concrete Insulated; (e) Comparison of Simulated Mechanical Responses and Analytical Solutions (KENPAVE)

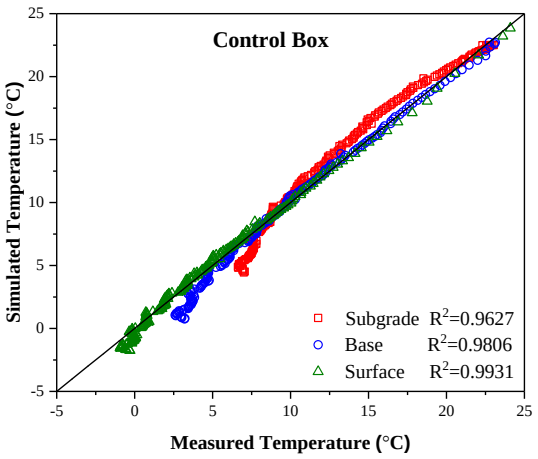

(a)

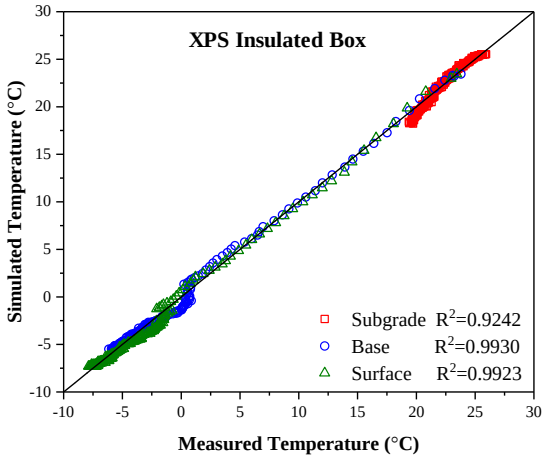

(b)

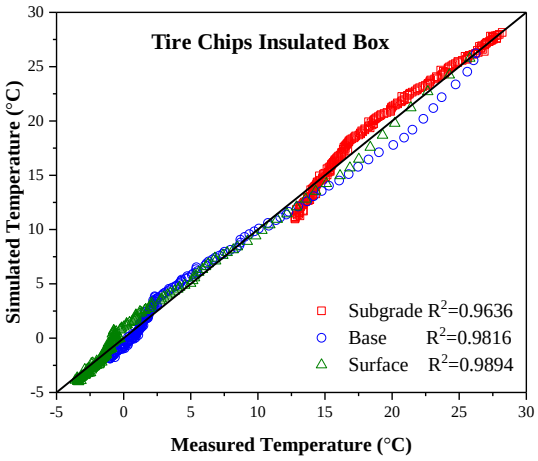

(c)

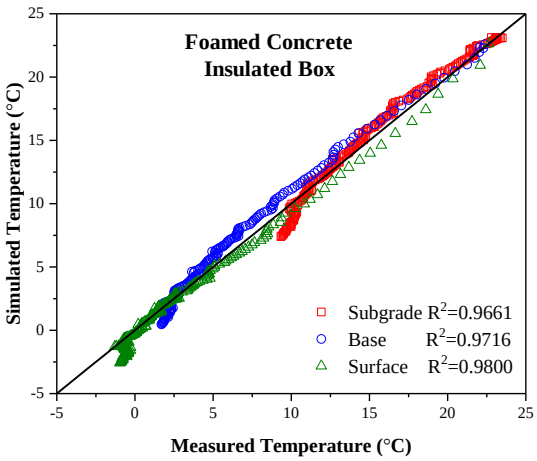

(d)

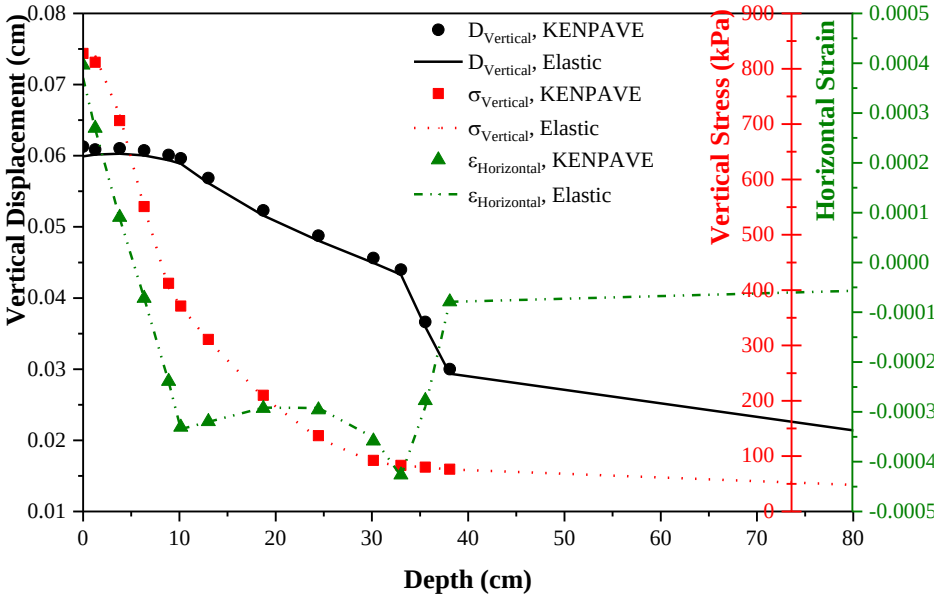

(e)

The comparison of the analytical solution and numerical solutions were presented in Figure 23. The R-square values of the vertical displacement, vertical stress, and horizontal strain between the analytical solution and elastic constitutive numerical solution are 99.83%, 99.97%, and 99.90%, respectively. The relatively high R^2 values indicated that the proposed FE model could accurately predict the mechanical responses of pavement structures. This suggests that boundary conditions, the load applied, and mesh the generated in the FEM model have no significant effects on the results.

5.6 Design Approach for Insulated Pavements

A mechanistic-empirical design procedure was proposed for designing insulated pavement structures while also balancing thermal and mechanical performances. The design of insulated pavements is based on the mechanistic-empirical pavement design

guide (MEPDG) [46, 105] and the thermal design process found in the Unified Facilities Criteria (UFC, 3-250-1) [45]. The proposed design approach is based on three principles as follows:

(1) An insulation lay can reduce the temperature variation of the layers underneath while it may also accelerate the temperature variation of the layers above the insulation. For this reason, two thermal criteria must be taken into account, one for the temperature variation in the subgrade, and the other is for temperature distribution in the base layer (lay above insulation).

(2) Increasing the insulation thickness will reduce variation in subgrade temperatures but may increase the variation in base and HMA temperatures.

(3) The temperature variation was evaluated by the standard deviation of the predicted daily temperature. The proposed FEM model took the daily air temperature in 2020 as the temperature input and then predicted the whole year's daily temperature distribution. The standard deviation of the temperature in the base layer and subgrade layer was calculated as an evaluation of the temperature variability. A smaller temperature standard deviation indicates the temperature is more stable, i.e., the insulating effect is better.

Figure 24 presents the flow chart of the proposed thermally-mechanically balanced design approach. This approach involves two stages, thermal and mechanical designs. The detail of each step is presented as follows:

Figure 24

The Procedure of Determining the Design Table Based on the Proposed Finite Element Model and Mechanistic-Empirical Pavement Design Guideline

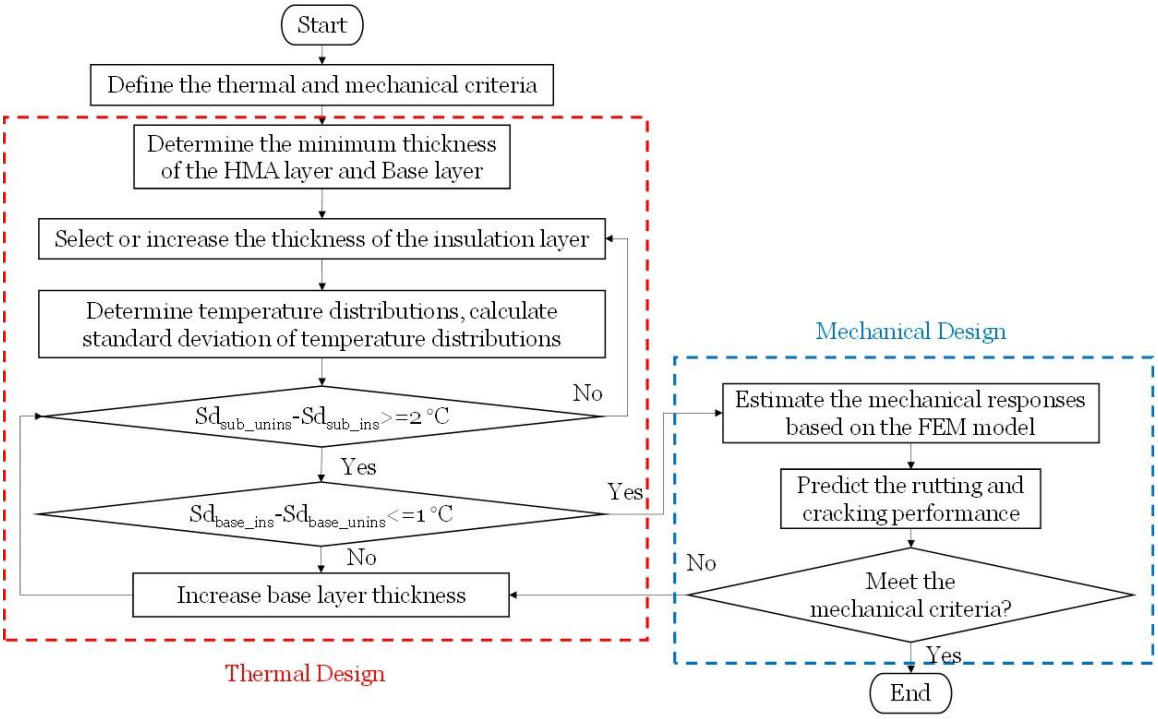

Step 1: Select the thermal and mechanical criteria.

Two thermal criteria were established in the thermal design. The first criterion is related to the temperature variation in the subgrade layer to ensure that low variation in insulated subgrade temperatures throughout the life of the pavement structure. The second criterion is related to the temperature variation of the HMA and base layers. In this study, the standard deviation (SD_{base} and $SD_{subgrade}$) of temperatures was used for characterizing the variation in subgrade and base layer temperatures.

Step 2: Determine the minimum thickness of the HMA layer and base layer.

According to UFC 3-250-1, the vertical stress on an insulation layer caused by dead and wheel loads should not exceed one-third of the compressive strength of the insulating material. Trials in a layered elastic analysis software such as KENPAVE can be used to determine the recommended minimum thicknesses for the base and HMA layers.

Step 3: Select or increase the insulation thickness.

The selection of type and thickness of the insulation layer should combine the local climate and local availability of materials. The increment of adding the thickness of the insulation layer is recommended as 2.5 cm.

Step 4: Determine temperature distributions and determine standard deviations.

The temperature distributions of the base and subgrade layer are determined using the proposed FEM model. In addition, the temperature distribution for the same structure without the insulation layer is calculated using the FEMs. The standard deviation is then determined.

Step 5: Evaluate the thermal adequacy of the current pavement structure.

Based on the calculated standard deviation values, the thermal adequacy of the insulated pavement structure is determined. As shown in Figure 24, a pavement structure is considered thermally adequate if:

1. $(SD_{sub\_unins} - SD_{sub\_ins})$ is greater than or equal to 2°C; and,

2. $(SD_{base\_ins} - SD_{base\_unins})$ is less than or equal to 1°C.

If both these conditions are not met, the thickness of the base layer is increased (usually by 2.5 cm) until the design (or pavement structure) is thermally adequate. If the

first condition is not met, then, as shown in Figure 24, the thickness of the insulation layer is increased (usually by 2.5 cm) until both conditions are satisfied. Once a pavement structure is thermally adequate, it can then be evaluated for mechanical performance adequacy as presented in the following section. It is worthy to note that the selection of parameters to indicate the thermal performance could be different. Other parameters such as the coefficient of variation or the largest frost depth of the year are also suitable in the design process. The threshold of thermal adequacy should be different based on the local climatic conditions. In this study, the standard deviation of the temperature changes was adopted.

Step 6: Estimate the mechanical responses based on the FEM model.

Linear elastic FEMs are used for determining the mechanical responses (critical stresses and strains) in thermally adequate insulated pavement structures. In particular, the mechanical responses targeted are: 1) vertical strains in sublayers (for rutting) and 2) tensile strains at the bottom of the HMA (for cracking)

Step 7: Predict Rutting and Cracking Performance

Using the mechanistic responses, the total rutting and number of loading repetitions to failure (N_f) are calculated using the MEPDG transfer functions. These equations are presented in Table 9.

Table 9

Equations and Parameters for Performance Prediction

Equations	Parameter
Rutting depth in the HMA layer	
$k_Z = (C_1 + C_2 D) \times 0.328196^D$	T = layer temperature
$C_1 = -0.1039 \times {h_{HMA}}^2 + 2.4868 \times h_{HMA} - 17.324$	ε_r = resilient strain in the sublayer
	k_Z = depth confinement factor
$C_2 = 0.0172 \times {h_{HMA}}^2 - 1.7331 \times h_{HMA} + 27.428$	C_1, C_2 = coefficients to calculate the depth confinement factor
	h_{HMA} = thickness of the HMA layer
	k_1, k_2, k_3 = calibration parameters, k_1=-3.35412, k_2=-1.5606, k_3=0.4791
	β_{1r}, β_{2r}, β_{3r} = local or mixture field calibration factors, $\beta_{1r} = \beta_{2r} = \beta_{3r} = 1$
Rutting depth in the unbound layer	
$log(\beta) = -0.61119 - 0.017638(W_c)$	h_{soil} = thickness of the unbound layer
$\rho = 10^9 \left(\frac{C_0}{(1-(10^9)^\beta)}\right)^{\frac{1}{\beta}}$	β_{s1} = local calibration factor, β_{s1} = 1 in this study
	β, ρ = material properties
$log\left(\frac{\varepsilon_0}{\varepsilon_r}\right) = 0.74168 + 0.08109 W_c - 0.00001215 M_r$	W_c = water content
	h_{soil} = thickness of the unbound layer
	C_0 = -4.8928
	ε_V = average vertical resilient strain
	$\varepsilon_0/\varepsilon_r$ = strain ratio
	M_r = resilient modulus
	k_1 = 2.03 for granular materials, and k_1 = 1.35 for fine-grained materials

Equations	Parameter
Bottom-up alligator cracking in the HMA layer	
$C = 10^{M}$ $M = 4.84\left(\frac{V_{be}}{V_a + V_{be}} - 0.69\right)$ $C_h = \frac{1}{0.000398 + \frac{0.003602}{1 + e^{(11.02 - 3.49 \times h_{HMA})}}}$	C = constant depending on mix properties V_{be} = effective asphalt content by volume V_a = air voids of HMA ε_t = tensile strain at the critical location C_h = thickness correction term h_{HMA} = thickness of the HMA layer k_{f1}, k_{f2}, k_{f3} = global field calibration parameters, k_{f1} = 0.007566, k_{f2} = -3.9492. k_{f3} = -1.281 β_{f1}, β_{f2}, β_{f3} = local calibration factors, $\beta_{f1} = \beta_{f2} = \beta_{f3} = 1$

Based on the mechanical response, the distresses were predicted based on Equation 5-7:

$$\Delta_{p(HMA)} = \beta_{1r} k_z \varepsilon_{r(HMA)} 10^{k_{1r}} n^{k_{2r}\beta_{2r}} T^{k_{3r}\beta_{3r}} \quad (32)$$

$$\Delta_{p(soil)} = h_{soil} \beta_{s1} k_1 \varepsilon_v \left(\frac{\varepsilon_0}{\varepsilon_r}\right) e^{-\left(\frac{\rho}{N}\right)^{\beta}} \quad (33)$$

$$N_{f-HMA} = k_{f1}(C)(C_H)\beta_{f1}(\varepsilon_t)^{k_{f2}\beta_{f2}}(E_{HMA})^{k_{f3}\beta_{f3}} \quad (34)$$

where $\Delta_{p(HMA)}$ is the accumulated permanent deformation in the HMA layer, $\Delta_{p(HMA)}$ is the accumulated permanent deformation in the unbound layer, $N_{f\text{-}HMA}$ is the allowable number of axle-load applications for a flexible pavement and HMA overlays. The prediction equation for the thermal cracking was not adopted in this study because

this equation was mainly used for the crack caused by a thermal contraction in the HMA layer. This equation didn't consider the effect of frost heave, which contributes more to crack initiation than the thermal contraction effect. In this study, the fitting parameters are all adopted as the global value in the MEPDG guideline, the equations and parameters used in this study are shown in Table 9 [46].

Step 8: Evaluate Mechanical Performance Adequacy

If the current design meets the rutting and cracking criteria, then the design is considered complete. If the design does not meet these requirements, the thickness of the HMA and base layers are increased until the performance criteria are satisfied. As discussed previously, thermal adequacy is evaluated if the thickness of the HMA and base were increased until the design is meeting both thermal and mechanical criteria.

The threshold and measures used in this study are only an example. Other measures of mechanical and thermal adequacy (e.g., the coefficient of variation of the temperature change) and threshold could be used as well.

5.7 Demonstration of Insulated Pavement Design Approach and Development of Design Tables

To supply an easy way to design an insulated pavement, this section provided design tables based on the proposed approach. Using the insulated pavement design approach presented above, sample design tables for Alaska weather conditions (Table 10 and Table 11) were developed. These design tables present a method for designing insulated pavement structures without running numerical simulations. These design tables

were developed for maximum rutting of 1.27 cm (0.5 inches) and maximum cracking of 20%.

Table 10 lists the maximum allowable load repetitions (traffic) under some typical inputs. The maximum allowable load repetitions are equal to the equivalent single axle load (ESAL). Under the given design criteria, rutting is the primary distress for insulated pavement since the calculated allowable load repetitions based on bottom-up cracking are almost two times larger than that based on rutting. The calculation of rutting depth is dominated by the vertical strain in the subgrade and the insulation strength. For insulated pavements with the same thicknesses in the HMA layer and base layer, pavements with a thicker insulation layer can bear more load repetitions. This is because a thicker insulation layer results in a deeper subgrade layer, thus the rutting depth is smaller, and the maximum allowable load repetition is larger. Increasing the depth of the insulation layer also increases the bearing capacity of pavement structures. For example, in Table 10, under the same surface thickness and insulation thickness, pavements with a thicker base layer (i.e., the insulation layer is deeper) have a higher maximum load repetition. In addition, different insulating materials show different responses when compared with uninsulated pavement. For example, in comparison to the uninsulated pavement, the pavements insulated by XPS boards and foamed concrete can bear more load repetitions (from 6% to 2123% more) because of the thickness of the overlay layers (layers above the subgrade layer) is larger. However, the tire chips insulated pavement can bear more traffic repetitions only when the overlay thickness is greater than 35 cm due to its smaller modulus.

Table 11 presented the temperature standard deviation at the subgrade layer under different thickness inputs. A lower standard deviation indicates fewer temperature variations in the subgrade layer for the entire year of consideration, which implies a better insulation effect. The temperature variability results show that the temperature of the subgrade layer in the insulated pavements is more stable than that in the uninsulated pavements, and a thicker insulation layer results in less temperature variation in the subgrade layer. Increasing the depth of the insulation layer slightly decreases the temperature variation in the subgrade layer. Besides, the insulating effects are directly dependent on the thermal conductivity of the insulation layer (the thermal conductivity: XPS< foamed concrete < tire chips). With the increase of the insulation depth, the insulating effect decreases. Taking the 2.5 cm XPS board insulated pavements as an example, the standard deviation of the subgrade layer decreases 31.6% for a 20 cm overlay structure (HMA =10 cm and base = 10 cm), while when the overlay thickness increases to 40 cm (HMA = 20 cm and base layer = 20 cm), the standard deviation decreases only 29.1%.

An example of using Table 10 and Table 11 to determine the appropriate insulated structure is presented as follows. Assuming the required maximum load repetition is 10 million, Table 4 indicates that multiple design scenarios are possible to satisfy this requirement, among which one design could be a pavement structure with a 10 cm thick HMA layer, a 20 cm thick base layer, and a 2.5 cm thick XPS insulation layer. According to Table 11, the temperature standard deviation difference between the insulated and uninsulated pavement = 5.09-3.58 = 1.51 ℃ < 2 ℃ (according to step 5 in

section 5). Therefore, this specific design does not satisfy the thermal design criteria. Another pavement structure needs to be selected and tested from Table 10 and Table 11 until the mechanical and thermal criteria are satisfied.

Table 10

Alaska's Insulated Pavements Mechanical Performance Design Table for Maximum Allowable Load Repetitions (Unit: Million)

HMA (cm)															
							10								
Base (cm)			10				15						20		
Insulation	0	2.5	5	7.5	10	0	2.5	5	7.5	10	0	2.5	5	7.5	10
XPS		0.35	0.55	0.80	1.09		2.00	3.40	5.21	7.82		**11.41**	18.05	27.28	38.12
Tire Chips	0.33	0.22	0.48	0.75	0.96	1.64	1.36	3.68	6.78	9.97	10.40	8.65	24.37	47.02	65.67
FC		0.95	2.79	6.29	15.12		5.01	13.60	25.10	51.20		22.36	45.41	70.64	109.99
HMA (cm)															
							15								
Base (cm)			10				15						20		
Insulation	0	2.5	5	7.5	10	0	2.5	5	7.5	10	0	2.5	5	7.5	10
XPS		5.75	9.57	15.15	21.60		27.22	41.66	60.70	82.22		89.60	121.86	159.50	194.96
TC	4.58	3.68	10.62	21.00	31.12	23.06	19.33	53.59	98.85	136.60	65.61	75.23	170.21	259.08	326.20
FC		13.33	31.69	56.90	101.80		49.11	92.66	135.28	200.74		130.07	188.85	247.15	316.39

HMA (cm)															
							20								
Base (cm)			10					15					20		
Insulation	0	2.5	5	7.5	10	0	2.5	5	7.5	10	0	2.5	5	7.5	10
XPS	66.97	78.31	116.68	148.11	199.72	151.03	202.59	234.32	314.00	361.03	289.56	373.40	438.92	552.30	614.01
TC		60.88	160.44	246.81	343.92		174.35	317.86	494.75	586.47		439.00	525.00	656.00	753.00
FC		116.85	197.39	243.98	352.03		266.69	320.34	428.33	511.11		438.71	524.84	656.09	752.97

Note: XPS, TC, FC represent the maximum allowable load repetitions of the XPS, tire chips, and foamed concrete insulated pavement. The values from this table are calculated based on the assumption that the rutting depth of the insulation layer is equal to the elastic deformation of the insulating materials.

Table 11

Alaska's Thermal Design for Control of Subgrade Temperature Variability (Standard Deviation) (Unit: ºC)

HMA (cm)															
							10								
Base (cm)			10				15						20		
Insulation (cm)	0	2.5	5	7.5	10	0	2.5	5	7.5	10	0	2.5	5	7.5	10
SD_XPS (ºC)		3.74	2.79	2.20	1.80		3.65	2.73	2.16	1.77		**3.58**	2.68	2.13	1.75
SD_Tire Chips (ºC)	5.47	4.84	4.34	3.92	3.56	5.29	4.71	4.22	3.81	3.48	**5.09**	4.58	4.10	3.72	3.40
SD_FC (ºC)		4.53	3.85	3.33	2.92		4.41	3.75	3.26	2.86		4.30	3.66	3.18	2.80
HMA (cm)							15								
Base (cm)			10				15						20		
Insulation (cm)	0	2.5	5	7.5	10	0	2.5	5	7.5	10	0	2.5	5	7.5	10
SD_XPS (ºC)		3.59	2.70	2.14	1.76		3.50	2.65	2.11	1.73		3.41	2.60	2.07	1.71
SD_Tire Chips (ºC)	5.18	4.60	4.15	3.77	3.43	5.00	4.48	4.04	3.67	3.35	4.85	4.34	3.94	3.58	3.27
SD_FC (ºC)		4.33	3.70	3.21	2.83		4.21	3.61	3.14	2.77		4.08	3.53	3.07	2.71

HMA (cm)															
	20														
Base (cm)	10					15					20				
Insulation (cm)	0	2.5	5	7.5	10	0	2.5	5	7.5	10	0	2.5	5	7.5	10
SD_XPS (°C)	4.91	3.47	2.62	2.09	1.72	4.76	3.38	2.57	2.05	1.70	4.61	3.27	2.53	2.02	1.67
SD_Tire Chips (°C)		4.42	3.98	3.61	3.31		4.29	3.87	3.52	3.23		4.14	3.77	3.44	3.16
SD_FC (°C)		4.15	3.55	3.10	2.73		4.04	3.48	3.03	2.68		3.91	3.39	2.97	2.63

5.8 Main Findings in This Chapter

In this study, a finite element model was adopted to predict the thermal and mechanical responses of the insulated pavement to develop a design table for insulated pavements. The model was calibrated with four large-scale pavement boxes, one was a control sample without an insulation layer, and the rest three were insulated with XPS, tire chips, and foamed concrete, respectively. The temperature distribution was collected by thermocouples embedded in different depths, and the thermal properties for each material were calculated based on the temperature distribution. According to the mechanical and thermal responses of the insulated pavement in different scenarios, the maximum axle load repetitions were calculated. Based on experimental and numerical data analyses, the following conclusions were drawn:

- Insulated pavement can be designed based on the proposed procedure. Once the traffic capacity is estimated, the FE model can calculate the responses over the whole year for local climate conditions, and the pavement performance can be evaluated by the MEPDG method.
- The proposed design approach considered not only the mechanical responses but also the thermal-induced material modulus degradation in the insulated pavement design. The calculated tensile strain and vertical strain resulting from vehicle loads vary in different seasons.
- The pavements insulated by XPS boards and foamed concrete can bear up to 50 times more load repetitions than uninsulated pavements, while the tire chips insulated pavement can bear more traffic repetitions only when the overlay thickness is greater than 35 cm.

- The temperature of the subgrade layer in the insulated pavements is more stable than that in the uninsulated pavements. The standard deviation of the subgrade temperature in the insulated boxes is 1-4 ºC less than that of the control box. Increasing the insulation thickness from 2.5 cm to 10 cm decreases the subgrade temperature standard deviation by 2 ºC.

However, further research related to the failure mechanism of the insulated is necessary to improve the accuracy of the design approach. The limitation of this study includes:

- The failure of the base and insulation layer was not considered in this study due to the complex mechanism of the Thermo-Hydro-Mechanical (THM) coupled process and the phase change effect during the deterioration process.
- Although this study adopted the empirical pavement performance prediction equations from MEPDG, field validation of the design approach is still warranted.

Chapter 6

Evaluating the Potential of Using Foamed Concrete as the Insulation Layer for Pavements in Cold Regions

6.1 Abstract

Insulated pavement structures help prevent frost penetration and its negative impacts on roadways and airfields in cold regions. The most commonly used insulating material in pavements is extruded polystyrene (XPS) boards. However, the utilization of XPS boards has several unavoidable drawbacks. For this reason, there is an increasing interest to explore alternative materials such as tire chips, bottom ash, and foamed glass aggregates as the insulation layer. This paper evaluates the potential of using foamed concrete as an insulation layer. To achieve this goal, a thermo-mechanical (TM) coupled model was developed to simulate the responses of insulated pavement with a foamed concrete insulation layer. In addition, the compressive strength and thermal conductivity of different densities of foamed concrete were tested to provide the material parameters for the developed model. The thermal aspects of the model were then calibrated by a large-scale insulated pavement test. The calibrated model was used for a parametric study to reveal the influence of the thickness, depth, and density of the foamed concrete layer on the thermal and mechanical performance. Simulation results show that the developed model can accurately predict the thermal performance of insulated pavements. Compared with the performance of uninsulated pavements, the foamed concrete-insulated pavement has better performance in resisting frost effect and traffic loading. The parametric study also found that a minimum thickness exists for a foamed concrete insulation layer to

ensure the subgrade layer is unfrozen. Increasing the thickness, depth, and density of a foamed concrete layer enhances its mechanical performance.

6.2 Introduction

To meet the challenge of building sustainable roadways under extreme climates, several strategies, such as selecting appropriate asphalt binders, replacing the frost-susceptible soils, and providing proper drainage, are employed [44, 49]. Recently, researchers showed an increased interest in exploring the application of insulated pavements in cold regions [20, 23, 84]. An insulated pavement is a pavement structure with a thermal insulation layer embedded above the frost-susceptible layers (usually the subgrade layer). Numerous studies proved the efficiency of pavement insulation layers in minimizing the frost heave effect in practice since 1967 [64]. However, questions are raised about using appropriate materials for insulating pavements. For example, the most commonly used pavement insulation material is extruded polystyrene (XPS) boards. This material is used because of its excellent insulating efficiency and good mechanical strength. However, XPS boards suffer from several major drawbacks. These include: 1) degradation of the long-term field insulation ability with moisture accumulation [67] and 2) the requirement for a time-consuming, labor intensive, and detailed approach for installing and sealing these boards [49]. To address these limitations, considerable literature has been published exploring the potential of using alternative materials (e.g., tire chips, bottom ash, and foamed glass aggregates [12, 13, 24, 25, 65, 69]) for insulating pavements. In addition to these materials, the application of a new insulating material named foamed concrete has received considerable attention in many engineering areas [73, 106].

Foamed concrete is a light cellular concrete with air entrapped by a suitable foaming agent, which processes self-compacting, lightweight, thermal insulation, low strength, and fireproof properties [107, 108]. By properly controlling the foaming agent dosage, foamed concrete with densities ranging from 400 kg/m^3 to 1600 kg/m^3 can be obtained [109]. Compared with other conventional insulating materials, foamed concrete has a number of attractive features. First, the self-compacting feature saves labor costs and simplifies the construction process. Second, experimental tests revealed that up to 67% of the cement used in foamed concrete could be replaced by fly ash without any significant strength degradation, which provides economical and safe disposal of these waste residues [110]. Foamed concrete is also one of the materials successfully used for different civil engineering applications including: cavity filling, fire insulation, thermal and acoustic insulation, trench reinstatement, and soil stabilization [111-113]. In the aspect of pavement engineering, foamed concrete was used for base layers to improve drainage or non-load bearing components [76]. However, there has been little discussion about using foamed concrete as an insulation layer in road construction.

A major problem with the application of foamed concrete in insulated pavements is selecting optimum parameters that balance the mechanical strength and insulating effect. The thermal and mechanical properties of foamed concrete are highly dependent on factors including density, cement type, and water/cement ratio [78]. In addition, the usage of additives such as fly ash, sand, and fibers also influence foamed concrete properties [78, 107, 114, 115]. With a determined type of foamed concrete, density selection has the greatest effect on the compressive strength and insulating effect. A number of studies reported that the compressive strength of varying densities differs by a

factor of ten [116, 117]. More importantly, the influence of density on the compressive strength and insulating effect is contradictory. Increasing the density of foamed concrete would increase the compressive strength while decreasing the insulating effect [118]. Therefore, selecting the appropriate density of foamed concrete poses a significant challenge for the application in insulated pavements.

6.3 Study Goal and Objectives

This study aims to explore the potential of utilizing foamed concrete as an insulation layer for pavements in cold regions. To achieve this goal, the following specific objectives were completed:

(1) Develop a thermal-mechanical (TM) coupled finite element (FE) model to predict the thermal and mechanical performance of insulated pavements.

(2) Establish the relationship between foamed concrete density and thermal/mechanical properties through laboratory testing.

(3) Conduct full-scale testing of foamed concrete insulated pavement structure to calibrate and validate the FE model.

(4) Perform a parametric study to investigate the influence of thickness, depth within pavement, and density of a foamed concrete layer on the thermal and mechanical performance of pavement structures.

6.4 Experimental Work

6.4.1 Foamed Concrete Samples Test

A series of laboratory tests were performed to measure the material properties of foamed concretes with varying densities. The density, compressive strength, thermal conductivity, and porosity of foamed concrete were measured. Foamed concretes with

densities of 480 kg/m^3 (30 lb/ft^3), 640 kg/m^3 (40 lb/ft^3), 800 kg/m^3 (50 lb/ft^3), and 960 kg/m^3 (60 lb/ft^3) were manufactured. Seven samples were made for each density, including 4 samples used for the compressive strength test and 3 samples used for the thermal conductivity test.

6.4.1.1 Materials Used in the Foamed Concrete Test. In this test, the foamed concrete was mixed with water, cement, and foam agent. The water-cement ratio of the cement paste is 0.5. The cement used in the foamed concrete was type II Portland cement. The size of the specimen is 7.62 cm in diameter and 15.24 cm in length.

6.4.1.2 Foamed Concrete Test Procedure. The manufacturing of foamed concrete followed the procedure of ASTM C796-97 [109]. Before the manufacturing of the test samples, a trial-and-error process was adopted to determine the appropriate amount of foam that guarantees the minimum difference between the actual and target cast density. The foamed concrete samples were prepared by the pre-foaming method. The portland cement was firstly mixed with water by a paddle mixer until a homogeneous mortar without lumps of undispersed cement was obtained. Then the pre-formed foam was produced by the foam generator and added to the mix immediately after preparation. The foam and mortar were mixed for at least 2 minutes until all foam was uniformly distributed. The mixed concrete was then placed in a pre-weighed cylinder mold by two lifts. Each lift is approximately half of the mold. After each lift, the mold was lightly tapped 10 to 15 times to close voids and release entrapped air. After filling the mold, the surface was covered to prevent evaporation without marring the surface. The weight of each sample was recorded to calculate the cast density. The average density of foamed concrete samples in this study is listed in Figure 25.

Figure 25

Densities of the Foamed Concrete Samples

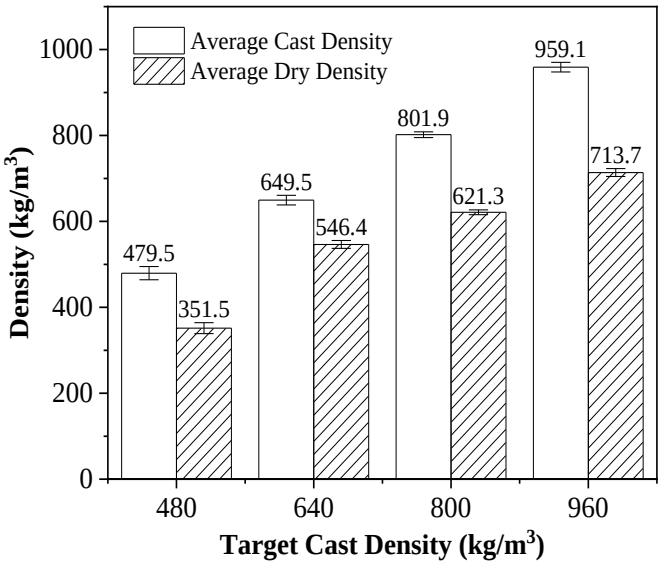

The samples were demolded 3 days after molding. Then the samples were maintained in a humid room with a controlled temperature of 23 °C and relative humidity of 50%. On day 28 after molding, four samples were used for the compressive strength test and three samples were used for the thermal conductivity testing at each density. After the compressive strength test and thermal conductivity test, the foamed concrete samples were used to conduct a porosity test. The apparatus used in this study is shown in Figure 26.

The compressive strength test followed the procedure of ASTM C495/C495M [119]. During the test, the day 28 samples were aligned with the center of the loading thrust. Then a 1.5 MPa/min load was applied to the sample until the maximum load was reached. The thermal conductivity test followed the procedure of ASTM D5334-14 [120]. The samples were placed in the humid room for 25 days to reach thermal equilibrium

before inserting the needle into the sample. The porosity test followed the procedure of ASTM C20-00(2015) [121]. The porosity of the foamed concrete sample was determined based on the weight difference before and after the saturating and boiling process.

Figure 26

Apparatus Used for (a) Compressive Strength Test; (b) Thermal Conductivity Test

(a)

(b)

6.4.2 Large-Scale Insulated Pavement Test

After the laboratory-scale foamed concrete test, a large-scale insulated sample was produced and measured under a cooling system. The purpose of the large-scale pavement test is to calibrate the heat transfer and temperature prediction model in the FE simulation.

Figure 27 shows the schematic view of the insulated pavement sample. The whole pavement sample was stored in a wooden box. The inner width and length of the box are 122 cm, and the height is 79 cm. The inner sides and bottom of the wooden box were

insulated by 5 cm thick extruded polystyrene boards to minimize the influence from the environment. The pavement sample contained a 10 cm thick hot mix asphalt (HMA) layer as the surface layer, a 13 cm thick recycled concrete layer as the base layer, a 5 cm thick foamed concrete layer as the insulation layer, and a 51 cm thick clayey sand layer as the subgrade layer. To monitor the temperature distribution, the pavement samples were instrumented with thermocouples at different depths between each other as shown in Figure 27. To create a constant freezing environment, a frosted panel made with pipes and chillers was placed on the top of the pavement sample for 200 hours. The temperature of the frosted panel was set as -15 ºC.

Figure 27

Schematic View and the Test Setup of the Large-Scale Pavement Test

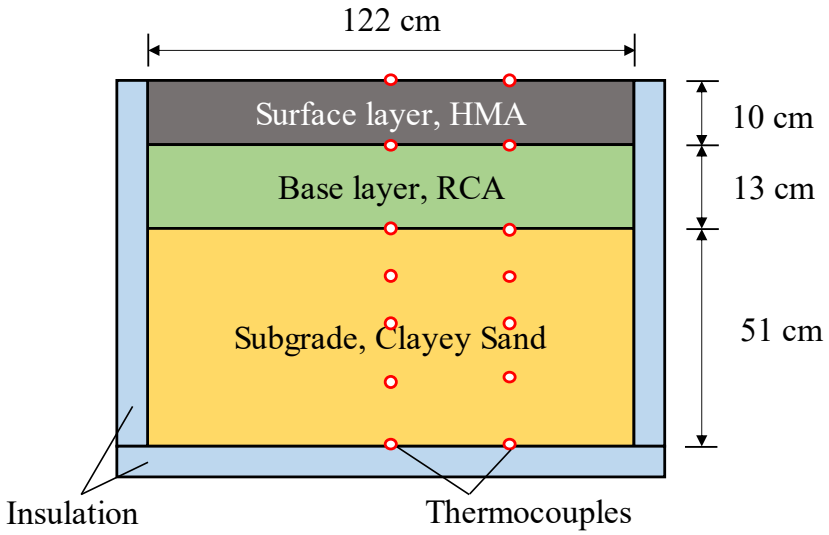

(a)

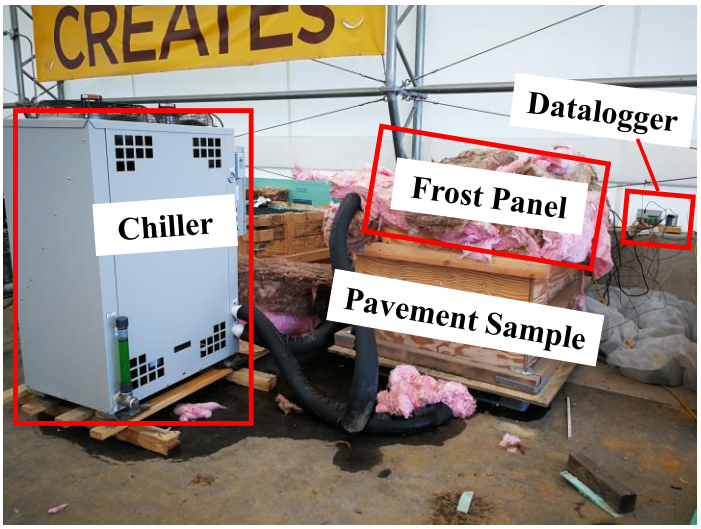

(b)

6.4.2.1 Material Used in the Large-Scale Insulated Pavement Test. The HMA used in this study was a dense-graded mixture with a nominal maximum sieve size of 9.5 mm, which satisfies the New Jersey Department of Transportation (NJDOT) specifications. The mix was prepared using an optimum binder content of 5.8% (by total weight of mix) and a binder grade of PG 64-22.

The recycled concrete aggregates used in the pavement box include 56% coarse materials (retained on Sieve No. 4), 35% sandy materials (passing Sieve No. 4), and 9% fines (passing sieve No. 200). The optimum moisture content to achieve maximum dry density for RCA was determined as 12.4% using the modified Proctor test (AASHTO T180) [122]. The recycled concrete aggregates were mixed with water in a concrete mixer (outside the wooden box) to reach the optimum moisture content before filling into the box.

The foamed concrete used in the pavement box followed the identical manufacturing procedure as the laboratory-scale foamed concrete test. The cement type,

water/cement ratio, and foam type were the same as the foamed concrete test. The density used in the large-scale pavement box was 880 kg/m^3.

A frost susceptible clayey sand from a local New Jersey contractor was used as the subgrade layer for the pavement boxes. This material contains 35.2% (by weight) fine materials that pass sieve No. 200 (i.e., < 75μm). The subgrade material had a Proctor test optimum moisture content of 12.1%. According to the Unified Soil Classification System (USCS), the soil can be classified as clay of low plasticity (CL). The subgrade clayey sand was first dried for 24 hours, then sieved through the No. 4 sieve (4.75 mm). Before filling into the wooden box, the clayey sand was mixed with water outside the box to reach the optimum moisture content.

6.4.2.2 Procedure for Preparing the Large-Scale Insulated Pavement Sample. The insulated pavement sample was constructed from the bottom up inside a wooden box. Before filling the box, the designed thickness for each layer was marked to the internal wall of the wooden box to ensure the designed thickness has been achieved.

The construction of the pavement structure started by placing four 12 cm lifts of the subgrade to achieve a total thickness of 48 cm. When filling those layers, the weight of clayey sand used for each layer and the thickness of each layer was recorded. The amount of clayey sand used for the next layer was then adjusted based on the previous soil weight and thickness.

The insulation layer of the pavement sample was produced by pouring the mixed foamed concrete on the top of the subgrade layer. The foamed concrete layer was cured for seven days to obtain an initial strength before constructing the base layer.

For the surface layer, the HMA mix was preheated to 175℃ to facilitate placement and compaction. Like the unbound layers, the weight of HMA materials was controlled by placing the same amount of material to compact a 10 cm thick surface layer. Compaction of all layers was performed using a vibratory plate compactor. In addition, thermocouples were installed at the bottom of each lift from the bottom of the sample to the top surface as shown in Figure 27. Each lift has two thermocouples, one at the midpoint and the other at the quarter-point. These thermocouples were connected to a data acquisition system for the continuous recording of temperature (rate of recording: 1 point every 5 minutes).

6.5 Finite Element Model Description

6.5.1 Model Configuration

In this study, a 2-dimensional symmetric thermal-mechanical coupled flexible pavements model was developed using the commercial FE software. The FE model was first set as the same size as the large-scale pavement test in this study: 122 cm in width and 79 cm in height. The thicknesses of the surface, base, insulation, and subgrade layers were 10 cm, 13 cm, 5 cm, and 51 cm, respectively. After comparing the measured performance from the experiment and the predicted performance from the FE model, the width of the FE model was then set as 4 m to simulate the performance of a real flexible pavement. In this stage, the thickness of each layer in the FE model varied based on the density of foamed concrete. The FE model adopted the thermal properties measured from the foamed concrete experiments performed in this study. The mechanical property of the surface, base, and subgrade layers used the global calibration values from the Mechanistic-empirical Pavement Design Guide (MEPDG) [46]. The Young's modulus of the foamed

concrete layer was estimated based on the compressive strength measured in this study. The relation between Young's modulus and compressive strength adopted the empirical equation developed by Zhang and Wang [123]:

$$E_c = 0.3743 f_c^{0.671} \quad (35)$$

where E_c and f_c are Young's modulus and compressive strength of the foamed concrete, respectively.

The material property adopted in the FE model was summarized in Table 12.

Table 12

Material Properties Used in the FE Model

Layer	Density [kg/m^3]	Thermal Conductivity [W/(m·K)]	Heat Capacity [J/(kg·K)]	Young's Modulus [MPa]
Surface	1905	1.00	3963	500
Base	2007	2.20	1838	200
Insulation	Depend on foamed concrete density			
Subgrade	1948	2.81	2941	80

The symmetric 2D FE model was meshed by triangular elements as shown in Figure 28. The mechanical boundary conditions for the model included assigning its sides and bottom with fixed constraints. Layers were fully bonded at the interface. No heat exchange was allowed on the model's sides and bottom to ensure that a one-dimensional heat transfer process is simulated. A static load of 827 kPa (120 psi) was applied on the top surface of the model to mimic the tire load of a single axle truck with a static load of

80 kN (18-kips). The length of the line load was calculated based on the following equations [47]:

$$F = 4A_c \cdot P_t \tag{36}$$

$$L = \sqrt{\frac{A_c}{0.5227}} \tag{37}$$

where F is the static load (80 kN), A_c is the tire contact area, P_t is the truck tire pressure (827 kPa or 120 psi), L is the length of the static load.

In addition, the temperature of the top surface was set as the input boundary condition. When comparing the FE model with the large-scale pavement test, the temperature of the top surface of the FE model was set to be the same as the experimentally measured temperature of the pavement sample's top surface. When performing the parametric study, the top surface temperature was set as the daily historic average temperature of Juneau, Alaska. The historic temperature was acquired from the National Oceanic and Atmospheric Administration (NOAA).

Figure 28

Mesh and Boundary Conditions of the FE Model

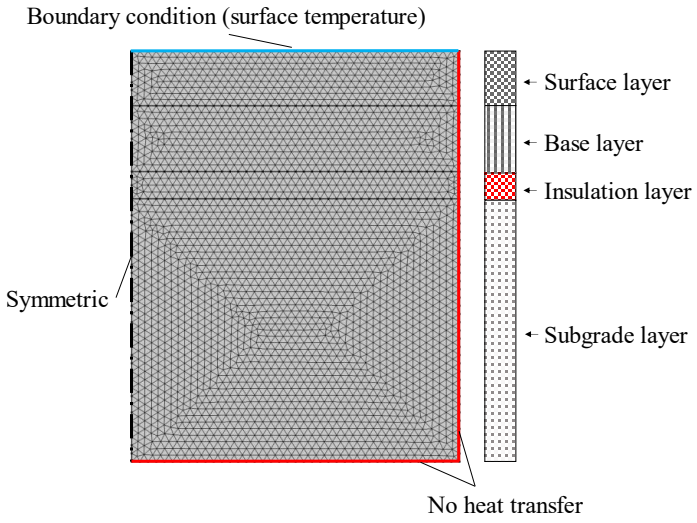

6.5.2 Governing Equations

6.5.2.1 Phase Change Process and Model Assumptions. The distresses of pavements in cold regions, such as frost heave and thaw weakening, are mainly attributed to the phase change process of the moisture in unbound, granular layers. The phase change process influences both the mechanical and the thermal behavior of granular layers. Phase change influences the mechanical behavior by changing the stiffness of the frozen area. In addition, moisture would expend when turning from an unfrozen state to a frozen state. Phase change influences the heat transfer process in two ways: one is the different thermal properties between the unfrozen water and ice; the other is the latent heat when unfrozen water turns to ice. Therefore, in this study, a thermal-mechanical coupled model was developed with the consideration of the phase change process in the granular layers (i.e., the base and subgrade layer). The model was built based on the following assumptions:

(1). Phase change only happens in the base and subgrade layers. For the surface and insulation layer, the moisture content is assumed to be zero.

(2). Moisture movement is neglected, and the convection term in the thermal field is set to zero.

(3). The effects of the surface's albedo, incoming solar radiation, wind speed, and the air phase are neglected.

6.5.2.2 Thermal Field. A modified Fourier's equation was adopted as shown in the following equation:

$$(\rho C)_{eq}\frac{\partial T}{\partial t} + \nabla \cdot \left(-k_{eq}\nabla T\right) = Q \tag{38}$$

where $(\rho C)_{eq}$ is the equivalent product of the density (ρ) and heat capacity (C), T is temperature, t is time, k_{eq} is the equivalent thermal conductivity, Q is the heat source.

The equivalent terms in Eq. (4) are calculated by the following equations:

$$(\rho C)_{eq} = \begin{cases} \rho_s C_s & \text{Surface and insulation layers} \\ \rho_s C_s V_s + \rho_w C_w V_w & \text{Base and subgrade layers} \end{cases} \tag{39}$$

$$k_{eq} = \begin{cases} k_s & \text{Surface and insulation layers} \\ k_s V_s + k_w V_w & \text{Base and subgrade layers} \end{cases} \tag{40}$$

where the subscript s and w denote solid mass and water, V is the volumetric content.

The density (ρ_w), heat capacity (C_w), and thermal conductivity (k_w) of water were calculated by Eq. (41) – (45):

$$\rho_w = \theta_i \rho_i + \theta_{uw}\rho_{uw} \tag{41}$$

$$C_w = \frac{1}{\rho_w}(\theta_i \rho_i C_i + \theta_{uw}\rho_{uw}C_{uw}) + L\frac{\partial \alpha_m}{\partial t} \tag{42}$$

$$\alpha_m = \frac{1}{2}\frac{\theta_{uw}\rho_{uw} - \theta_i\rho_i}{\theta_i\rho_i + \theta_{uw}\rho_{uw}} \quad (43)$$

$$k_w = \theta_i k_i + \theta_{uw} k_{uw} \quad (44)$$

$$\theta_i + \theta_{uw} = 1 \quad (45)$$

where the subscript *i* and *uw* denote ice and unfrozen water. *L* is the latent heat of water (334kJ/kg), and α_m is the phase transition between ice and unfrozen water. The phase transition indicates the phase change process.

6.5.2.3 Mechanical Field. A viscoelastic constitutive model was adopted to simulate the mechanical behavior of the HMA layer, and elastic models were used for the rest of the layers. The relaxation modulus of asphalt mixture was modeled as a generalized Maxwell solid model in terms of the Prony series, as shown in Eq. (46) [86, 124]:

$$E(t_r) = E_0\left(1 - \sum_{i=1}^{N} E_i\left(1 - e^{\frac{-t_r}{t_i}}\right)\right) \quad (46)$$

where E_0 is instantaneous elastic modulus, E_i and τ_i are Prony series parameters, t_r is reduced time. The Prony series parameters adopted the values obtained from laboratory tests by Katicha [85].

6.5.2.4 Coupling Process. The thermal and mechanical processes in the FE model are coupled through the temperature dependency of resilient modulus for the HMA layer. The temperature dependency of asphalt concrete modulus is characterized by the time-temperature superposition principle. The relation between the time-temperature shift

factor and the temperature can be expressed by the Williams-Landell-Ferry (WLF) function:

$$\log a_T = -\frac{C_1(T - T_R)}{C_2 + (T - T_R)} \quad 47)$$

where T_R is the reference temperature (in this study, 21.1 °C), C_1 and C_2 are regression parameters (in this study, C_1 = 11.59, C_2 = 62.35 K). T_R, C_1 and C_2 were assigned with values from related literature [86].

For the base and subgrade layers, the thermo-mechanical (TM) coupling was achieved by defining the mechanical properties (i.e., Young's modulus and Poisson's ratio) as a function of the ice content inside the granular materials. The Young's modulus and Poisson's ratio of the granular layers were defined as [125]:

$$E = \frac{[V_s E_s(1 - 2\upsilon_i) + V_w \theta_i E_i(1 - 2\upsilon_s)][V_s E_s(1 + \upsilon_i) + V_w \theta_i E_i(1 + \upsilon_s)]}{V_s E_s(1 + \upsilon_i)(1 - 2\upsilon_i) + V_w \theta_i E_i(1 + \upsilon_s)(1 - 2\upsilon_s)} \quad 48)$$

$$\upsilon = \frac{V_s E_s \upsilon_s(1 + \upsilon_i)(1 - 2\upsilon_i) + V_w \theta_i E_i \upsilon_i(1 + \upsilon_s)(1 - 2\upsilon_s)}{V_s E_s(1 + \upsilon_i)(1 - 2\upsilon_i) + V_w \theta_i E_i(1 + \upsilon_s)(1 - 2\upsilon_s)} \quad 49)$$

where E, υ are the equivalent Young's modulus and equivalent Poisson's ratio of the granular layers, V_s and V_w are the volumetric content of the soil matrix and water (including unfrozen water and ice), E_s and E_i are Young's modulus of the soil solids and ice, θ_i is the ice content in Eq. (7)-(11). According to Eq. (14) – (15), for unfrozen soil (i.e., θ_i =0), the equivalent Young's modulus $E = V_s E_s$; and the equivalent Poisson's ration $\upsilon = \upsilon_s$.

6.5.3 Insulated Pavement Performance Prediction

After calibrating the proposed FE model with the foamed concrete tests, the model was then used to perform a parametric study to predict the thermal and mechanical performance of insulated pavement with different densities of foamed concrete. The thermal performance indicates the largest frost depth (the depth that the temperature is

colder than 0 ºC) under a natural environment. This was estimated by predicting the temperature distribution of the insulated pavement structure. The mechanical performance includes rutting and bottom-up cracking. These performances were predicted by two steps: first, calculating the vertical and tensile strains at the critical locations, then estimating the performance based on the mechanistic-empirical transfer function in MEPDG [46]:

$$\Delta_{p(HMA)} = \beta_{1r} k_z \varepsilon_{r(HMA)} 10^{k_{1r}} N^{k_{2r}\beta_{2r}} T^{k_{3r}\beta_{3r}} \quad (50)$$

$$\Delta_{p(soil)} = h_{soil} \beta_{s1} k_1 \varepsilon_v \left(\frac{\varepsilon_0}{\varepsilon_r}\right) e^{-\left(\frac{\rho}{N}\right)^{\beta}} \quad (51)$$

$$N = k_{f1}(C)(C_H)\beta_{f1}(\varepsilon_t)^{k_{f2}\beta_{f2}}(E_{HMA})^{k_{f3}\beta_{f3}} \quad (52)$$

where $\Delta_{p(HMA)}$ and $\Delta_{p(soil)}$ are the rutting depth of the HMA layer and the granular layer, N is the allowable number of axle-load applications (N = 1,000,000 in this study), β, β_{1r}, β_{2r}, β_{3r}, β_{f1}, β_{f2}, β_{f3}, k_z, k_{1r}, k_{2r}, k_{3r}, k_1, k_{f1}, k_{f2}, k_{f3} are calibration factors, which adopted the global values in the MEPDG guideline, ε_r is the vertical elastic strain, ε_v is the average vertical elastic strain, ε_t is the tensile strain at the bottom of the HMA layer, C and C_H are parameters calculated based on the thickness and material property of the HMA layer. The detailed equations can be found in the MEPDG guideline [46].

6.6 Results and Discussion

6.6.1 Compressive Strength, Thermal Conductivity, and Porosity of Foamed Concrete

The relationship between cast density and compressive strength, thermal conductivity, and porosity is shown in Figure 29. It can be observed that the compressive strength, thermal conductivity, and porosity vary with the density of foamed concrete. Foamed concrete with higher cast density tends to result in a larger compressive strength and thermal conductivity and a smaller porosity. This conclusion agrees with the

experimental results performed by other researchers [126]. The 28-day compressive strength of the foamed concrete ranges from 0.44 – 2.54 MPa, the thermal conductivity ranges from 0.11 – 0.24 W/(m·K), and the porosity ranges from 0.30 – 0.46. All those values are located in a similar range as related studies [78].

In addition, foamed concrete with different densities exhibit different failure modes. For foamed concrete with higher density (800 and 960 kg/m^3), the concrete failed mainly because of the longitudinal cracks, whereas for lower density foamed concrete (480 kg/m^3), the concrete failed by crushing at the top, with no longitudinal crack found in these samples. For the foam concrete with medium density (640 kg/m^3), the failure mode combined the performance of both high density and low density concretes. The broken samples with medium density presented both throughout cracks and top crush regions, as shown in Figure 29.

Figure 29

Foamed Concrete Test Results: (a) Compressive Strength; (b) Thermal Conductivity; (c) Porosity; and (d) Image of Broken Samples

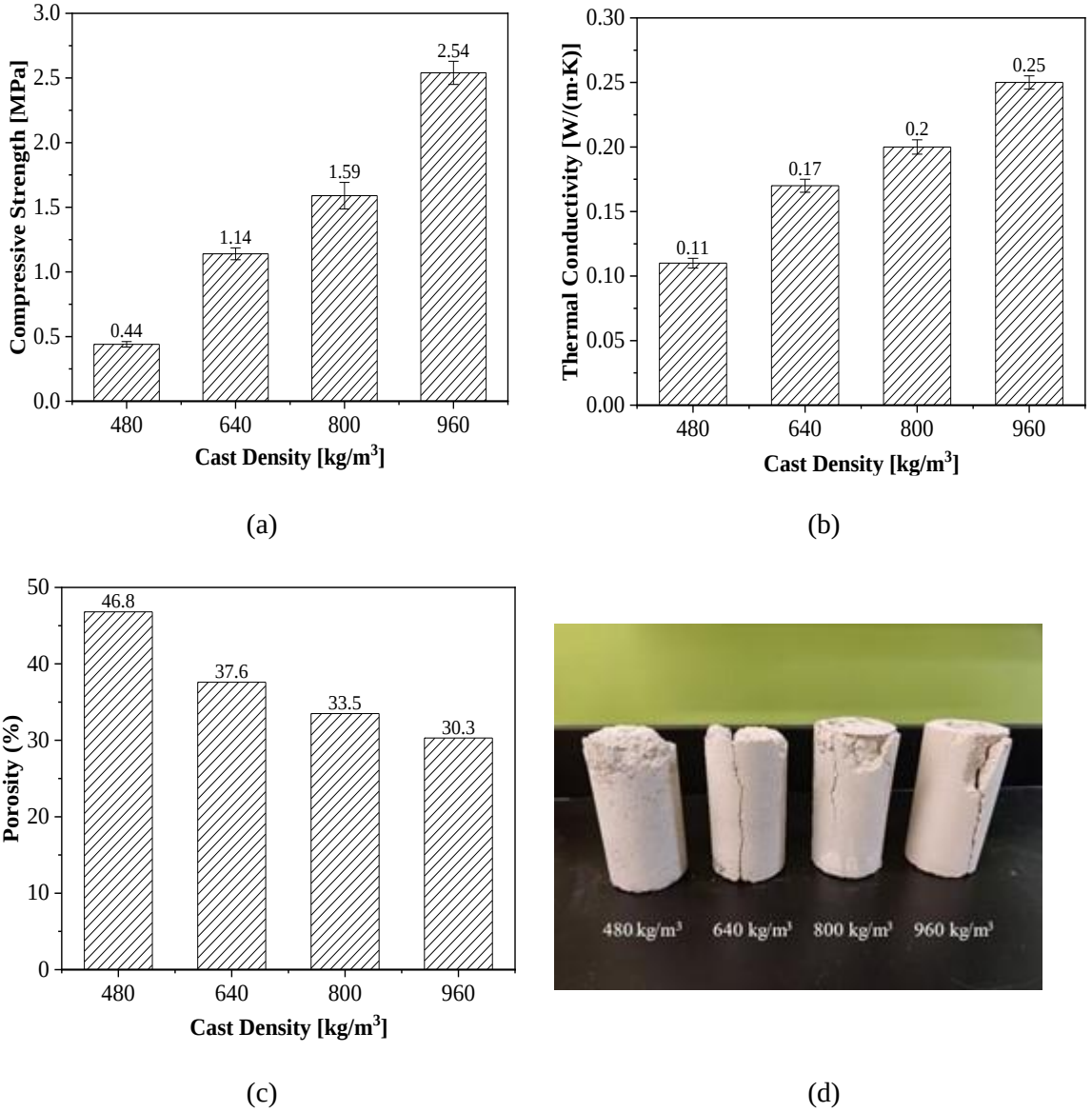

6.6.2 Thermal Performance of the Large-Scale Insulated Pavement Box

To validate the accuracy of the proposed FE model, the temperature distribution of a pavement structure with a foamed concrete insulation layer was recorded. The measured

temperature distribution was then compared with the predicted values given by the FE model. The material properties of the surface, base, and subgrade layers in the FE model adopted the measured material properties from the large-scale pavement box. The material properties of the foamed concrete insulation layer used the interpolation value calculated from the foamed concrete test results (Figure 29).

The measured and predicted temperature distribution of the insulated pavement box under a constantly freezing panel was shown in Figure 30. The temperatures of the surface, base, and subgrade shown in Figure 30. indicate the temperatures of the bottom of the surface layer, the bottom of the base layer, and the middle of the subgrade layer. According to the comparison between the measured and predicted temperature distribution, the developed model is capable of accurately predicting the thermal performance of insulated pavements.

Figure 30

Measured and Predicted Temperature Distribution of the Large-Scale Pavement Box

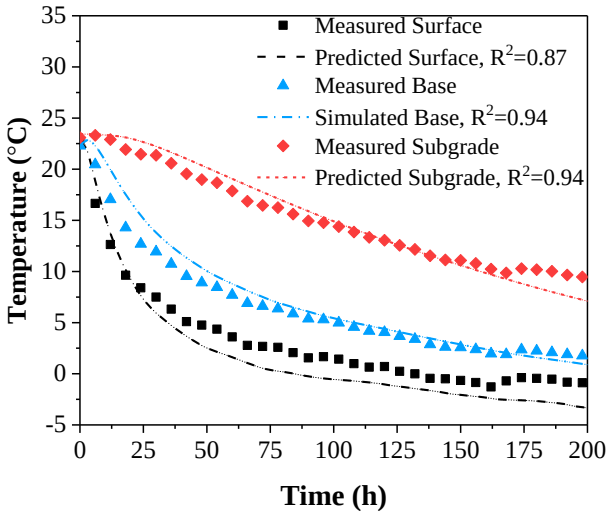

6.6.3 Parametric Study using the Developed FE Model

To investigate the influence of the density of a foamed concrete layer on the mechanical and thermal performance of an insulated pavement structure, a parametric study was performed based on the calibrated model. For each density, the thermal and mechanical performance of seven different structures as shown in Table 13 was estimated. The structures in Table 13 can be divided into two groups: group 1 (No.1 to No.5, with varying insulation thickness) and group 2 (No.1, No.3, No.6 to No.11, with varying insulation depth).

Table 13

Structure Matrix for the Parametric Study

No.	Surface (cm)	Base (cm)	Insulation (cm)	Subgrade (cm)
1	10	12	0	100
2	10	12	2.5	100
3	10	12	5	100
4	10	12	7.5	100
5	10	12	10	100
6	10	15	0	100
7	10	15	5	100
8	10	18	0	100
9	10	18	5	100
10	10	21	0	100
11	10	21	5	100

The parametric study results are presented in Figure 31. The frozen depth shown in the figure was the largest depth of the location where the temperature was 0 ºC. The insulation depth shown in Figure 31 (d) and (f) was the distance from the pavement surface to the top of the insulation layer. The maximum allowable traffic in (e) and (f) was calculated based on the empirical equation of estimating the bottom-up cracking.

Figure 31 (a) shows the influence of the density and insulation thickness (No.1 to No.5) on the frost depth (as indicated by different bars). The colors of this figure represent the layers of the insulated pavement. The simulation results indicated that compared with the uninsulated section, the foamed concrete insulation layer decreased the frost depth by 55% - 59%. When the thickness of the insulation layer was 2.5 cm, using a foamed concrete with high density (larger than 480 kg/m^3) would result in a frozen area in the subgrade layer, which might cause frost heave and thaw weakening if the subgrade is frost susceptible. For a foamed concrete layer with a thickness higher than 2.5 cm, the insulation layer could efficiently prevent the frost front from reaching the subgrade layer. In addition, when the thickness of the foamed concrete layer is larger than 2.5 cm, the density of the foamed concrete and the thickness of the insulation layer has little influence on the frozen depth.

Figure 31 (b) presents the influence of the density and depth (No. 1, No. 2, and No. 6 to No. 11) of the foamed concrete layer on the frozen depth. All uninsulated pavements failed to prevent the frost front from penetrating the subgrade layer. This result indicates that for a fixed thickness of the foamed concrete layer, adding the depth of the insulation layer would increase the frozen depth. When the depth of the insulation layer was deeper than 28 cm, insulated pavement with a higher density of foamed

concrete has a smaller frozen depth. This is because the insulation layer accelerates the temperature decreasing of the layers above the insulation layer [48]. An insulated pavement with a better insulation layer (i.e., lower thermal conductivity) has a stronger effect on the layers above the insulation layer.

The relationship between the density, thickness, and depth of the foamed concrete layer and the mechanical performance is presented in Figure 31 (c) to (f). These results show that adding a foamed concrete layer increased the mechanical performance of pavements. Compared with the uninsulated pavement, the foamed concrete insulated pavement has 4% to 20% less rutting depth and 23% to 180% more maximum allowable traffic. The influences of the thickness and depth on the mechanical performance are linear. A foamed concrete insulated pavement with a higher insulation thickness has better mechanical performance (i.e., a smaller rutting depth and a higher maximum allowable traffic). Increasing the insulation depth results in a better mechanical performance. Using foamed concrete with a higher density will enhance the mechanical performance of an insulated pavement.

These results were estimated based on the climate of Juneau, Alaska and the material properties measured in this study. With different types of foamed concrete or under different climates, the results might be different.

Figure 31

Influence of Foamed Concrete's Density and Pavement Structure on the Thermal and Mechanical Performance: (a), (b) Frozen Depth; (c), (d) Rutting Depth; (e), (f) Maximum Allowable Traffic

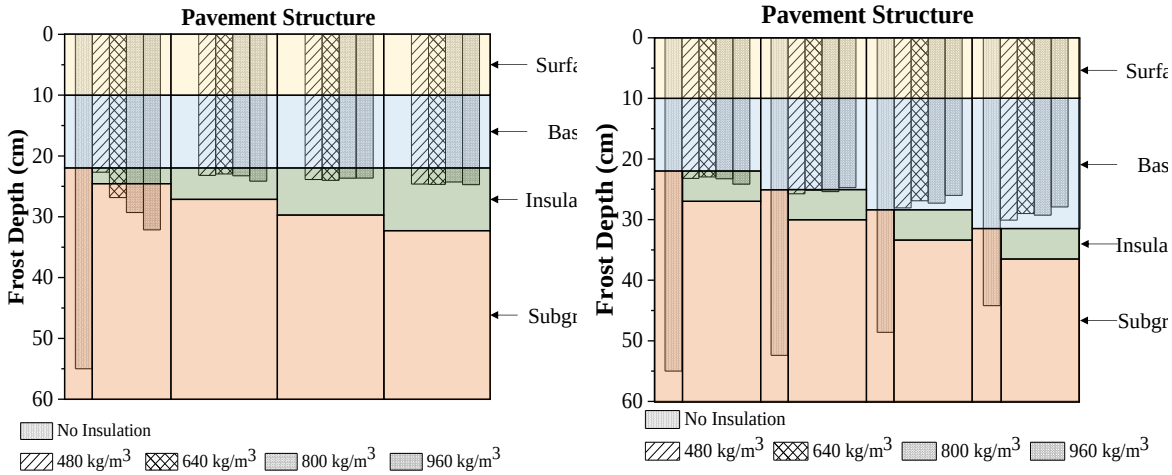

(a) (b)

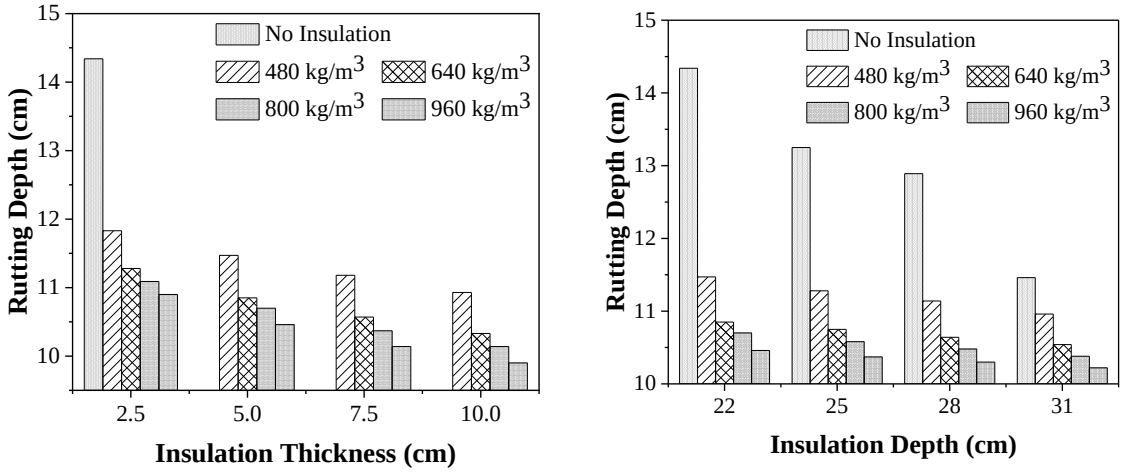

(c) (d)

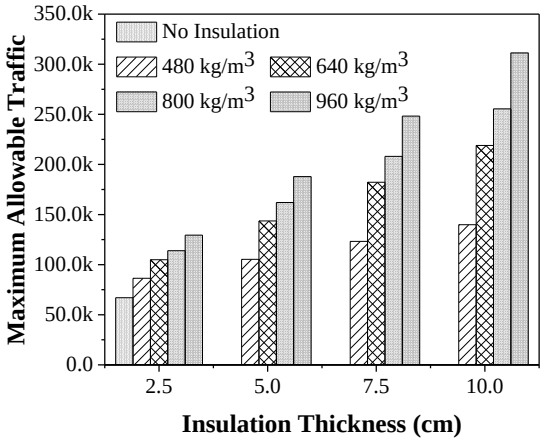

(e)

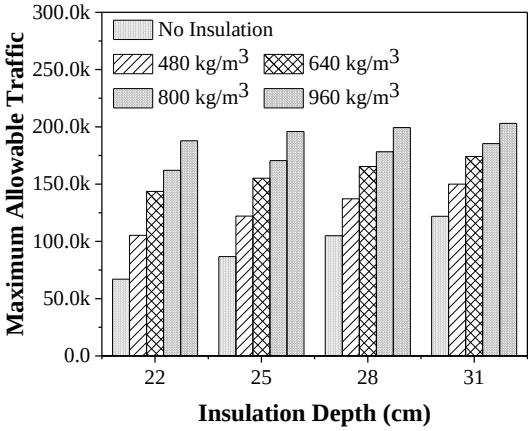

(f)

6.7 Main Findings in This Chapter

This chapter investigated the potential of using foamed concrete as an insulation layer in pavements in cold regions. To achieve this goal, a TM coupled model was developed to evaluate the application of foamed concrete as an insulation layer in flexible pavements. In addition, the compressive strength and thermal conductivity of foamed concrete with different densities were measured for a purpose of providing the relationship between the density and thermal/mechanical properties of foamed concretes. The temperature distribution of a large-scale insulated pavement structure was also measured and compared with the predicted values given by the TM coupled model. In the end, the mechanical and thermal performances of insulated pavement structures with different densities of foamed concrete were estimated based on the developed model and the empirical equations from the MEPDG guideline. Based on the analyses conducted as part of this study, the following conclusions were drawn:

(1) The model developed throughout this study is capable of accurately predicting the thermal performance of insulated pavements. The R^2s between the

predicted measured temperature from the large-scale box and the predicted temperature from the FE model in all layers are higher than 0.87.

(2) The average compressive strength of the foamed concrete samples with density of 480 kg/m^3 is 0.44 MPa, and that of the samples with density of 960 kg/m^3 is 2.54 MPa.

(3) The average thermal conductivity of 480 kg/m^3 foamed concrete samples is 0.11, and that of the 960 kg/m^3 samples is 0.25.

(4) Compared with the performance of uninsulated pavements, the foamed concrete insulated pavement has better performance in resisting frost effect and traffic loading. The foamed concrete insulation layer decreased the frost depth by 55% - 59%. Compared with the uninsulated pavement, the foamed concrete insulated pavement has 4% to 20% less rutting depth and 23% to 180% more maximum allowable traffic.

(5) To ensure the subgrade layer unfrozen, there is a minimum insulation thickness for a foamed concrete layer. In this study, for a foamed concrete layer with a density larger than 480 kg/m^3, the minimum thickness was 5 cm.

(6) Increasing the depth of the insulation layer from 15 cm to 21 cm will increase the maximum allowable traffic by 61%, while also increasing the frozen depth by 32%. Using foamed concrete with higher density result in a better mechanical performance.

Chapter 7

Cost Analysis of Insulated Pavement Structures

The purpose of this chapter is to present the results of a cost analysis conducted to compare the costs of insulated and uninsulated pavement structures. To facilitate the cost comparisons, equivalent pavement insulated pavement structures were designed. In this chapter, the designs of thermally and mechanically equivalent uninsulated (control) and insulated (four sections) are presented. This chapter also presents a cost comparison of the insulated pavement structures.

7.1 Equivalent Pavement Structure Analysis

The Finite Element Models (FEMs) developed as part of Chapter 5 were used to design thermally and mechanically equivalent insulated pavement structures. That is, determine the thickness of insulation layer that leads to similar thermal and mechanical performance.

A pavement structure insulated with 5 cm of XPS boards was used for establishing a baseline temperature distribution on top of the insulated subgrade layer. Thermal equivalency among insulated sections is defined as the condition where the temperature distribution at top of the insulated subgrade layer in each of the insulated sections is similar (standard deviation difference less than 1 ºC) to that of the baseline XPS insulated section. Mechanical equivalency was checked to ensure that all sections met a rutting threshold of 1.3 cm and a bottom-up cracking of less than 20% under 1,000,000 load repetitions. The thermal equivalency dictated the designs as the pavement structures generated by the thermal design step (Chapter 6) are mechanically adequate.

7.1.1 Design Inputs and Approach

Table 14 presents the thermal and mechanical properties used for the HMA, RCA base, insulation materials, and the subgrade layer. The thicknesses insulation layer (in the section containing insulation materials) were varied with their final thickness determined using the FEMs developed in Chapter 5. Using the FEMs, for each insulation material the thickness of the insulation layer was increased until the temperature distribution on top of the subgrade layer was similar to that of the baseline XPS insulated section. The similarity here means that the difference in the standard deviation of temperatures at the top of the subgrade layer for an insulated section was within 0.5 ºC to that of the XPS insulated baseline section.

Table 14 also shows that an uninsulated (control) section was designed to meet thermal equivalency criteria. For this section, the thickness of the base layer in the FEM was increased until the standard deviation of temperatures on top of the subgrade in this section was within 0.5 ºC of the XPS insulated section.

In addition to the material properties, the thermal field used in the FEMs for designing equivalent pavement structures was the same. To elaborate more, the thermal field in the FEMs was based on a 12-month daily temperature (January through December, 2019) variation in Alaska. The temperature data was obtained from the National Oceanic and Atmospheric Administration (NOAA; https://www.ncdc.noaa.gov/cdo-web/datatools). The initial temperature within the pavement layers was determined according to the BELLS temperature prediction model.

Table 14

Thermal and Mechanical Properties Used in Finite Element Models (FEMs) for Conducting Cost Comparisons

Materials	E (psi)	ν	k (BTU/h·ft·°F)	C (BTU/lb·°F)	Thickness (in.)
HMA	500,000	0.35	1.02	0.34	4
Base	100,000	0.25	$0.0001T^2$-0.0259T+2.35	0.33	Varies for uninsulated; 5 for insulated sections
XPS Boards	1,000	0.35	0.06	0.45	2
Tire Chips	150	0.35	0.22	0.27	Varies
Foam Glass Aggregates	10,000	0.35	0.11	0.56	Varies
Foamed Concrete	160,000	0.35	0.11	0.69	Varies
Subgrade	10,000	0.4	$0.00007T^2$-0.0144T+1.78	0.95	100

7.1.2 Discussion of Equivalent Pavement Sections

Table 15 presents the thermally and mechanically equivalent insulated pavement structures. A 2-inch thick XPS insulation layer is equivalent to 52 inches thick base layer (in the uninsulated, control section), a 7-inch thick tire chips layer, a 4-inch thick foam glass aggregates layer, or a 4-inch thick foamed concrete layer. This observation was expected as XPS had the best thermal insulation properties, followed by foamed glass aggregates and foamed concrete, and finally tire chips (please refer to Table 15 above for thermal properties).

Table 15

Thermally and Mechanically Equivalent Pavement Structures

Layers	Control (Uninsulated)	XPS (Baseline)	Tire Chips	Foamed Glass Aggregates	Foamed Concrete
HMA (in.)	4	4	4	4	4
Base (in.)	52	5	5	5	5
Insulation Layer (in.)	NA	2	7	4	4
Subgrade (in.)	100	100	100	100	100

7.2 Economic Cost Analysis of Different Insulating Materials

The cost analysis performed in this study focused on material costs and construction cost (labor cost, mobilization cost, etc.). The future routine and preventive maintenance costs, resurfacing and rehabilitation costs, and the associated administrative costs were not included in the analysis due to their high unpredictability for insulated pavements (Smith, 2006).

7.2.1 Cost Analysis Assumptions

The factors considered when conducting the cost comparisons are summarized as follows:

(1). The pavement structures are constructed as a new roadway; that is, there is a need to excavate the existing natural ground to place the paving materials;

(2). Only materials, labor, excavation, and mobilization costs are considered in the analysis. That is, the initial costs for constructing insulated pavement structures. As such,

there was no need to establish a discount rate for comparing costs as all the considered costs are current (time value of money is not a factor for these costs);

(3). Penalty factors are applied to costs if the construction activities are labor intensive (e.g., XPS boards) or require a time for curing and strength gaining (e.g., foamed concrete); and,

(4). Material costs are calculated for constructing a 12 ft. wide, 1-mile long lane of insulated roadway.

7.2.2 Materials, Labor, Mobilization and Excavation Costs

The material costs are those costs of all the materials used in constructing an insulated pavement structure. For any particular material, its cost can be calculated as shown in Equation 53:

$$Material\ Cost = Unit\ Cost\ (per\ cubic\ yard) \times Materials\ Volume \quad (53)$$

Labor costs represent the sum of all wages paid to employees. The mobilization cost represents the cost of getting the related equipment and crew to the job site. The excavation costs represent the cost of excavating the current ground level to the designed subgrade level.

Table 16 presents the costs for all materials used in the five thermally and mechanically equivalent pavement structures (Section 7.1). These costs along with the layer thicknesses will be used to determine the total materials costs. That is, for a 1-mile long, 12-ft wide lane of roadway.

Table 16

Unit Cost of Materials Per Cubic Yards

Material	Unit Cost ($/yd^3)
Hot Mix Asphalt	160
Recycled Concrete Aggregates	20
XPS Boards	165
Tire Chips	24
Foam Glass Aggregates	76
Foamed Concrete	195

The labor, mobilization and excavation costs are summarized in Table 17. As can be seen from this table the labor costs are given as the hourly rate for each laborer ($50/hour). It is assumed that 10 laborers are needed for completing all construction activities. A one-time mobilization cost of $5000 is estimated for transporting equipment and laborers to the construction site for constructing a typical roadway. The excavation cost per cubic yard is estimated at $100 (Table 17).

Table 17

Unit Construction Cost Used in the Cost Analysis

Item	Unit Costs
Labor cost (per laborer)	50 ($/hr)
Mobilization (one-time)	$5000
Excavation	100 ($/yd^3)

7.2.3 Total Construction Period and Penalty Factors

In this analysis, it is estimated that a total of 7 days (10 hours of work per day) is required to construct a typical pavement structure (1 mile long, 12 ft wide lane). A typical pavement structure here refers to a pavement that does not require any specialized construction equipment. Under this category, the control, foamed glass aggregate, and tire chip sections are considered typical with no penalty factor applied.

In the case of the XPS and foamed concrete insulated sections, delays in construction activities are expected. For instance, the XPS boards require a laborious process of installing the boards and ensuring the joints in between boards are sealed properly. Therefore, a penalty factor is of 1.5 is applied to increase the time needed (and in effect labor costs) for completing construction activities for the XPS insulated section. For the foamed concrete, additional time will be needed to place forms and pour the foamed concrete layer. More time in this case is also needed to allow the foamed concrete to cure and gain strength (at least 7 days). Because of these extra delays in construction schedule, a penalty factor of 2 is applied to the time needed for constructing foamed concrete insulated pavement structures in comparison to others. Both factors are also applied to the mobilization costs to reflect differences among the sections in terms of equipment and mobilization needs.

7.2.4 Discussion of Cost Analysis Results

Using the information provided in the previous sections along with the equivalent pavement structures data (Table 17), the materials, labor, and excavation costs are estimated for all thermally and mechanically equivalent pavement structures. Figure 32 presents the costs calculated per section. As can be seen from this figure, the control

section had the highest total cost of $1.96M. This was expected because more RCA base materials and higher excavation costs were needed for ensuring the subgrade in this section is insulated (i.e., temperature is similar to that of the XPS insulated section).

Figure 32 also shows that the cost of constructing an XPS insulated pavement structure was around $0.98M, followed by foamed glass aggregates at a cost of $0.99M, tire chips at a cost of $1.03M and finally foamed concrete at $1.12M. From these costs it can be seen that a cost-saving of roughly $1M can be attained when comparing insulated pavement structures to uninsulated pavement structures (the control). All insulating materials; therefore, are cost-effective options than just using regular base materials as the insulation layer. In addition, when comparing the costs of different insulation materials, it can be seen that XPS, tire chips, and foamed glass aggregates had similar costs (within $0.04M difference). This suggests that all these materials have similar cost-effectiveness.

Figure 32

Costs Summary of Equivalent Structures

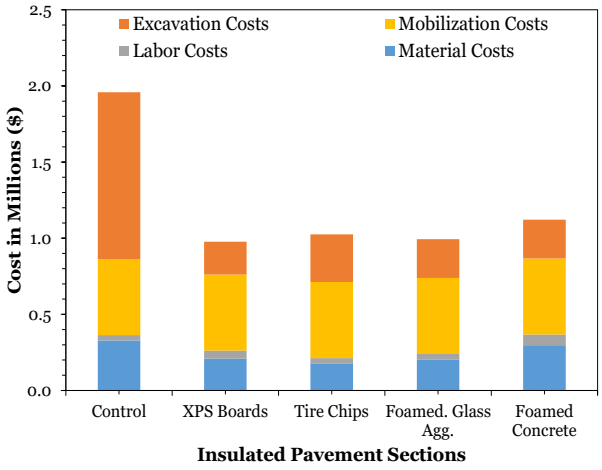

7.3 Main Findings in This Chapter

This chapter analyzed the cost-effectiveness of different insulating materials used in this study. The main findings can be summarized as follows:

(1) According to the equivalent thickness, a 5 cm thick XPS board layer had an equivalent performance as a 40 cm thick tire chips layer, a 25 cm thick FGA layer, a 30 cm thick foamed concrete layer, or a 68 cm thick base layer.

(2) To reach a similar thermal performance, the cost of building a uninsulated pavement is the most expensive ($1.96M), followed by the foamed concrete insulated pavement ($1.12M), tire chips insulated pavement ($1.03M), foamed glass aggregates insulated pavement ($0.99M), and XPS insulated pavement ($0.98M).

Chapter 8

Summary, Conclusions and Recommendations

8.1 Summary of Findings

Based on the experimental test and parametric studies, the major findings are as follows:

(1). The temperature decreases of the subgrade layer in insulated boxes, depending on the materials, ranges from 5.8 ºC to 15.4 ºC, while in the control box, it is 16.9 ºC. In contrast, the temperature decrease of the surface layer in insulated boxes ranges from 24.2 ºC to 30.8 ºC, which is larger than that in the control box (24.4 ºC).

(2). The performance of different insulating materials was evaluated and graded based on six indicators related to short-term temperature decrease and long-term temperature variation. The grades show that XPS boards presented the best insulating effect on the subgrade layer (grades 14.2/20 and 14/20 in the subgrade layer), but also caused the most significant variation in the surface layer (grades -0.8/10 and 2/10).

(3). XPS boards have the best overall performance (65.8/100), followed by foamed glass aggregates (60.1/100), foamed concrete (52.7/100), tire chips (48.8/100), and the control box (38.8/100).

(4). The pavements insulated by XPS boards and foamed concrete can bear up to 50 times more load repetitions than uninsulated pavements, while the tire chips insulated pavement can bear more traffic repetitions only when the overlay thickness is greater than 35 cm.

(5). The standard deviation of the subgrade temperature in the insulated boxes is 1-4 ºC less than that of the control box. Increasing the insulation thickness from 2.5 cm to 10 cm decreases the subgrade temperature standard deviation by 2 ºC.

(6). The average compressive strength of the foamed concrete samples with density of 480 kg/m3 is 0.44 MPa, and that of the samples with density of 960 kg/m3 is 2.54 MPa. The average thermal conductivity of 480 kg/m3 foamed concrete samples is 0.11, and that of the 960 kg/m3 samples is 0.25.

(7). Compared with the performance of uninsulated pavements, the foamed concrete insulation layer decreased the frost depth by 55% - 59%. Compared with the uninsulated pavement, the foamed concrete insulated pavement has 4% to 20% less rutting depth and 23% to 180% more maximum allowable traffic.

(8). Increasing the depth of the insulation layer from 15 cm to 21 cm will increase the maximum allowable traffic by 61%, while also increasing the frozen depth by 32%.

(9). According to the equivalent thickness, a 5 cm thick XPS board layer had an equivalent performance as a 40 cm thick tire chips layer, a 25 cm thick FGA layer, a 30 cm thick foamed concrete layer, or a 68 cm thick base layer.

(10). To reach a similar thermal performance, the cost of building an uninsulated pavement is the most expensive ($1.96M), followed by the foamed concrete insulated pavement ($1.12M), tire chips insulated pavement ($1.03M), foamed glass aggregates insulated pavement ($0.99M), and XPS insulated pavement ($0.98M).

8.2 Conclusions

(1). An insulation layer reduces the temperature variation in the layers below within a pavement structure. The same insulation layer also increases the rate of change of temperatures in layers above it.

(2). Temperature distribution results in the subgrade layers of the insulated large pavement boxes showed that XPS boards are the most effective at insulating the subgrade layer. But XPS boards also show the greatest negative influence on the surface layer.

(3). The ranking of the overall performance of the insulation materials is: XPS boards (best insulator), foamed glass aggregates, foamed concrete, and finally tire chips.

(4). Most of the insulated pavement structures can bear more rutting repetitions compare with uninsulated pavement. For insulated pavement with weak materials such as tire chips, the maximum load repetitions is less than that of the uninsulated pavement when the insulation thickness is not thick enough.

(5). With the same thickness of the surface, base, and subgrade layers, the insulated pavements have less temperature variation compared to the uninsulated pavements. A thicker insulation layer result in a smaller temperature variation.

(6). Foamed concrete with a higher density has a better mechanical performance and a worse insulating effect.

(7). Compared with the performance of uninsulated pavements, the foamed concrete insulated pavement has better performance in resisting frost effect and traffic loading.

(8). Increasing the depth of the insulation layer will achieve a better mechanical performance, while also increasing the frozen depth. Using a foamed concrete with a higher density result in a better mechanical performance.

(9). The use of insulation materials saves approximately $1M dollars in mate-rials, labor, mobilization, and excavation costs to build a 1 mile long, 12 ft. wide lane of a roadway. This is in comparison to the option of insulating using traditional construction materials (i.e., not using any of the four insulation materials).

8.3 Recommendations

Based on the conclusions and findings from this study, the following recommendations for future research are provided:

(1). The design approach provides example threshold values for controlling the variability within the subgrade and base layers in insulated pavement structures. As such, additional research is needed to develop realistic thresholds for the variability of the temperatures in these layers

(2). Validation of the design approach using full-scale, accelerated testing is also necessary. This would provide additional information about how well the insulated pavement structures designed using the approached developed in this study perform in the field. Adjustment to the design approach might be necessary based on these findings.

(3). The drainage conditions caused by insulating materials such as XPS boards need to be investigated. XPS boards are waterproof materials and the existence of XPS boards insulation layer might cause drainage problems for pavement structures.

(4). To achieve a better thermal performance, the insulated pavement structure is better than uninsulated pavements. Among the materials investigated in this study, XPS boards have the best overall thermal performance, foamed concrete and foamed glass aggregates also have relatively good thermal performance and better mechanical performance than the XPS boards.

(5). The life-cycle cost analysis of insulated pavements needs to be investigated.

(6). This study used FEM simulation to investigate the mechanical performance of the insulated pavement structures. For the future study, experimental tests need to be performed to supply the data for calibration process.

(7). This study collected a considerable amount of temperature data of pavement boxes under the nature environment, these data could be used for temperature prediction with the help of artificial intelligence method.

(8). The influence of interface between different layers in the FEM simulations needs to be considered.

References

1. Ma, H., et al., *Determination of allowable subgrade frost heave with the pavement roughness index in numerical analysis.* Sciences in Cold and Arid Regions, 2018. **7**(5): p. 587-593.

2. Salour, F. and S. Erlingsson. *The Influence of Groundwater Level on the Structural Behaviour of a Pavement Structure Using FWD*. in *Proceedings of the international conferences on the bearing capacity of roads, railways and airfields*. 2013.

3. Viklander, P., *Permeability and volume changes in till due to cyclic freeze/thaw.* Canadian Geotechnical Journal, 1998. **35**(3): p. 471-477.

4. Simonsen, E., V.C. Janoo, and U. Isacsson, *Resilient properties of unbound road materials during seasonal frost conditions.* Journal of Cold Regions Engineering, 2002. **16**(1): p. 28-50.

5. Chamberlain, E., I. Iskandar, and S. Hunsicker, *Effect of freeze-thaw cycles on the permeability and macrostructure of soils.* Cold Region Research and Engineering Laboratory, 1990. **90**(1): p. 145-155.

6. Zimmie, T. and C. La Plante. *Effect of freeze/thaw cycles on the permeability of a fine-grained soil*. in *Hazardous and Industrial Wastes- Proceedings of the Mid-Atlantic Industrial Waste Conference*. 1990.

7. Christopher, B.R., et al., *Geotechnical aspects of pavements*. 2006, United States. Federal Highway Administration.

8. Officials, T., *AASHTO Guide for Design of Pavement Structures, 1993*. Vol. 1. 1993: Aashto.

9. Kuosa, H., et al., *Pervious pavement winter performance-State-of-the-Art and recommendations for Finnish winter conditions.* VTT Tutkimusraportti VTT, 2014.

10. Booth, J.R., *Some factors affecting the long-term thermal insulating performance of extruded polystyrene foams*, in *Insulation Materials: Testing and Applications, 2nd Volume*. 1991, ASTM International.

11. Gandahl, R. *The use of plastic foam insulation in roads*. in *Proceedings of the 4th Canadian Permafrost Conference*. 1982.

12. Lee, J., et al., *Shredded tires and rubber-sand as lightweight backfill.* Journal of geotechnical and geoenvironmental engineering, 1999. **125**(2): p. 132-141.

13. Haghi, N.T., et al., *Using field data to evaluate bottom ash as pavement insulation layer.* Transportation Research Record, 2014. **2433**(1): p. 39-47.

14. Ghosh, A., A. Ghosh, and S. Neogi, *Reuse of fly ash and bottom ash in mortars with improved thermal conductivity performance for buildings.* Heliyon, 2018. **4**(11): p. e00934.

15. Raj, A., D. Sathyan, and K. Mini, *Physical and functional characteristics of foam concrete: A review.* Construction and Building Materials, 2019. **221**: p. 787-799.

16. Mydin, M.A.O. and H. Awang, *A review on mechanical and thermal properties of lightweight foamed concrete at ambient temperature.* Sustainable Building and Infrastructure Systems: Our Future Today, 2011: p. 388.

17. Emersleben, A. and N. Meyer, *The use of recycled glass for the construction of pavements*, in *GeoCongress 2012: State of the Art and Practice in Geotechnical Engineering*. 2012. p. 1642-1649.

18. Arulrajah, A., et al., *Engineering and environmental properties of foamed recycled glass as a lightweight engineering material.* Journal of Cleaner Production, 2015. **94**: p. 369-375.

19. Lee, C.-T., *Production of alumino-borosilicate foamed glass body from waste LCD glass.* Journal of Industrial and Engineering Chemistry, 2013. **19**(6): p. 1916-1925.

20. Penner, E., *Insulated road study.* Transportation Research Record, 1976(612): p. 80-83.

21. Esch, D., *Long Term Evaluation of Insulated Roads and Airfields in Alaska, Alaska Department of Transportation and Public Facilities*. 1994, Report no. FHWA-AKRD-94-18, Fairbanks, Alaska.

22. Kestler, M.A. and R.L. Berg, *Case study of insulated pavement in Jackman, Maine.* Transportation research record, 1995(1481).

23. Côté, J. and J.-M. Konrad, *A field study of hoarfrost formation on insulated pavements.* Canadian geotechnical journal, 2002. **39**(3): p. 547-560.

24. Dore, G., et al., *Use of alternative materials in pavement frost protection: Material characteristics and performance modeling.* Transportation research record, 1995(1481).

25. Field, D., et al. *Edmonton experience with bottom ash and other insulating materials for mitigation of frost heave induced damage in pavements*. in *2011 CONFERENCE AND EXHIBITION OF THE TRANSPORTATION ASSOCIATION OF CANADA. TRANSPORTATION SUCCESSES: LET'S BUILD ON THEM. 2011 Congress et Exhibition de l'Association des Transports du Canada. Les Succes en Transports: Une Tremplin vers l'AvenirTransportation Association of Canada (TAC)*. 2011.

26. Cortes, D.D., et al., *Thermal conductivity of hydrate‐bearing sediments.* Journal of Geophysical Research: Solid Earth, 2009. **114**(B11).

27. Kersten, M.S., *Thermal properties of soils*. 1952, Transportation Research Board.

28. Van Rooyen, M. and H.F. Winterkorn. *Structural and textural influences on thermal conductivity of soils*. in *Highway Research Board Proceedings*. 1957.

29. Johansen, O., *Thermal conductivity of soils*, in *CRREL Draft Translation 637, 1977*. 1975: Trondheim, Norway.

30. Gavriliev, R.I., *Generalized relationships between thermal and physical properties for various types of soils and peat*, in *Frozen Soils Under Engineering Impact*. 1984: Novosibirsk, Russia. p. 14-28.

31. Becker, B.R., A. Misra, and B.A. Fricke, *Development of correlations for soil thermal conductivity.* International Communications in Heat and Mass Transfer, 1992. **19**(1): p. 59-68.

32. De Vries, D.A., *Thermal conductivity of soil.* Mededelingen van deLandbouwhogeschool te Wageningen, 1952. **52**(1): p. 1-73 (translated by Building Research Station, Library Communication No. 759, England).

33. Gemant, A., *How to compute thermal soil conductivities.* Heating, Piping, and Air Conditioning, 1952. **24**(1): p. 122-123.

34. DeVera, A.L. and W. Strieder, *Upper and Lower Bounds on the Thermal Conductivity of a Random, Two-Phase Material.* The Journal of Physical Chemistry, 1977. **81**(18): p. 1783-1790.

35. Maxwell, J.C. and J.J. Thompson, *A treatise on electricity and magnetism*. 1904: Clarendon.

36. Kumlutas, D., I.H. Tavman, and M.T. Coban, *Thermal conductivity of particle filled polyethylene composite materials.* Composites Science and Technology, 2003. **63**(1): p. 113-117.

37. Hashin, Z. and S. Shtrikman, *A variational approach to the theory of the effective magnetic permeability of multi-phase materials.* Journal of Applied Physics, 1962. **33**(10): p. 3125-3131.

38. Nimick, F.B. and J.R. Leith, *A model for thermal-conductivity of granular porous media.* Journal of Heat Transfer-Transactions of the Asme, 1992. **114**(2): p. 505-508.

39. Tarnawski, V.R., et al., *Inter-particle contact heat transfer in soil systems at moderate temperatures.* International Journal of Energy Research, 2002. **26**(15): p. 1345-1358.

40. Gori, F. and S. Corasaniti, *Theoretical prediction of the thermal conductivity and temperature variation inside Mars soil analogues.* Planetary and Space Science, 2004. **52**(1-3): p. 91-99.

41. Ho, D., M. Harr, and G. Leonards, *Transient temperature distribution in insulated pavements—predictions vs. observations.* Canadian Geotechnical Journal, 1970. **7**(3): p. 275-284.

42. Frivik, P., et al., *Thermal design of pavement structures in seasonal frost areas.* 1977.

43. Dempsey, B.J. and M.R. Thompson, *A heat transfer model for evaluating frost action and temperature-related effects in multilayered pavement systems.* Highway Research Record, 1970(342).

44. Smith, B.S., *Design and construction of pavements in cold regions: state of the practice.* 2006.

45. (UFC), U.F.C., *Pavement Design for Roads and Parking Areas*. 2016.

46. AASHTO, *Mechanistic-Empirical Pavement Design Guide: A Manual of Practice.* 2008.

47. Huang, Y.H., *Pavement analysis and design.* 2004.

48. Côté, J. and J.-M. Konrad, *Granular protection design to minimize differential icing on insulated pavements.* Canadian geotechnical journal, 2006. **43**(3): p. 260-272.

49. Doré, G. and H.K. Zubeck, *Cold regions pavement engineering*. Vol. 401. 2009: ASCE Press Reston, Virginia.

50. Berg, R.L., G.L. Guymon, and T.C. Johnson, *Mathematical model to correlate frost heave of pavements with laboratory predictions*. 1980, COLD REGIONS RESEARCH AND ENGINEERING LAB HANOVER NH.

51. Konrad, J.-M. and N. Lemieux, *Influence of fines on frost heave characteristics of a well-graded base-course material.* Canadian geotechnical journal, 2005. **42**(2): p. 515-527.

52. Sarsembayeva, A. and P.E. Collins, *Evaluation of frost heave and moisture/chemical migration mechanisms in highway subsoil using a laboratory simulation method.* Cold Regions Science and Technology, 2017. **133**: p. 26-35.

53. Teng, J., et al., *Modelling frost heave in unsaturated coarse-grained soils.* ACTA GEOTECHNICA, 2020.

54. Simonsen, E. and U. Isacsson, *Thaw weakening of pavement structures in cold regions.* Cold regions science and technology, 1999. **29**(2): p. 135-151.

55. Qi, J., P.A. Vermeer, and G. Cheng, *A review of the influence of freeze‐thaw cycles on soil geotechnical properties.* Permafrost and periglacial processes, 2006. **17**(3): p. 245-252.

56. Qi, J., W. Ma, and C. Song, *Influence of freeze–thaw on engineering properties of a silty soil.* Cold regions science and technology, 2008. **53**(3): p. 397-404.

57. Wang, S.-l., et al., *Volume change behaviour and microstructure of stabilized loess under cyclic freeze–thaw conditions.* Canadian Journal of Civil Engineering, 2016. **43**(10): p. 865-874.

58. O'Neill, K., *The physics of mathematical frost heave models: A review.* Cold regions science and technology, 1983. **6**(3): p. 275-291.

59. Padilla, F. and J.-P. Villeneuve, *Modeling and experimental studies of frost heave including solute effects.* Cold Regions Science and Technology, 1992. **20**(2): p. 183-194.

60. Selvadurai, A., J. Hu, and I. Konuk, *Computational modelling of frost heave induced soil–pipeline interaction: I. Modelling of frost heave.* Cold regions science and technology, 1999. **29**(3): p. 215-228.

61. Shoop, S.A. and S.R. Bigl, *Moisture migration during freeze and thaw of unsaturated soils: modeling and large scale experiments.* Cold Regions Science and Technology, 1997. **25**(1): p. 33-45.

62. Tian, Z., Heitman, J., Horton, R., Ren, T., *Determining Soil Ice Contents During Freezing and Thawing with Thermo-Time Domain Reflectometry.* Vadose Zone Journal, 2015.

63. Qiang Ma, H.F., Henglin Xiao, Yongli Liu, Jun Zhang, Qian Deng, *Model test study on mechanical properties of pipe under the soil freeze-thaw condition.* Cold Regions Science and Technology, 2020.

64. Penner, E., *Experimental pavement structures insulated with a polyurethane and extruded polystyrene foam.* Physics of Snow and Ice: proceedings, 1967. **1**(2): p. 1311-1322.

65. Haghi, S.N.T., *Use of Waste/Recycled Material as Insulation in Road Construction.* 2019.

66. UFC, *Pavement Design for Roads and Parking Areas*. 2016.

67. Connor, B., *Comparison of Polystyrene Expanded and Extruded Foam Insulation in Roadway and Airport Embankments*. 2019.

68. Kardos, A.J. and S.A. Durham, *Strength, durability, and environmental properties of concrete utilizing recycled tire particles for pavement applications.* Construction and Building Materials, 2015. **98**: p. 832-845.

69. Shao, J. and J. Zarling, *Thermal conductivity of recycled tire rubber to be used as insulating fill beneath roadways*. 1995.

70. Tavafzadeh Haghi, N., et al., *Capital Cost Comparison of Pavements Comprised of Insulation Layers: Case Study in Edmonton, Canada.* Journal of Construction Engineering and Management, 2019. **145**(7): p. 04019038.

71. Tavafzadeh Haghi, N., L. Hashemian, and A. Bayat, *The effect of insulation layers on pavement strength during non-freeze–thaw season.* International Journal of Pavement Engineering, 2018. **19**(6): p. 543-552.

72. Huang, Y., et al., *Performance Evaluation of Different Insulating Materials using Field Temperature and Moisture Data.* Transportation Research Record, 2021: p. 03611981211003572.

73. Kearsley, E. and P. Wainwright, *Porosity and permeability of foamed concrete.* Cement and concrete research, 2001. **31**(5): p. 805-812.

74. Nambiar, E.K. and K. Ramamurthy, *Air‐void characterisation of foam concrete.* Cement and concrete research, 2007. **37**(2): p. 221-230.

75. Zhang, Z., et al., *Mechanical, thermal insulation, thermal resistance and acoustic absorption properties of geopolymer foam concrete.* Cement and Concrete Composites, 2015. **62**: p. 97-105.

76. Decký, M., et al., *Foam concrete as new material in road constructions.* Procedia engineering, 2016. **161**: p. 428-433.

77. Li, J., et al. *Seismic performance of pre-cast self-insulation shear walls made by a new type of foam concrete with high strength and low thermal conductivity*. in *Structures*. 2020. Elsevier.

78. Amran, Y.M., N. Farzadnia, and A.A. Ali, *Properties and applications of foamed concrete; a review.* Construction and Building Materials, 2015. **101**: p. 990-1005.

79. Segui, P., J.-P. Bilodeau, and G. Doré, *Mechanical Behavior of Pavement Structures Containing Foam Glass Aggregates Insulation Layer: Laboratory and In Situ Study*, in *Cold Regions Engineering 2019*. 2019, American Society of Civil Engineers Reston, VA. p. 213-221.

80. Segui, P., et al., *Thermal Behavior of Flexible Pavement Containing Foam Glass Aggregates as Thermal Insulation Layer*, in *Cold Regions Engineering 2019*. 2019, American Society of Civil Engineers Reston, VA. p. 204-212.

81. Liu, Z. and X. Yu, *Coupled thermo-hydro-mechanical model for porous materials under frost action: theory and implementation.* Acta Geotechnica, 2011. **6**(2): p. 51-65.

82. Farouki, O.T., *The thermal properties of soils in cold regions.* Cold Regions Science and Technology, 1981. **5**(1): p. 67-75.

83. Ghazavi, M. and M. Roustaie, *The influence of freeze–thaw cycles on the unconfined compressive strength of fiber-reinforced clay.* Cold regions science and technology, 2010. **61**(2-3): p. 125-131.

84. Khazanovich, L., et al., *Design and construction guidelines for thermally insulated concrete pavements.* 2013.

85. Katicha, S., *Analysis of Hot Mix Asphalt (HMA) Linear Viscoelastic and Bimodular Properties Using Uniaxial Compression and Indirect Tension (IDT) Tests*. 2007, Virginia Tech.

86. Li, M. and H. Wang, *Development of ANN-GA program for backcalculation of pavement moduli under FWD testing with viscoelastic and nonlinear parameters.* International Journal of Pavement Engineering, 2019. **20**(4): p. 490-498.

87. Delatte, N., *Concrete Pavement Design, Construction, and Performance*. 2018.

88. Mallick, R.B., and Tahar El-Korchi, *Pavement Engineering: Principles and Practice*. 2017.

89. Cui, K., et al., *The coupling effects of freeze-thaw cycles and salinization due to snowfall on the rammed earth used in historical freeze-thaw cycles relics in northwest China.* Cold Regions Science and Technology, 2019. **160**: p. 288-299.

90. Sterpi, D., *Effect of freeze–thaw cycles on the hydraulic conductivity of a compacted clayey silt and influence of the compaction energy.* Soils and foundations, 2015. **55**(5): p. 1326-1332.

91. Esch, D.C., *Long-term evaluations of insulated roads and airfields in Alaska.* Transportation research record, 1995(1481).

92. Yoshihara, H., N. Ataka, and M. Maruta, *Measurement of the Young's modulus and shear modulus of extruded polystyrene foam by the longitudinal and flexural vibration methods.* Journal of Cellular Plastics, 2018. **54**(2): p. 199-216.

93. Chen, J., H. Wang, and P. Xie, *Pavement temperature prediction: Theoretical models and critical affecting factors.* Applied Thermal Engineering, 2019. **158**: p. 113755.

94. Lukanen, E.O., et al., *Temperature predictions and adjustment factors for asphalt pavement*. 2000, Turner-Fairbank Highway Research Center.

95. Braley, W.A. and J.P. Zarling. *MUT1D: user-friendly one-dimensional thermal model*. in *Cold Regions Engineering*. 1991. ASCE.

96. Hermansson, Å., *Simulation model for calculating pavement temperatures including maximum temperature.* Transportation Research Record, 2000. **1699**(1): p. 134-141.

97. Hermansson, Å., *Mathematical model for calculation of pavement temperatures: comparison of calculated and measured temperatures.* Transportation Research Record, 2001. **1764**(1): p. 180-188.

98. Hermansson, Å., *Mathematical model for paved surface summer and winter temperature: comparison of calculated and measured temperatures.* Cold regions science and technology, 2004. **40**(1-2): p. 1-17.

99. Chen, J., H. Wang, and H. Zhu, *Analytical approach for evaluating temperature field of thermal modified asphalt pavement and urban heat island effect.* Applied Thermal Engineering, 2017. **113**: p. 739-748.

100. Van Donk, S. and E.W. Tollner, *Apparent thermal conductivity of mulch materials exposed to forced convection.* Transactions of the ASAE, 2000. **43**(5): p. 1117.

101. Wang, H., I.L. Al-Qadi, and I. Stanciulescu, *Simulation of tyre–pavement interaction for predicting contact stresses at static and various rolling conditions.* International Journal of Pavement Engineering, 2012. **13**(4): p. 310-321.

102. Penner, E., *Thermal conductivity of frozen soils.* Canadian Journal of Earth Sciences, 1970. **7**(3): p. 982-987.

103. Tian, Z., et al., *A simplified de V ries ‐based model to estimate thermal conductivity of unfrozen and frozen soil.* European Journal of Soil Science, 2016. **67**(5): p. 564-572.

104. Kay, B., et al., *The importance of water migration in the measurement of the thermal conductivity of unsaturated frozen soils.* Cold Regions Science and Technology, 1981. **5**(2): p. 95-106.

105. Jasim, A.F., H. Wang, and T. Bennert, *Evaluation of Clustered Traffic Inputs for Mechanistic-Empirical Pavement Design: Case Study in New Jersey.* Transportation Research Record, 2019. **2673**(11): p. 332-348.

106. Katicha, S.W. and G.W. Flintsch. *Use of fractional order viscoelastic models to characterize asphalt concrete*. in *Transportation and Development Institute Congress 2011: Integrated Transportation and Development for a Better Tomorrow*. 2011.

107. Ramamurthy, K., E.K. Nambiar, and G.I.S. Ranjani, *A classification of studies on properties of foam concrete.* Cement and concrete composites, 2009. **31**(6): p. 388-396.

108. Wei, S., et al., *Characterization and simulation of microstructure and thermal properties of foamed concrete.* Construction and building materials, 2013. **47**: p. 1278-1291.

109. ASTM, *Standard test method for foaming agents for use in producing cellular concrete using preformed foam.* 2012.

110. Kearsley, E. and P. Wainwright, *The effect of high fly ash content on the compressive strength of foamed concrete.* Cement and concrete research, 2001. **31**(1): p. 105-112.

111. Jones, M. and A. McCarthy. *Behaviour and assessment of foamed concrete for construction applications*. in *Use of foamed concrete in construction: Proceedings of the international conference held at the University of Dundee, Scotland, UK on 5 July 2005*. 2005. Thomas Telford Publishing.

112. Richard, T., et al., *Cellular concrete-A potential load-bearing insulation for cryogenic applications?* IEEE Transactions on Magnetics, 1975. **11**(2): p. 500-503.

113. Zahari, N.M., et al. *Foamed concrete: potential application in thermal insulation*. in *Malaysian Technical Universities Conference on Engineering and Technology*. 2009.

114. Kearsley, E. *Just foamed concrete–an overview*. in *Creating with Concrete: Proceedings International Conference (and Seminars) Held at the University of Dundee, Scotland, UK on 6-10 September 1999Thomas*. 1999.

115. Yamamoto, M., et al. *Fiber reinforced foamed mortar with multiple cracks in flexure*. in *International RILEM Workshop on High Performance Fiber Reinforced Cementitious Composites in Structural Applications*. 2006. RILEM Publications SARL.

116. Tam, C., et al., *Relationship between strength and volumetric composition of moist-cured cellular concrete.* Magazine of Concrete Research, 1987. **39**(138): p. 12-18.

117. Aldridge, D., *Foamed concrete.* Concrete, 2000. **34**(4): p. 20-2.

118. Jones, M. and A. McCarthy, *Heat of hydration in foamed concrete: Effect of mix constituents and plastic density.* Cement and concrete research, 2006. **36**(6): p. 1032-1041.

119. ASTM, *Standard test method for compressive strength of lightweight insulating concrete.* 2012.

120. ASTM, D., *Standard test method for determination of thermal conductivity of soil and soft rock by thermal needle probe procedure.* ASTM Data Ser. Publ., 2008. **5334**: p. 1-8.

121. Standard, A., *C20-00 Standard test methods for apparent porosity, water absorption, apparent specific gravity, and bulk density of burned refractory brick and shapes by boiling water.* ASTM Int., West Conshohocken, 2010.

122. AASHTO, *Standard method of test for moisture-density relations of soils using a 4.54-kg (10-lb) rammer and a 457-mm (18-in.) drop.* AASHTO T 180-10, 2010.

123. Zhang, Z. and H. Wang, *The pore characteristics of geopolymer foam concrete and their impact on the compressive strength and modulus.* Frontiers in Materials, 2016. **3**: p. 38.

124. Park, S. and R. Schapery, *Methods of interconversion between linear viscoelastic material functions. Part I—A numerical method based on Prony series.* International journal of solids and structures, 1999. **36**(11): p. 1653-1675.

125. Zhu, Z., J. Ning, and W. Ma, *A constitutive model of frozen soil with damage and numerical simulation for the coupled problem.* Science China Physics, Mechanics and Astronomy, 2010. **53**(4): p. 699-711.

126. Nambiar, E.K. and K. Ramamurthy, *Models relating mixture composition to the density and strength of foam concrete using response surface methodology.* Cement and Concrete Composites, 2006. **28**(9): p. 752-760.